NASA
Technical
Paper
2727

September 1987

# Subsonic Longitudinal and Lateral-Directional Characteristics of a Forward-Swept-Wing Fighter Configuration at Angles of Attack up to 47°

Michael J. Mann,
Jarrett K. Huffman,
and Charles H. Fox, Jr.

NASA

NASA
Technical
Paper
2727

1987

# Subsonic Longitudinal and Lateral-Directional Characteristics of a Forward-Swept-Wing Fighter Configuration at Angles of Attack up to 47°

Michael J. Mann,
Jarrett K. Huffman,
and Charles H. Fox, Jr.

*Langley Research Center*
*Hampton, Virginia*

National Aeronautics
and Space Administration

**Scientific and Technical
Information Office**

## Summary

The subsonic lateral-directional and longitudinal characteristics of a forward-swept-wing fighter configuration were examined in wind-tunnel tests at Mach numbers of 0.2 and 0.5 for angles of attack from 7° to 47°. The wind-tunnel model was tested over a sideslip range of -15° to 15°. The effects of a canard, strakes, the vertical tail, and leading- and trailing-edge flaps were examined. The canard and strakes both reduced asymmetric moments and side forces at zero sideslip for angles of attack up to about 30°. The canard had a small influence on the lateral-directional stability; however, the strakes produced a substantial reduction in the lateral stability for angles of attack greater than about 20°. The vertical tail improved directional stability up to an angle of attack of about 30°. Deflection of the leading-edge flaps to 20° at high angles of attack on the strake and canard configurations degraded both lateral and directional stability. Deflection of the trailing-edge flaps to 20° on the canard configuration generally increased the lateral and directional stability at high angle of attack. Once the basic wing-body configuration reached maximum lift, there was a very gradual decrease in lift up to the highest angle of attack tested. In the region of maximum lift, the strake configuration produced a more constant level of lift than the canard configuration as angle of attack was increased. It appeared that the canard configuration could be trimmed for the range of conditions of this study. The strake configuration was more longitudinally unstable and would require larger pitching moments than the canard configuration to trim. The leading- and trailing-edge flaps on the wing-body and the canard configurations were effective for increased lift only up to an angle of attack of about 40°. The leading-edge flap remained effective on the strake configuration over the entire angle-of-attack range tested.

## Introduction

Highly maneuverable aircraft are frequently required to operate at angles of attack well beyond maximum lift. Flight at these high angles of attack produces a variety of aerodynamic phenomena which strongly influence the aircraft stability and control (refs. 1 to 4). The aircraft forebody produces vortices which become asymmetric at high angles of attack and cause large side forces and yawing moments. For this reason, the shape of the forebody has a strong influence on the lateral-directional stability (ref. 5). Aircraft behavior at high angles of attack can also be strongly influenced by vortices generated on forebody strakes and the wing leading edge.

Experimental studies of the longitudinal and the lateral-directional characteristics of forward-swept-wing configurations at high angles of attack are reported in references 6 to 9. Reference 9 includes the effects of forebody strakes. Forward-swept wings exhibit different stall characteristics than aft-swept wings, and flow fields of forward-swept wings may also interact with the flow from the forebody, the forebody strakes, or a canard somewhat differently than the flow fields of aft-swept wings do. The present wind-tunnel investigation was conducted in order to determine the subsonic high angle-of-attack longitudinal and lateral-directional characteristics of a forward-swept-wing fighter configuration. The wing and the canard were designed to achieve good transonic maneuver performance (refs. 10 to 12). Although the wing was designed to operate in the presence of the canard, the configuration was also tested with forebody strakes. The effects of leading- and trailing-edge flaps, the vertical tail, and underwing or pylon-type vortex generators were also examined. The tests were conducted in the Langley 7- by 10-Foot High-Speed Tunnel at Mach numbers of 0.2 and 0.5 over an angle-of-attack range of -7° to 47° and a sideslip range of -15° to 15°.

## Symbols

The measurements and calculations were made in U.S. Customary Units. Force and moment coefficients are based on the geometry of the basic trapezoidal wing extended to the model centerline. (See table I and fig. 1.) Pitching moments are referred to a moment center 23.9 in. from the fuselage nose (15.6 percent of the mean aerodynamic chord) and 0.22 in. below the fuselage reference plane. The longitudinal data are referenced to the stability-axis system and the lateral-directional data are referenced to the body-axis system.

| | |
|---|---|
| $b$ | wing reference span, 26.6486 in. |
| $C$ | local wing chord, parallel to the plane of symmetry, in. |
| $C_D$ | drag coefficient, $\frac{\text{Drag}}{qS}$ |
| $C_L$ | lift coefficient, $\frac{\text{Lift}}{qS}$ |
| $C_{L_\alpha}$ | $= \partial C_L/\partial\alpha$, per deg |
| $C_l$ | rolling-moment coefficient, $\frac{\text{Rolling moment}}{qSb}$ |
| $C_{l_\beta}$ | $= \partial C_l/\partial\beta$, calculated by $\left(C_{l_{\beta=5°}} - C_{l_{\beta=-5°}}\right)/10°$ (lateral stability derivative, or dihedral effect), per deg |

$C_m$ pitching-moment coefficient, $\frac{\text{Pitching moment}}{qS\bar{c}}$

$C_n$ yawing-moment coefficient, $\frac{\text{Yawing moment}}{qSb}$

$C_{n_\beta}$ $= \partial C_n/\partial\beta$, calculated by $\left(C_{n_{\beta=5^\circ}} - C_{n_{\beta=-5^\circ}}\right)/10^\circ$ (directional stability derivative), per deg

$C_p$ pressure coefficient, $\frac{p_l - p}{q}$

$C_Y$ side-force coefficient, $\frac{\text{Side force}}{qS}$

$C_{Y_\beta}$ $= \partial C_Y/\partial\beta$, calculated by $\left(C_{Y_{\beta=5^\circ}} - C_{Y_{\beta=-5^\circ}}\right)/10^\circ$, per deg

$\bar{c}$ mean aerodynamic chord, 9.2589 in.

$L$ fuselage length, 38 in.

$L/D$ lift-drag ratio

$M$ free-stream Mach number

$p$ free-stream static pressure, psf

$p_l$ local static pressure, psf

$q$ free-stream dynamic pressure, psf

$S$ wing reference area, 1.5035 ft$^2$

$X$ local chordwise distance from wing leading edge parallel to plane of symmetry, in. (with strake on, $X$ is still measured from a straight line along wing leading edge extended to the fuselage)

$x'$ fuselage station, measured from model nose, in.

$\bar{x}$ distance from apex of strake measured parallel to plane of symmetry, in.

$y$ spanwise distance from plane of symmetry, in.

$\bar{y}$ spanwise distance measured from apex of strake, in.

$\alpha$ angle of attack, deg

$\beta$ angle of sideslip, deg

$\delta_c$ canard deflection, positive for leading edge up, deg

$\delta_{f,\mathrm{LE}}$ leading-edge flap deflection, measured chordwise, positive for leading edge down, deg

$\delta_{f,\mathrm{TE}}$ trailing-edge flap deflection, measured chordwise, positive for trailing edge down, deg

$\eta$ semispan location, $y/(b/2)$

Abbreviations:

FRP fuselage reference plane (see fig. 1(a))

WRP wing reference plane, parallel to FRP and 0.22 in. below it

## Apparatus and Tests

### Model Description

Drawings and details of the wind-tunnel model are presented in figure 1. Photographs of the model installed in the Langley 7- by 10-Foot High-Speed Tunnel are shown in figure 2. The geometric characteristics are given in table I. The model is representative of a highly maneuverable forward-swept-wing fighter configuration equipped with a canard or strakes or both. The incidence of the canard is variable and the wing leading- and trailing-edge flaps can be deflected (figs. 1(a) and 1(b)).

The airfoil sections of the wing and canard were designed by the use of transonic computational methods. The configuration is designed for a maneuver lift coefficient of 0.9 over a Mach range of 0.85 to 0.95 (refs. 10 and 11). The wing sections are 4.2 to 4.6 percent thick and have a leading-edge radius of 0.3 to 0.4 percent of the local wing chord over most of the span. The general shapes of the wing sections are shown in figure 1(b). The wing has an incidence of $-2^\circ$ at the fuselage juncture. The wing twist then increases in two linear segments between the fuselage juncture and $\eta = 0.90$ and is a constant $4^\circ$ outboard. The wing twist distribution is given in figure 1(c).

The leading- and trailing-edge flaps are 15 percent and 30 percent, respectively, of the local wing chord and extend from the fuselage juncture to the 0.84-semispan station (figs. 1(a) and 1(b)). The photographs of the model (fig. 2) show that the flaps are segmented; however, the segments are generally deflected as an integral unit.

The canard has the same aspect ratio as the wing (3.28) but is swept aft and is located above and ahead of the wing (fig. 1(a)).

The fuselage cross sections (fig. 1(d)) are circular fore and aft of the canopy region. The sides of the fuselage are flat in the region of the canard so that

the canard fits flush with the fuselage as it goes through a range of incidence angles. The fuselage has been area-ruled for low supersonic Mach numbers (ref. 10), and the cross-sectional area distributions of the fuselage and the other model components are shown in figure 1(e).

The forebody strakes are mounted below the fuselage reference plane and are blended into the wing leading edge as shown in figure 1(f). The planform coordinates of the strake leading edge are given in table II. A complete description of the strake design is given in reference 10.

Underwing or pylon-type vortex generators were mounted on the lower surface of the wing leading edge for some tests. The geometric details and wing locations of the vortex generators are given in figure 1(h).

### Tests and Corrections

The investigation was conducted in the Langley 7- by 10-Foot High-Speed Tunnel. This is a continuous-flow, single-return, atmospheric tunnel with a closed rectangular test section. A description and calibration of the tunnel is given in reference 13.

The tests were made at Mach numbers of 0.2 and 0.5, which corresponded to dynamic pressures of approximately 68 and 310 psf, respectively, and Reynolds numbers per foot of $1.35 \times 10^6$ and $3.00 \times 10^6$. Aerodynamic forces and moments were measured on a six-component strain-gauge balance mounted internally in the model. The model was tested over an angle-of-attack range of $-7°$ to $47°$ at sideslip angles of $0°$ and $\pm 5°$, and selected data were obtained at sideslip angles from $-15°$ to $15°$. The angles of attack and sideslip have been corrected for the effects of sting and balance bending under aerodynamic load. It should be noted that the model support system was designed specifically for stability testing. (See fig. 2.) It is expected that this support system produced pressure disturbances on the aft region of the model, which make the level of the drag data questionable for use in performance analysis.

Jet boundary and blockage corrections, based on the procedures of references 14 and 15, respectively, were applied to the data. Drag measurements were adjusted to the condition of free-stream static pressure acting over the model base.

Boundary-layer transition strips were applied to the model according to the method of reference 16. Strips about 0.06-in. wide of no. 120 carborundum grains were placed 0.6 in. aft (streamwise) of the leading edges of the wing, canard, vertical tail, and strake. A strip of the same width and grain size was placed 1.0 in. aft of the fuselage nose.

The wing and fuselage were instrumented with static-pressure orifices distributed in streamwise rows, as shown in figure 1(g). The left wing had orifices on the upper surface at semispan stations of $\eta = 0.25, 0.30, 0.35, 0.40, 0.45, 0.50, 0.65$, and 0.85. The right wing had upper-surface orifices at $\eta = 0.25$ and lower-surface orifices at $\eta = 0.25, 0.35, 0.50, 0.65$, and 0.85. All surface pressures were recorded by the use of differential pressure scanning valves mounted in the nose section of the model.

## Presentation of Results

The results of this study are presented in figures 3 to 17, which are organized into groups as indicated by the subheadings in the following list. The first four groups of figures present the characteristics of the model in the four basic configurations tested: the wing-body, the canard-wing-body, the strake-wing-body, and the strake-canard-wing-body configurations. The results are discussed in the same order as the figures. The effects of the canard, the strakes, the vertical tail, and the wing leading- and trailing-edge flaps are examined. The effects of flow field parameters such as Mach number and sideslip angle are examined for the various configurations. At appropriate places in the discussion, the configurations are compared by use of figure 15. The last two figures present some results for vortex generators and a segmented leading-edge flap. Unless otherwise specified, all the plotted data are with the vertical tail on.

All the plotted pressure distributions are for a sideslip angle of $0°$. All the upper-surface pressure distributions are plotted for the left wing, with the exception of figures 6 and 10. In figures 6 and 10, the right-wing upper-surface pressure distribution at $\eta = 0.25$ has been used to obtain a more closely spaced distribution of orifices at that span station.

### Wing-Body Configuration

## Results and Discussion

The longitudinal and lateral-directional characteristics are discussed separately. Pertinent results from the literature are discussed along with the results of this study.

### Longitudinal Characteristics

***Wing-body configuration.*** The longitudinal force and moment characteristics of the wing-body configuration at Mach numbers of 0.2 and 0.5 are shown in figure 3(a), and the wing and fuselage pressure distributions for a lift coefficient near 1.0 are plotted in figures 3(d) and 3(e). The wing leading- and trailing-edge flaps are deflected to 20°. Once the configuration reaches maximum $C_L$, there is a gradual decrease in lift with angle of attack and the curve becomes almost flat. The configuration is longitudinally stable for angles of attack up to 5° and becomes almost neutrally stable over most of the remainder of the angle-of-attack range. The wing pressure distributions seem to show some trailing-edge separation as indicated by the lack of good trailing-edge pressure recovery.[1] The fuselage pressure distribution shows a drop in pressure just aft of the juncture of the wing leading edge with the fuselage (fig. 3(e), $x'/L = 0.62$).

As shown in figure 4(a), deflection of the leading- and trailing-edge flaps produces substantial increases in $C_L$ for angles of attack up to about 40°. The flap deflection substantially reduces $L/D$ up to an angle of attack of 15°, but slightly increases $L/D$ for angles of attack of 15° to 25°. Corresponding to the increase in $L/D$ at $\alpha = 15°$, the wing pressure distributions in figure 4(d) show less leading-edge flow separation with the flaps deflected.

[1] The denser orifice spacing on the wing at $\eta = 0.25$ in figure 6(h) (canard off) shows a pressure peak which is not apparent in figure 3(d).

***Canard-wing-body configuration.*** Figures 6(a) and 6(b) show that as angle of attack is increased, the addition of the canard produces an increasing increment of lift up to the angle of attack for maximum lift, after which the lift increment becomes approximately constant. Because of the additional lift ahead of the moment reference center, the canard makes the configuration longitudinally unstable at both Mach numbers for angles of attack up to about 20°. Above this angle of attack, the configuration with the canard is almost neutrally stable.

Figures 6(g) to 6(r) show the effects of the canard on the wing and fuselage pressure distributions at various angles of attack for Mach numbers of 0.2 and 0.5. Figures 6(k) and 6(l), for angles of attack of about 23° and 25°, show a higher leading-edge suction peak on the wing at $\eta = 0.35$ and 0.50 with the canard on. The induced downwash on the wing from the canard reduces the local angle of attack at the wing leading edge and, therefore, reduces the flow separation on the wing leading edge. As shown in figures 6(a) and 6(b), for a given lift coefficient ($C_L = 1.4$, for example) $L/D$ is higher with the canard on than with the canard off. The reduced flow separation on the wing caused by the favorable interference from the canard would partly explain this increased $L/D$. Of course, the additional area of the canard allows the lift to be achieved at a lower angle of attack, where flow separation is further reduced, and this effect also contributes to a higher $L/D$. The effect of Mach number with the canard on is shown in figure 7(a) and is small.

Figures 6(m) and 6(n) show that the canard induces higher velocities and, therefore, an adverse pressure gradient at the middle of the fuselage. Since the gradient steepens as the Mach number increases, it appears that this gradient will develop into a shock wave at higher Mach numbers. (See tabulated data in ref. 10.)

The effects of the leading- and trailing-edge flap deflections on the canard configuration at a Mach number of 0.2 are shown in figure 8(a). Deflection of the leading-edge flap increases $C_{L_\alpha}$, and deflection of both the leading- and trailing-edge flaps produces a substantial increase in maximum $C_L$. As in the case of the wing-body configuration, the flaps are only effective for increased lift up to an angle of attack of approximately 40°. Figure 8(d) shows that deflection of the leading-edge flap greatly reduces the leading-edge pressure peak over most of the wing. This lower pressure peak eliminates a severe adverse pressure gradient and reduces the tendency for flow separation. ($L/D$ increases for essentially constant $\alpha$ and $C_L$, as shown in the figure.)

The effects of a change in incidence of the all-movable canard from 0° to −20° are shown in figure 9(a). It appears that the canard generates sufficient pitching moment to trim this configuration over a wide range of angles of attack.

***Strake-wing-body configuration.*** Figures 10(a) and 10(b) show the effects of the strakes on the longitudinal force and moment characteristics, and figures 15(a) and 15(b) make a direct comparison between the strake and canard configurations. In the region of maximum $C_L$, the strake configuration produces a more constant value of $C_L$ than the canard configuration. The strake configuration is much more longitudinally unstable than the canard configuration and would require larger moment increments to trim. The effect of Mach number for the strake configuration is shown in figure 11(a) and is small.

Figures 10(g) to 10(r) show the effects of the strake on the wing and fuselage pressure distributions at various angles of attack for Mach numbers of 0.2 and 0.5. The format is the same as that used for the canard configuration. The strake-wing juncture is at $\eta = 0.32$, so the pressure measurements at $\eta = 0.25$ are behind the strake. With the strake on, $X/C$ still refers to $X$ measured from a line along the wing leading edge extended to the fuselage. With the strake off, figures 10(g) and 10(h) show a peak in the pressure at $\eta = 0.25$ at the leading-edge flap hinge line of $X/C = 0.15$. This peak is gone with the strake on because in that case there is no flap deflection at that span station. Figure 10(k), for $\alpha \approx 23°$, shows that the strake reduces the leading-edge suction peak along the wing leading edge. Apparently the strake produces an upwash on the wing leading edge which promotes separation at a lower angle of attack than if the strake were not present. The fuselage pressure distributions show that the addition of the strake reduces the longitudinal pressure gradients on the fuselage (figs. 10(i), 10(j), 10(m), and 10(n), for example).

Figure 13(a) shows that deflection of the leading-edge flap to 20° on the strake configuration has a small effect on the longitudinal forces and the pitching moment. Above an angle of attack of 12°, the flap remains effective for increased lift up to the highest angle of attack tested. Similar to the wing-body case (fig. 4(d)), figure 13(d) shows that deflection of the leading-edge flap at $\alpha \approx 15°$ reduces the leading-edge separation on the wing between $\eta = 0.35$ and $\eta = 0.65$.

***Strake-canard-wing-body configuration.*** Results for the strake-canard configuration at Mach numbers of 0.2 and 0.5 are shown in figure 14(a) and are compared with the canard and strake configurations in

figures 15(a) and 15(b). The strake-canard configuration produces somewhat higher maximum $C_L$ and requires larger pitching-moment increments to trim than either the canard or the strake configuration.

***Vortex generators and segmented leading-edge flap.*** Figure 16(a) shows that the vortex generators used in this study have very little effect on the longitudinal forces and pitching moment. Figure 17(a) shows that deflection of the inboard segment of the leading-edge flap has almost no effect on the longitudinal forces and pitching moment. Therefore, the increase in maximum $C_L$ and the reduced drag caused by deflection of the entire leading-edge flap are apparently due to the outboard segment of that flap.

## Lateral-Directional Characteristics

The lateral-directional aerodynamic symmetry and stability of each configuration are now discussed. Aerodynamic symmetry is defined as the condition of the flow when the model is at zero sideslip and the side force, yawing moment, and rolling moment are essentially zero. Any significant nonzero values of these quantities at zero sideslip are termed asymmetric forces and moments.

***Wing-body configuration.*** The results for the wing-body configuration are shown in figures 3 to 5. Figure 3(b) shows the lateral-directional characteristics of the wing-body configuration (vertical tail on) with leading- and trailing-edge flaps deflected to 20° at Mach numbers of 0.2 and 0.5 and zero sideslip. This configuration generally exhibits lateral-directional aerodynamic symmetry for angles of attack up to about 15°. Above this angle of attack, this configuration, with these flap deflections, develops very large asymmetric side forces, yawing moments, and rolling moments. The yawing moment even changes sign as the angle of attack is increased.

Figure 3(c) shows that this configuration is generally directionally stable (positive values of $C_{n_\beta}$) at low angles of attack and becomes directionally unstable at high angles of attack. The configuration is laterally unstable at low angles of attack and becomes laterally stable (negative values of $C_{l_\beta}$) at high angles of attack. The effect of an increase in Mach number is to produce lateral stability at a lower angle of attack and to reduce somewhat the directional stability.

The effect of the vertical tail on lateral-directional stability of the wing-body configuration at a Mach number of 0.2 is shown in figures 3(f) and 5 for leading- and trailing-edge flap deflections of 20° and 0°, respectively. The vertical tail has essentially the same effect for both flap deflections. The basic wing-body configuration (vertical tail off) is generally directionally unstable over the entire angle-of-attack range, and the vertical tail increases the directional stability for angles of attack up to about 30°. With the flaps undeflected (fig. 5), the vertical tail makes the configuration directionally stable for angles of attack up to 22°. At high $\alpha$, the vertical tail is apparently immersed in separated flow so that its effectiveness is lost.

Figure 3(g) shows the variation of $C_Y$, $C_n$, and $C_l$ with the sideslip angle for sideslip angles from 15° to −15°. This figure illustrates that the $\beta$ derivatives, which are computed from measurements made at $\beta = \pm 5°$, are generally representative of the derivatives over the sideslip-angle range from 15° to −15°. An exception is the variation of $C_n$ and $C_l$ at an angle of attack of 24.1°. Because of the nonlinear behavior of these data, the actual values of $C_{n_\beta}$ and $C_{l_\beta}$ at $\alpha = 24.1°$ vary considerably with $\beta$, and for some values of $\beta$ differ from the average values in figure 3(c), which are computed for data points at $\beta = \pm 5°$.

Figure 4 illustrates the effects of deflection of the leading- and trailing-edge flaps to 20° at a Mach number of 0.2. The flap deflection in general increases the maximum values of the asymmetric moments and side force (fig. 4(b)). The effect of the flaps on $C_{n_\beta}$ is to increase stability over most of the angle-of-attack range, with a substantial increase occurring at low $\alpha$ (fig. 4(c)). The effect of the flaps on $C_{l_\beta}$ is to decrease stability at low $\alpha$ and to increase stability at high $\alpha$.

***Canard-wing-body configuration.*** Figures 6(c) and 6(d) show that the addition of the canard greatly reduces the asymmetric moments and side forces at zero sideslip. With the canard installed, the model is close to aerodynamic symmetry for angles of attack up to about 40° at a Mach number of 0.2 and up to about 30° at a Mach number of 0.5. Above these angles of attack some significant yawing moments and side forces do develop. Generally, the addition of the canard has only a small effect on both the directional and the lateral stability at Mach numbers of 0.2 and 0.5 (figs. 6(e) and 6(f)). The influence of the canard on stability is essentially the same with or without the vertical tail (figs. 6(e) and 6(s)). The effect of Mach number with the canard installed is summarized in figures 7(b) and 7(c). Figure 7(g) shows that the variation of $C_Y$, $C_n$, and $C_l$ with $\beta$ is approximately linear for at least $\beta = \pm 10°$.

The effectiveness of the vertical tail with the canard on (fig. 7(f)) is essentially the same as with the canard off (fig. 3(f)). The vertical tail increases

the directional stability for angles of attack up to about 25°.

For a Mach number of 0.2, the effects of the leading- and trailing-edge flaps and the canard incidence on the side force and on the lateral-directional moments and stability are generally rather small (figs. 8(b), 8(c), 9(b), and 9(c)). These results contrast with the canard-off case (fig. 4(b)), in which the flap deflection significantly increases the asymmetric moments and side forces. Figure 8(c) shows that deflection of the leading-edge flap is somewhat directionally destabilizing at high $\alpha$ and is laterally destabilizing over most of the angle-of-attack range. Deflection of the trailing-edge flap generally increases the lateral and directional stability at high $\alpha$. These results contrast somewhat with the results reported in reference 4, which indicate that at high $\alpha$, the leading-edge flap provides favorable increments for lateral-directional stability but that favorable effects have not been consistently obtained by the use of the trailing-edge flap. For the canard-on case, figure 9(b) shows that the canard incidence affects $C_n$ at zero sideslip for angles of attack greater than 30°.

The vortex generators and deflection of only the inboard segment of the leading-edge flap have a minor effect on the lateral-directional characteristics at zero sideslip over most of the angle-of-attack range (figs. 16(b) and 17(b)). However, the trends in these data at the highest angles of attack suggest that these devices may develop significant asymmetric moments and side force for angles of attack above 43°.

***Strake-wing-body configuration.*** Similar to the situation with the canard, the addition of the strake to the wing-body configuration at zero sideslip reduces the asymmetric moments and side forces at both Mach numbers for angles of attack up to about 30° (figs. 10(c) and 10(d)). Also similar to the canard configuration, the strake configuration does develop significant asymmetric moments and side forces above this angle of attack. (See figs. 15(c) and 15(d) for a direct comparison of the two configurations.)

In contrast to the addition of the canard, the addition of the strake has a very strong influence on the lateral stability; however, the effect on the directional stability is small, as is the case with the canard configuration (figs. 10(e) and 10(f)). Generally, the strake stabilizes $C_{n_\beta}$ and $C_{l_\beta}$ at low angles of attack and destabilizes them at high angles of attack. Similar results are shown in figure 13 of reference 4 for the effect of a strake on the lateral-directional stability of an aft-swept wing configuration.

These effects of the strake on lateral stability can be explained by the lateral movement of the strake vortices at sideslip. As shown in the sketch below, looking forward for a positive sideslip angle, the windward vortex from the right strake moves inboard and the leeward vortex from the left strake moves outboard toward the wing tip. This lateral movement of the vortices produces a positive rolling moment as the vortices pass over the wing. This would explain the large increase in $C_{l_\beta}$ (destabilizing) at high $\alpha$ caused by the addition of the strake (figs. 10(e) and 10(f)). It is recognized, of course, that even with the strakes off there is a vortex system from the forebody. However, it is expected that these vortices behave differently than the strake vortices.

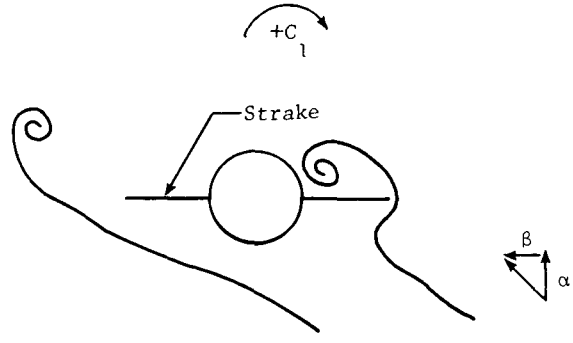


Figure 11(g) shows the lateral-directional characteristics for sideslip angles other than the ±5° used to calculate the stability derivatives for this configuration. Both $C_n$ and $C_l$ generally vary linearly with $\beta$ in a mean sense, with the exception of $C_n$ at $\alpha = 23.7°$. At the two higher angles of attack, the variation of $C_Y$ with $\beta$ has a nonlinear behavior which is not so pronounced for the wing-body or the canard-wing-body configurations (figs. 3(g) and 7(g)). This behavior is probably due to the inboard movement of the vortex from the right strake, which places the low pressure vortex core next to the fuselage and produces a positive side force at a positive sideslip. (See sketch.)

The effects of the strake on the $\beta$ derivatives for the configuration with and without the vertical tail (figs. 10(e) and 10(s)) are similar in character but slightly different in magnitude. The vertical tail increases directional stability for angles of attack up to about 30° (fig. 11(f)).

Figures 15(e) and 15(f) show that the strake configuration generally has a lower level of directional stability than the canard configuration for angles of attack greater than about 30° and a lower level of lateral stability for angles of attack greater than about 20°. Similar differences in lateral stability for an aft-swept wing configuration equipped with either strakes or canards are shown in figure 21 of reference 4.

The effects of Mach number on the lateral-directional characteristics of the strake configuration are summarized in figures 11(b) and 11(c).

Figure 12 shows that the leading- and trailing-edge flaps have a small influence on the lateral-directional coefficients at $\alpha \approx 36°$ for sideslip angles up to 15°. Figure 13(b) shows that deflection of the leading-edge flap to 20° produces a substantial asymmetry in the rolling moment at high $\alpha$. Deflection of the leading-edge flap degrades both lateral and directional stability at high $\alpha$ (fig. 13(c)), which is similar to the case of the canard configuration (fig. 8(c)). This contrasts with the deflection of both flaps on the wing-body configuration, which increases lateral and directional stability at high $\alpha$ (fig. 4(c)). At low $\alpha$, deflection of the leading-edge flap on the strake configuration generally increases directional stability (fig. 13(c)).

***Strake-canard-wing-body configuration.*** This configuration develops much larger asymmetrical moments and side forces at zero sideslip and high $\alpha$ than either the canard or the strake configuration (figs. 15(c) and 15(d)). The lateral-directional stability levels fall near or between those of the canard and strake configurations (figs. 15(e) and 15(f)). The variation of the lateral-directional coefficients with sideslip angle shown in figure 14(g) is similar to the results for the basic strake configuration (fig. 11(g)).

As for previous configurations, the addition of the vertical tail increases directional stability for angles of attack up to about 30° (fig. 14(f)). However, above this angle of attack, the vertical tail reduces both directional and lateral stability. This effect of the vertical tail at high $\alpha$ also occurs to a lesser extent for the strake configuration (fig. 11(f)). For the wing-body and canard configurations, this effect is either not present or is smaller in magnitude (figs. 3(f) and 7(f)). Therefore, it appears the vertical tail has a somewhat different effect on lateral-directional stability at high $\alpha$ when the strake is present. This suggests that there is some interaction between the strake vortices and the vertical tail at high $\alpha$.

***Summary of lateral-directional results.*** The $\beta$ derivatives computed for sideslip angles of $\pm 5°$ appear to be sufficiently accurate to provide a general description of the lateral-directional stability for sideslip angles up to approximately 10°. The addition of either the canard or the strake to the wing-body configuration at zero sideslip reduces the asymmetric moments and side forces for angles of attack up to about 30°. Above this angle of attack, asymmetric moments and side forces did develop. The canard has a small effect on the lateral-directional stability; however, the strake produces a very substantial reduction in lateral stability for angles of attack greater than about 20°. The strake configuration generally has a lower level of directional stability than the canard configuration for angles of attack greater than about 30° and a lower level of lateral stability for angles of attack greater than about 20°. Other studies have observed similar results on aft-swept wings for the effect of strakes on the lateral and directional stability and for the differences in lateral stability between canard and strake configurations. The stability levels for the current strake-canard configuration fall near or between the levels for the strake and canard configuration.

The vertical tail increases directional stability for all configurations for angles of attack up to about 30°. Above this angle of attack, the vertical tail is not effective and, in fact, reduces directional and lateral stability for the strake and strake-canard configurations. It appears, therefore, that the vertical tail has a somewhat different effect on lateral-directional stability at high $\alpha$ when the strake is present. Deflection of the leading-edge flap to 20° at high $\alpha$ on the strake and the canard configuration degrades both lateral and directional stability. Deflection of the trailing-edge flap to 20° on the canard configuration generally increases the lateral and directional stability at high $\alpha$.

## Summary of Results

The subsonic longitudinal and lateral-directional characteristics of a forward-swept wing configuration were examined in tests conducted at Mach numbers of 0.2 and 0.5 for angles of attack up to 47°. The forward-swept wing model of this study was designed as a highly maneuverable fighter configuration and the effects of both canards and strakes were examined. The results of this study may be summarized as follows:

1. Once the basic wing-body configuration reached maximum lift, there was a very gradual decrease in lift as angle of attack increased up to the highest angle tested.

2. The canard made the wing-body configuration longitudinally unstable for angles of attack up to about 20°. Above this angle of attack, the canard configuration was almost neutrally stable.

3. The all-movable canard generated sufficient pitching moment to trim the canard configuration for the range of conditions of this study.

4. In the region of maximum lift, the strake configuration produced a more constant level of lift as angle of attack was increased than the canard configuration.

5. The strake configuration was more longitudinally unstable and would require larger pitching moments to trim than the canard configuration.

6. Deflection of both the leading- and trailing-edge flaps to 20° on the wing-body and canard configurations increased lift for angles of attack up to about 40°, where the flaps were no longer effective.

7. Deflection of the leading-edge flap to 20° on the strake configuration remained effective for increased lift from an angle of attack of 12° to the highest angle of attack tested.

8. The canard and the strakes both reduced asymmetric moments and side forces at zero sideslip for angles of attack up to about 30°. Above this angle of attack, asymmetric moments and side forces did occur on the canard and strake configurations.

9. The canard had a small effect on the lateral-directional stability; however, the strakes produced a very substantial reduction in lateral stability for angles of attack greater than about 20°.

10. The strake configuration generally has a lower level of directional stability than the canard configuration for angles of attack greater than about 30° and a lower level of lateral stability for angles of attack greater than about 20°.

11. For all angles of attack, the lateral-directional stability levels of the strake-canard configuration fell near or between the levels for the strake and canard configurations.

12. The vertical tail was effective for increased directional stability of all configurations for angles of attack up to 30°. Above this angle of attack, the vertical tail reduced lateral and directional stability when the strake was present.

13. Deflection of the leading-edge flap to 20° at high angles of attack on the strake and canard configurations degraded both lateral and directional stability.

14. Deflection of the trailing-edge flaps to 20° on the canard configuration generally increased lateral and directional stability at high angles of attack.

NASA Langley Research Center
Hampton, Virginia 23665-5225
June 8, 1987

## References

1. High Angle-of-Attack Aerodynamics. AGARD-LS-121, Dec. 1982.
2. *High Angle of Attack Aerodynamics.* AGARD-CP-247, Jan. 1979.
3. *The Effects of Buffeting and Other Transonic Phenomena on Maneuvering Combat Aircraft.* AGARD-AR-82, July 1975.
4. Gilbert, William P.; and Nguyen, Luat T.: Impact of Recent Design Trends on Fighter Airplane Stall/Departure Characteristics. *Tactical Aircraft Research and Technology—Volume I,* NASA CP-2162, Part 1, 1981, pp. 369–401.
5. Carr, Peter C.; and Gilbert, William P.: *Effects of Fuselage Forebody Geometry on Low-Speed Lateral-Directional Characteristics of Twin-Tail Fighter Model at High Angles of Attack.* NASA TP-1592, 1979.
6. Murri, Daniel G.; Nguyen, Luat T.; and Grafton, Sue B.: *Wind-Tunnel Free-Flight Investigation of a Model of a Forward-Swept-Wing Fighter Configuration.* NASA TP-2230, 1984.
7. Huffman, Jarrett K.; and Fox, Charles H., Jr.: *The Effect of Canard Relative Size and Vertical Location on the Subsonic Longitudinal and Lateral-Directional Static Aerodynamic Characteristics for a Model With a Swept Forward Wing.* NASA TM-78739, 1979.
8. Huffman, Jarrett K.; and Fox, Charles H., Jr.: *Subsonic Longitudinal and Lateral-Directional Static Aerodynamic Characteristics for a Close-Coupled Wing-Canard Model in Both Swept Back and Swept Forward Configurations.* NASA TM-74092, 1978.
9. Huffman, Jarrett K.; and Fox, Charles H., Jr.: *Subsonic Longitudinal and Lateral-Directional Static Aerodynamic Characteristics for a Model With Swept Back and Swept Forward Wings.* NASA TM-74093, 1978.
10. Mann, Michael J.; and Mercer, Charles E.: *Forward-Swept-Wing Configuration Designed for High Maneuverability by Use of a Transonic Computational Method.* NASA TP-2628, 1986.
11. Mann, Michael J.; and Mercer, Charles E.: A Forward-Swept Wing Fighter Configuration Designed by a Transonic Computational Method. *J. Aircr.,* vol. 23, no. 6, June 1986, pp. 506–512.
12. Gainer, Thomas G.; Mann, Michael J.; and Huffman, Jarrett K.: *Low-Speed Investigation of Effects of Wing Leading- and Trailing-Edge Flap Deflections and Canard Incidence on a Fighter Configuration Equipped With a Forward-Swept Wing.* NASA TM-85795, 1984.
13. Fox, Charles H., Jr.; and Huffman, Jarrett K.: *Calibration and Test Capabilities of the Langley 7- by 10-Foot High-Speed Tunnel.* NASA TM X-74027, 1977.
14. Gillis, Clarence L.; Polhamus, Edward C.; and Gray, Joseph L., Jr.: *Charts for Determining Jet-Boundary Corrections for Complete Models in 7- by 10-Foot Closed Rectangular Wind Tunnels.* NACA WR L-123, 1945. (Formerly NACA ARR L5G31.)
15. Herriot, John G.: *Blockage Corrections for Three-Dimensional-Flow Closed-Throat Wind Tunnels, With Consideration of the Effect of Compressibility.* NACA Rep. 995, 1950. (Supersedes NACA RM A7B28.)
16. Braslow, Albert L.; and Knox, Eugene C.: *Simplified Method for Determination of Critical Height of Distributed Roughness Particles for Boundary-Layer Transition at Mach Numbers From 0 to 5.* NACA TN 4363, 1958.

Table I. Geometric Characteristics of Model

| | |
|---|---|
| **Wing (based on trapezoid extended to fuselage centerline):** | |
| Aspect ratio | 3.28 |
| Forward sweep of leading edge, deg | 20.234 |
| Forward sweep of trailing edge, deg | 49.184 |
| Forward sweep of quarter-chord line, deg | 29.505 |
| Taper ratio | 0.2142 |
| Area, $ft^2$ | 1.5035 |
| Span, in. | 26.6486 |
| Mean aerodynamic chord, in. | 9.2589 |
| Wing spanwise station of mean aerodynamic chord, in. | 5.225 |
| Fuselage station of 25-percent wing mean aerodynamic chord, in. | 23.770 |
| Root chord (at fuselage centerline), in. | 13.383 |
| Tip chord, in. | 2.867 |
| Dihedral, deg | 0 |
| Twist (washin from root to tip), deg | 6.0 |
| Incidence (root), deg | −2.0 |
| Airfoil sections | 4.2- to 4.6-percent-thick supercritical |
| **Canard (based on trapezoid extended to fuselage centerline, except as noted):** | |
| Leading-edge sweep, deg | 45 |
| Aspect ratio | 3.28 |
| Taper ratio | 0.2142 |
| Area, $in^2$ | 54.122 |
| Span, in. | 13.324 |
| Root chord (at fuselage centerline), in. | 6.691 |
| Tip chord, in. | 1.433 |
| Dihedral, deg | 10 |
| Airfoil sections | 5.1-percent-thick supercritical |
| Ratio of exposed area to wing reference area | 0.156 |
| **Fuselage:** | |
| Base cavity area, $in^2$ | 5.52 |
| **Vertical tail (based on exposed area):** | |
| Leading-edge sweep, deg | 54 |
| Aspect ratio | 1.02 |
| Taper ratio | 0.310 |
| Area, $in^2$ | 29.76 |
| Span, in. | 5.50 |
| Root chord, in. | 8.26 |
| Tip chord, in. | 2.56 |
| Airfoil section | 4-percent circular-arc biconvex |
| **Strakes (based on exposed area of each strake, except as noted):** | |
| Width, in. | 2.94 |
| Root chord, in. | 17.7 |
| Slenderness ratio (length/width) | 6.02 |
| Area, $in^2$ | 26.10 |
| Dihedral, deg | 3 |
| Ratio of exposed area of both strakes to wing reference area | 0.241 |

Table II. Strake Planform Leading-Edge Coordinates

| $\bar{x}$, in. | $\bar{y}$, in. |
|---|---|
| 0 | 0 |
| .058 | .052 |
| .132 | .104 |
| .220 | .156 |
| .318 | .208 |
| .428 | .261 |
| .744 | .395 |
| 1.114 | .529 |
| 1.535 | .665 |
| 2.004 | .803 |
| 2.520 | .941 |
| 3.083 | 1.081 |
| 3.695 | 1.222 |
| 4.356 | 1.364 |
| 5.070 | 1.508 |
| 5.840 | 1.653 |
| 6.673 | 1.800 |
| 7.577 | 1.949 |
| 8.568 | 2.100 |
| 9.662 | 2.254 |
| 10.889 | 2.411 |
| 12.304 | 2.573 |
| 14.039 | 2.743 |
| 16.803 | 2.941 |

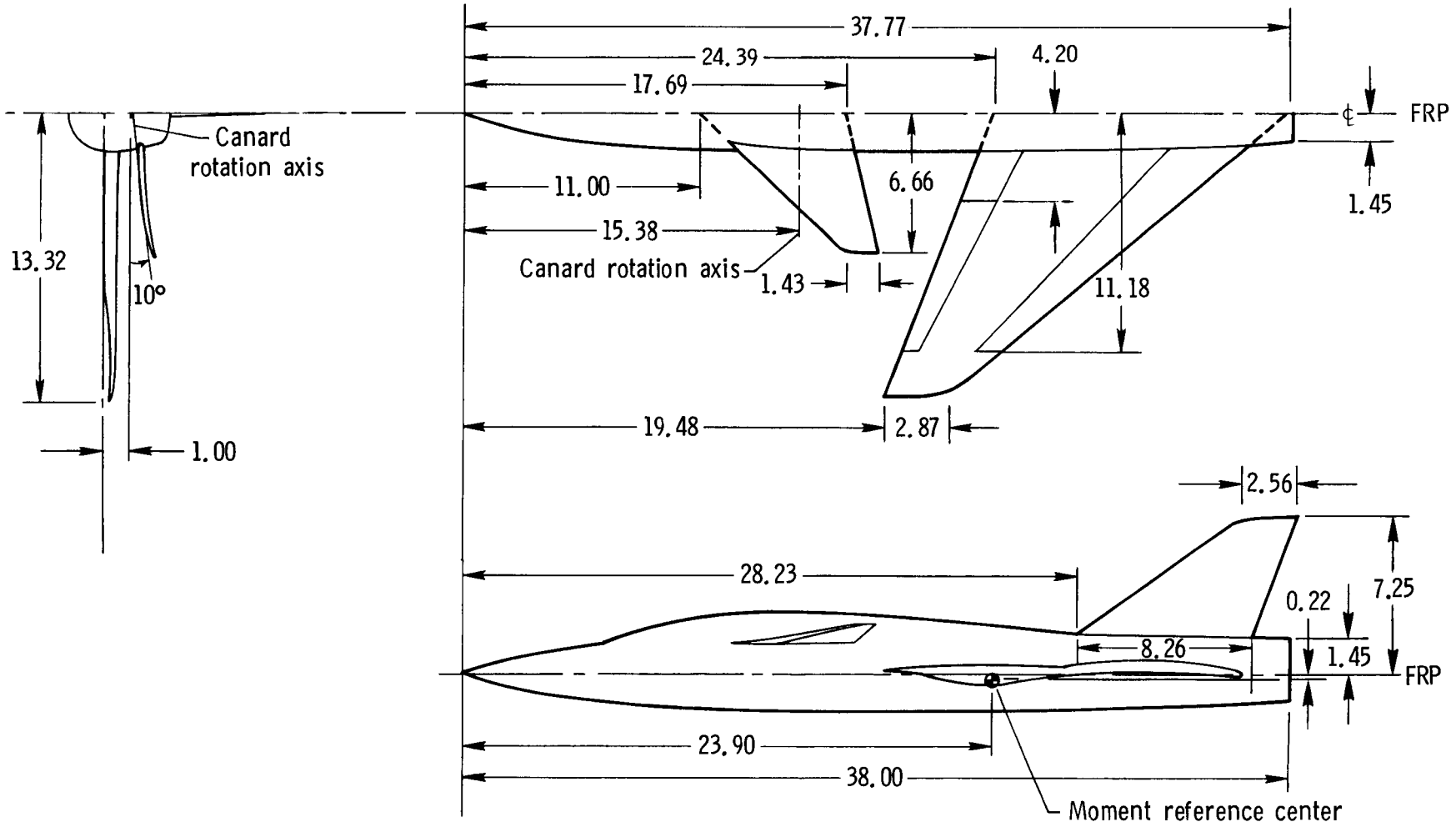


(a) General arrangement of model.

Figure 1. Geometric characteristics of model. Dimensions are in inches unless indicated otherwise.

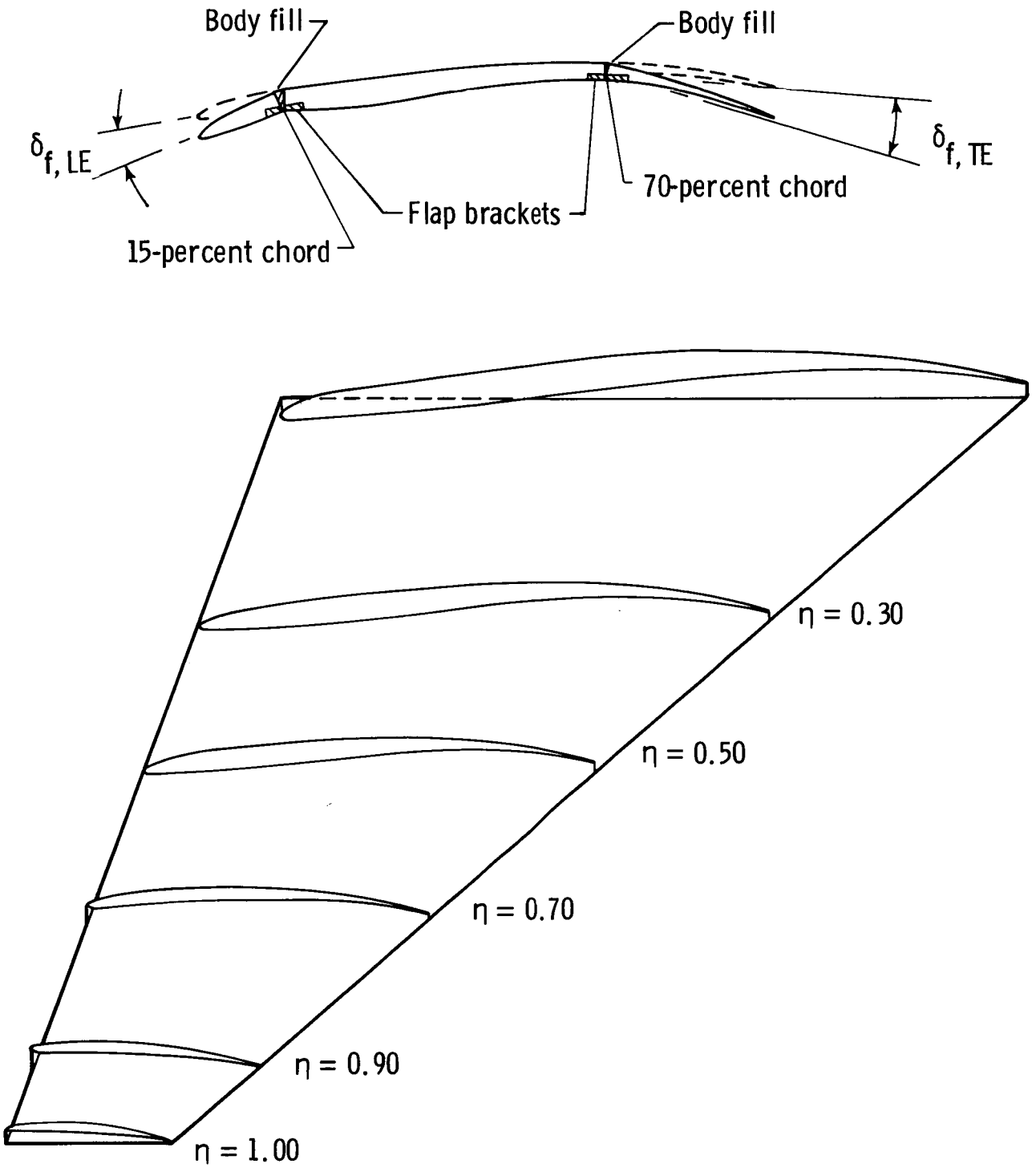


(b) Wing sections and flap locations.

Figure 1. Continued.

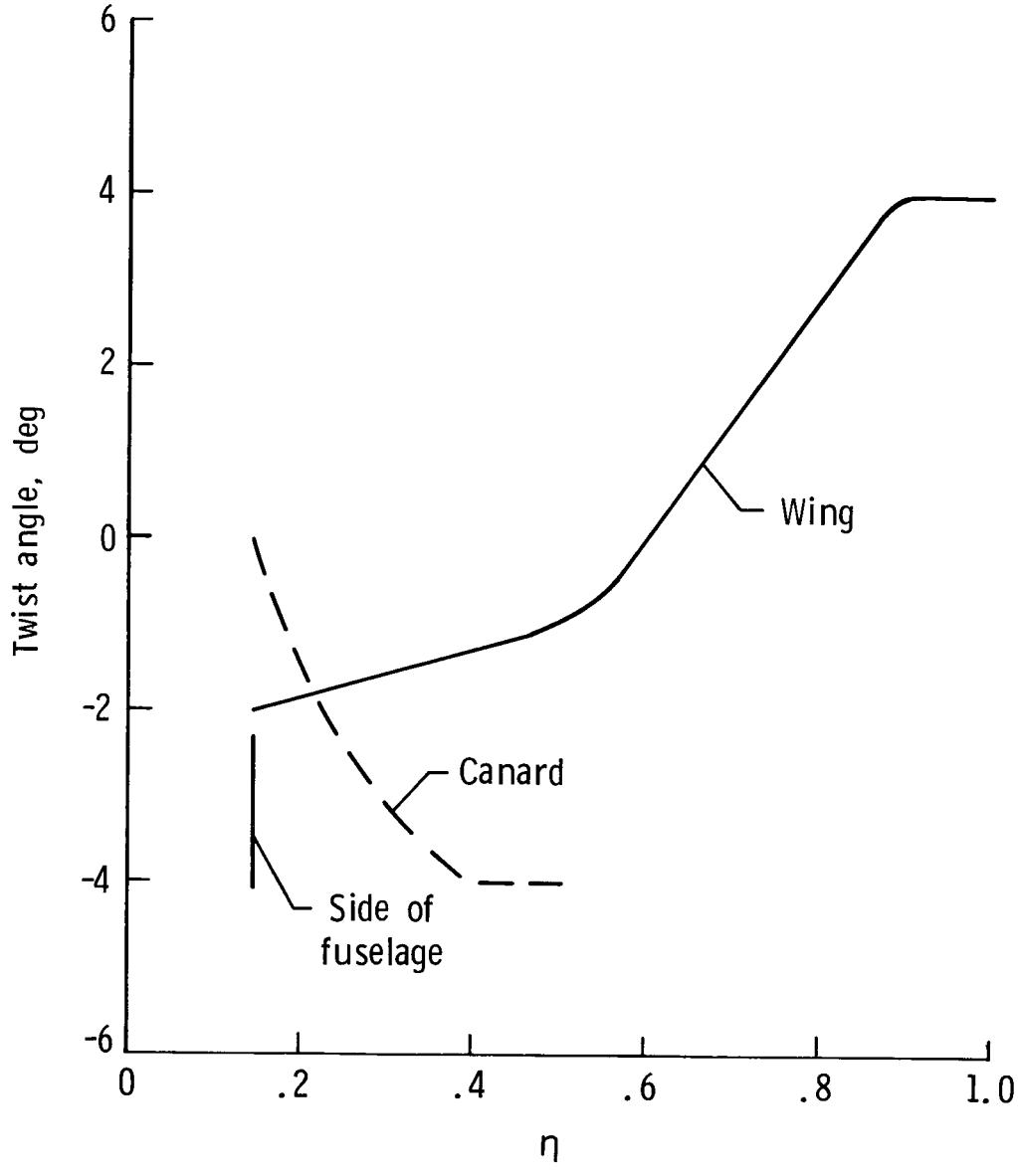


(c) Twist distributions for wing and canard.

Figure 1. Continued.

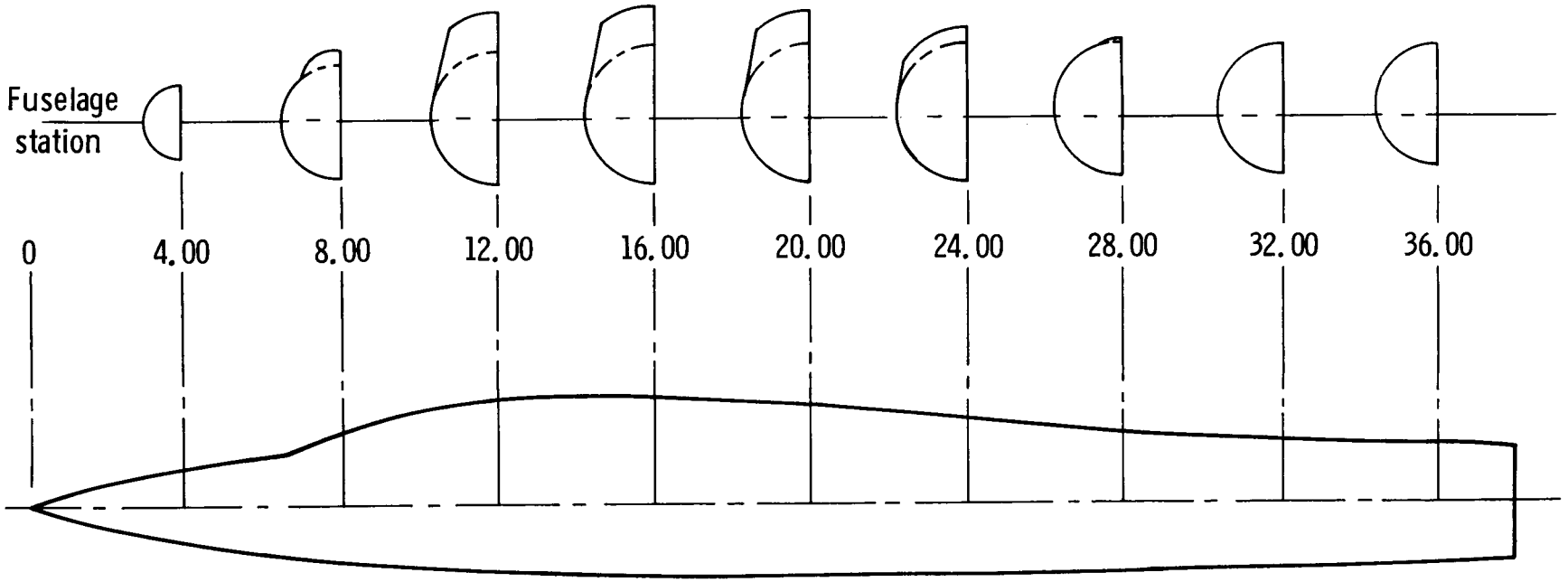


(d) Fuselage external contours.

Figure 1. Continued.

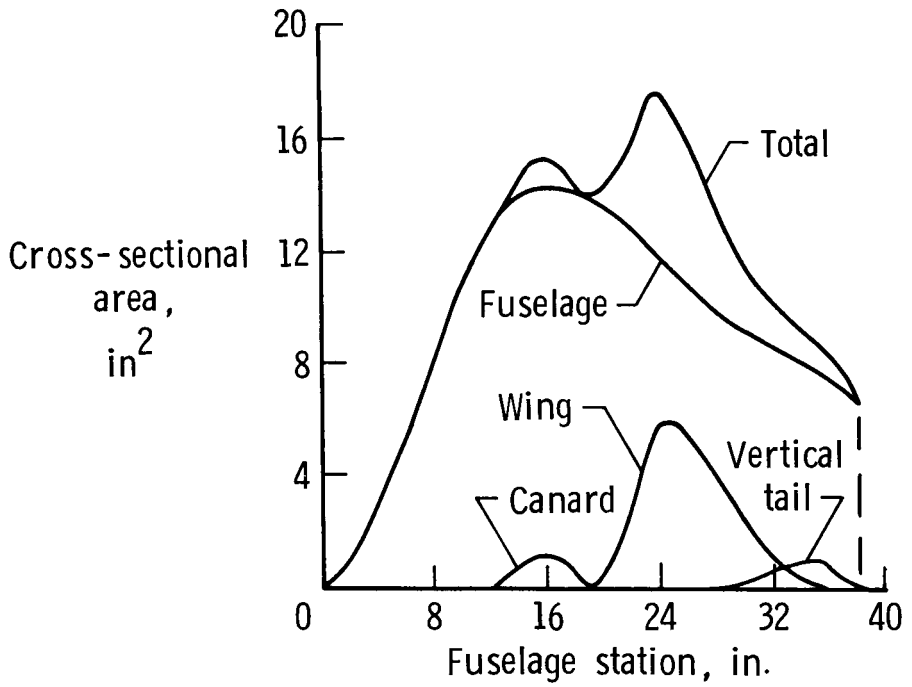


(e) Longitudinal variation of cross-sectional areas.

Figure 1. Continued.

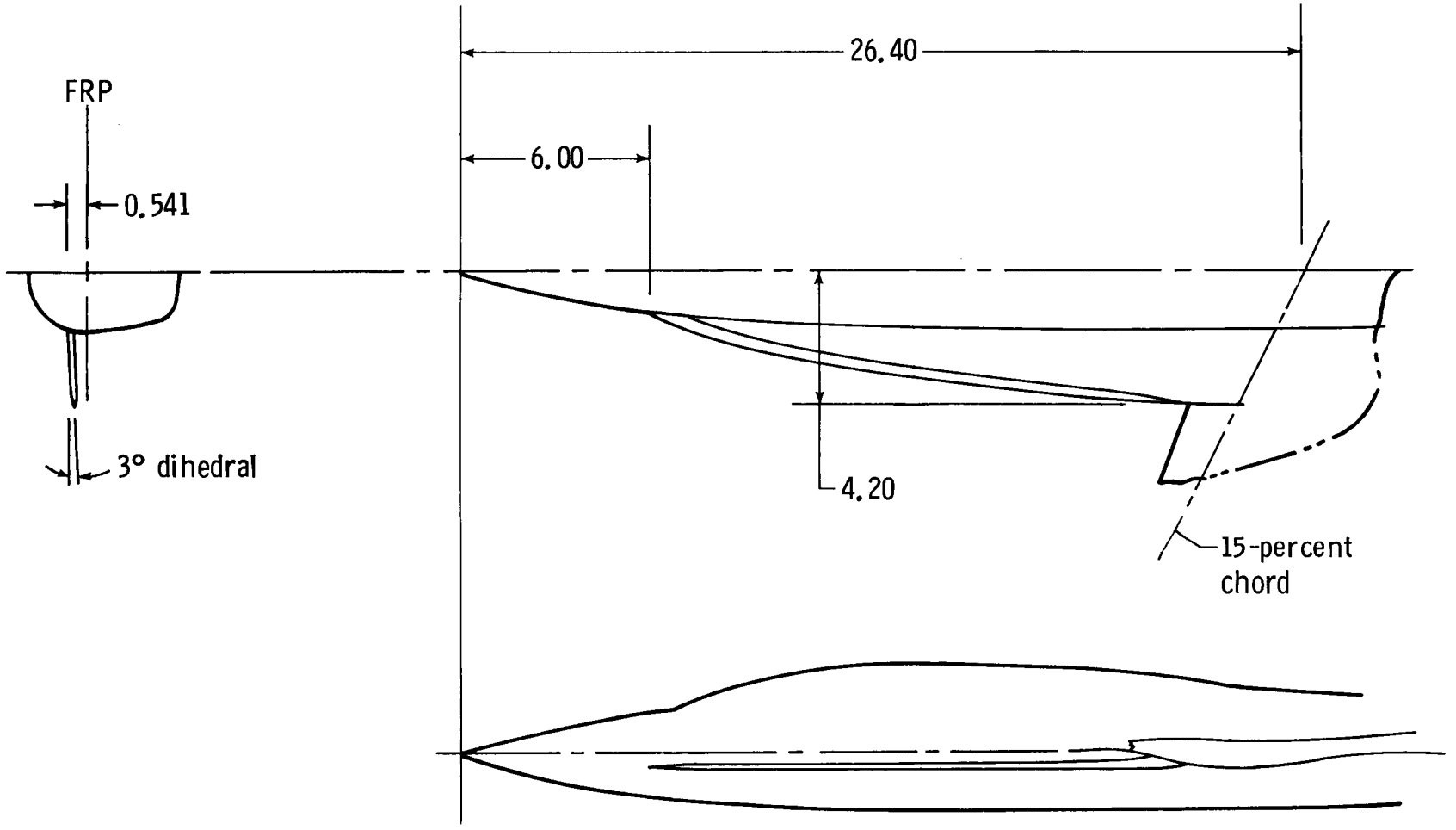


(f) Forebody strake.

Figure 1. Continued.

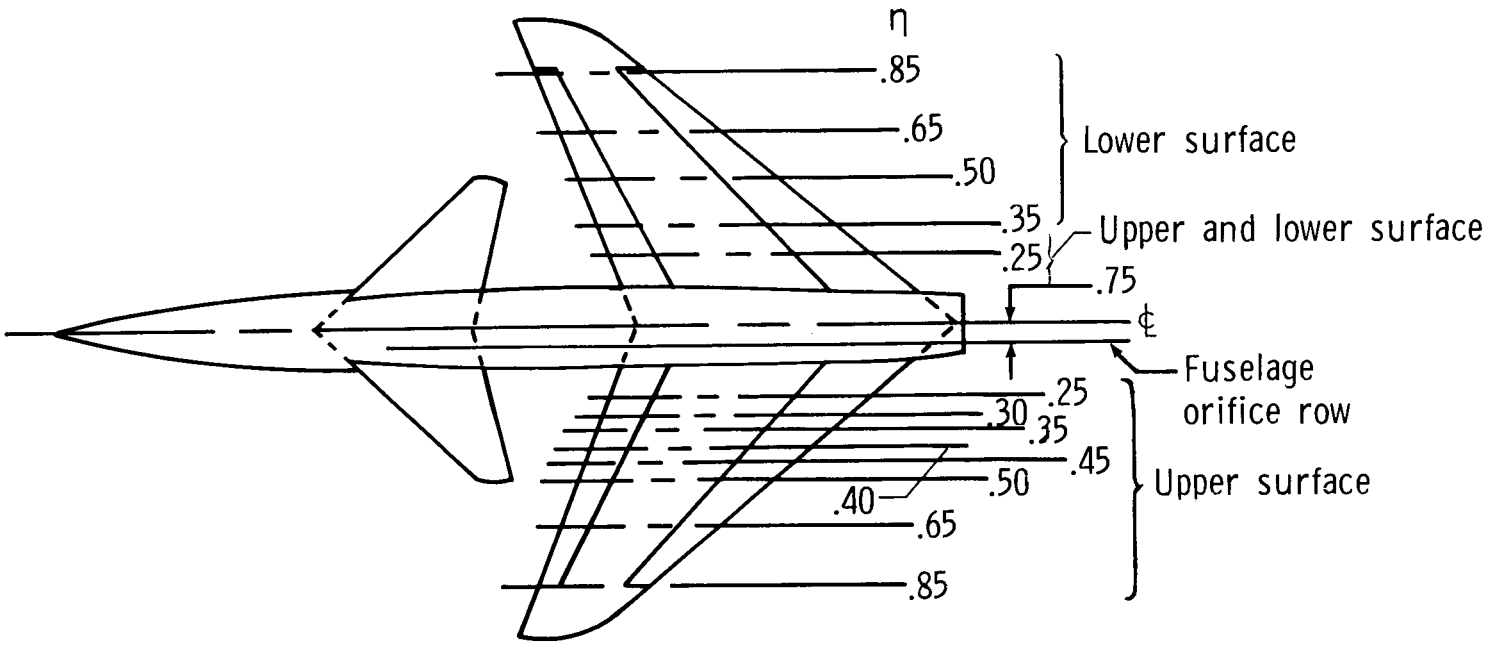


(g) Distribution of streamwise rows of pressure orifices.

Figure 1. Continued.

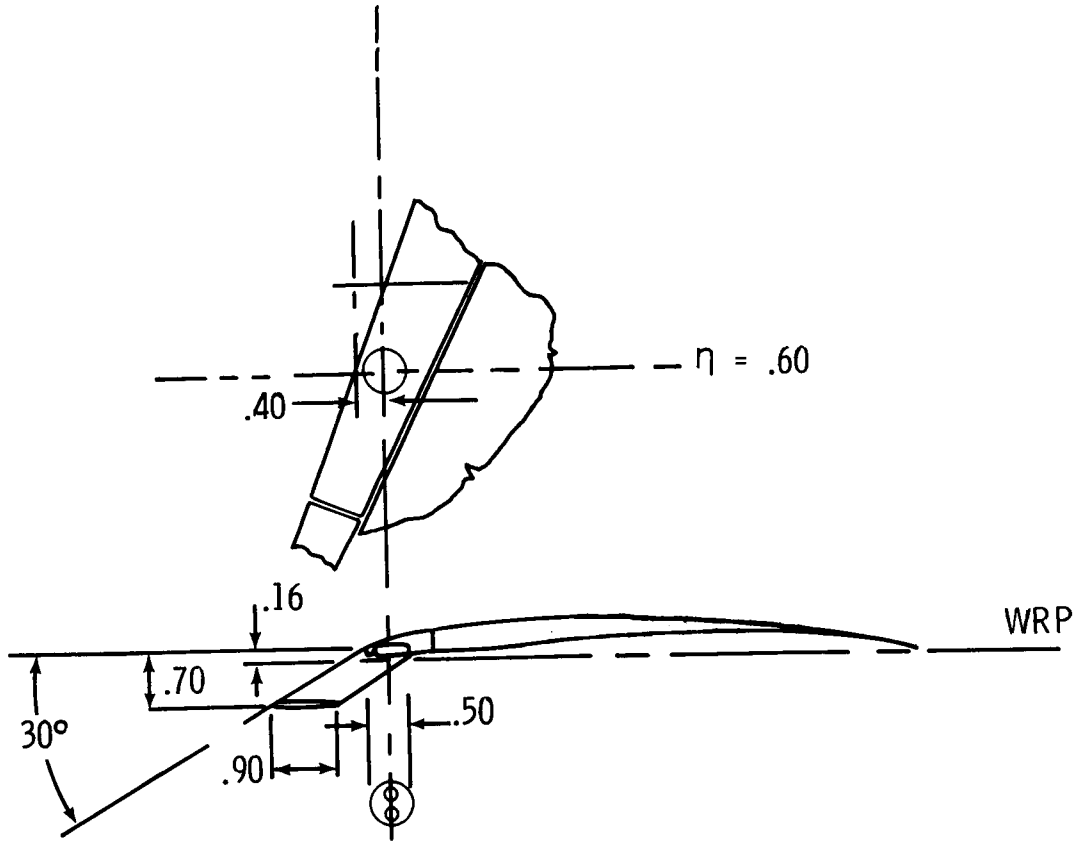


(h) Details of vortex generators.

Figure 1. Concluded.

L-84-6333

(a) Front-quarter bottom view with canard and strakes.

Figure 2. Model mounted in Langley 7- by 10-Foot High-Speed Tunnel.

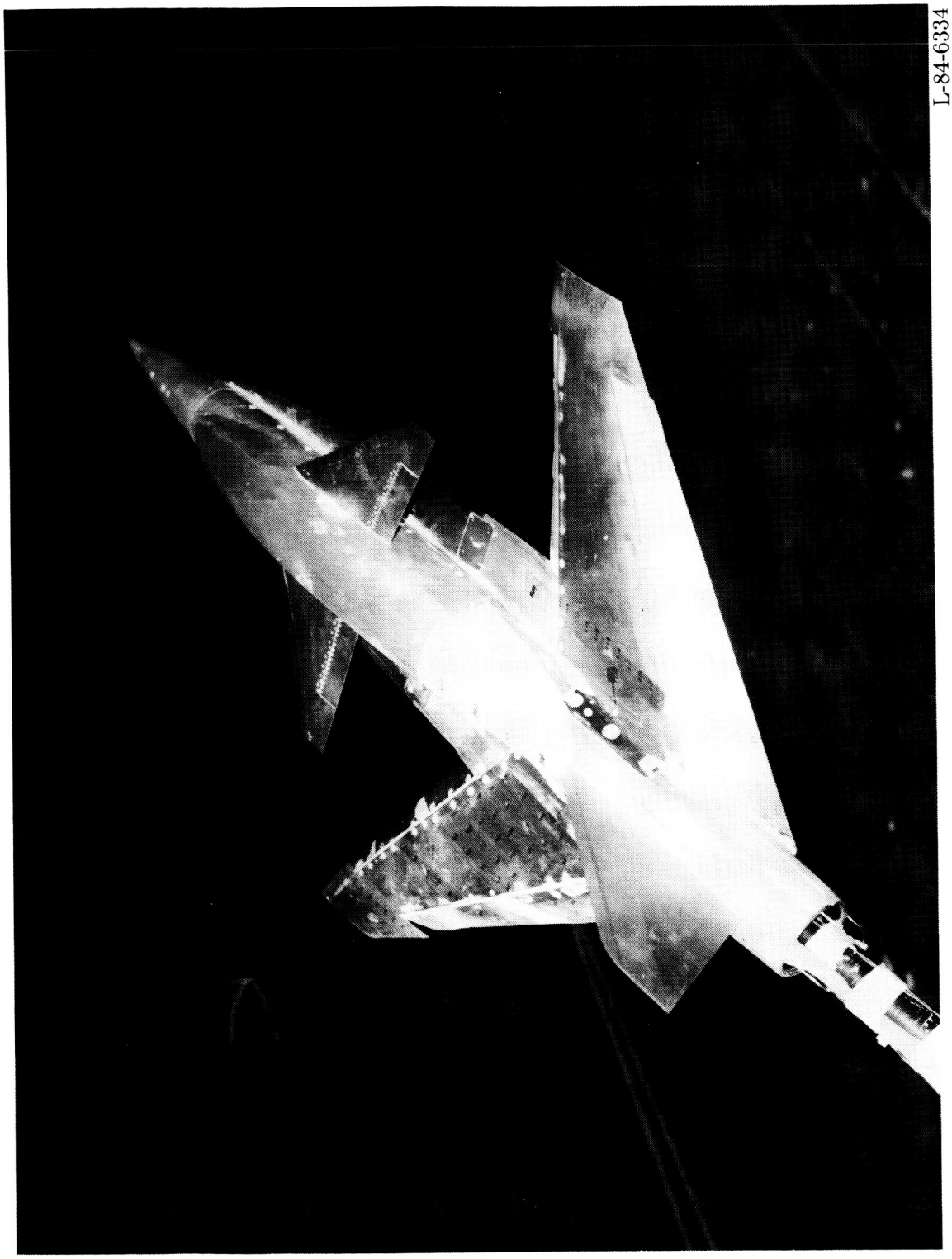

L-84-6334

(b) Rear-quarter top view with canard and strakes.

Figure 2. Continued.

L-83-922

(c) Rear-top view with canard.

Figure 2. Continued.

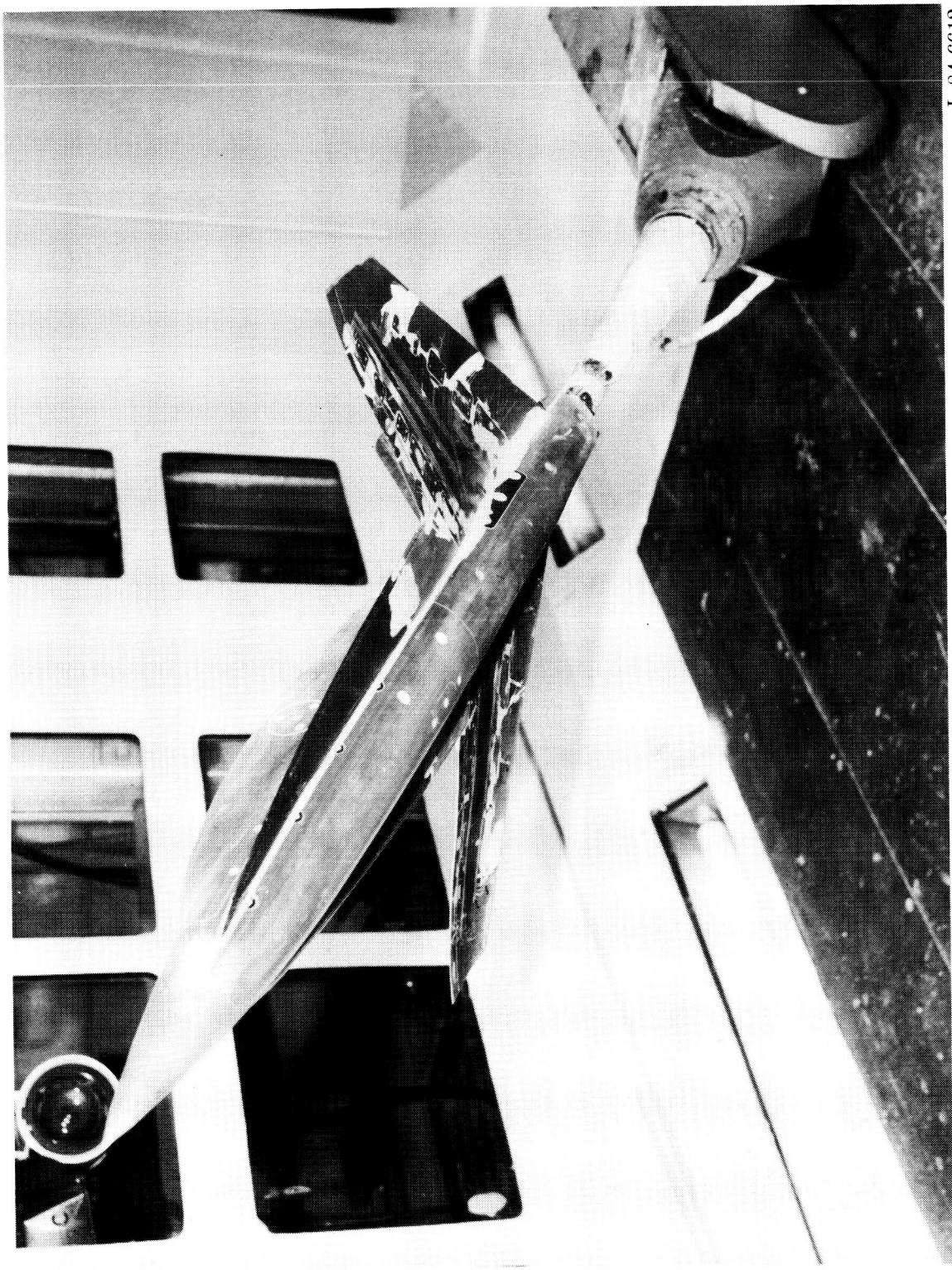

L-84-6612

(d) Front-quarter bottom view with strakes.

Figure 2. Concluded.

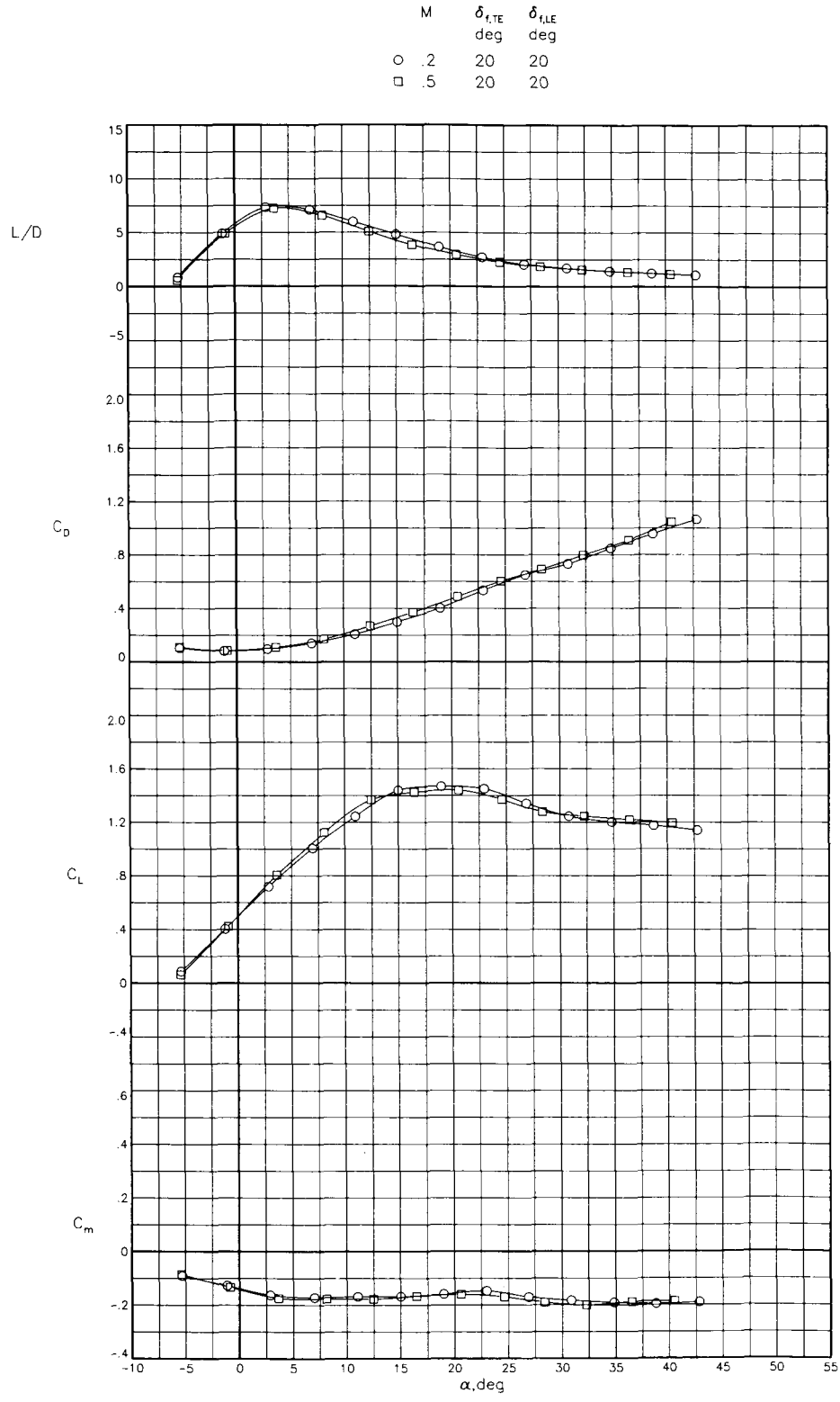


(a) Effect of Mach number on longitudinal characteristics. $\beta = 0°$.

Figure 3. Characteristics of wing-body configuration with canard and strake off. $\delta_{f,\mathrm{LE}} = \delta_{f,\mathrm{TE}} = 20°$.

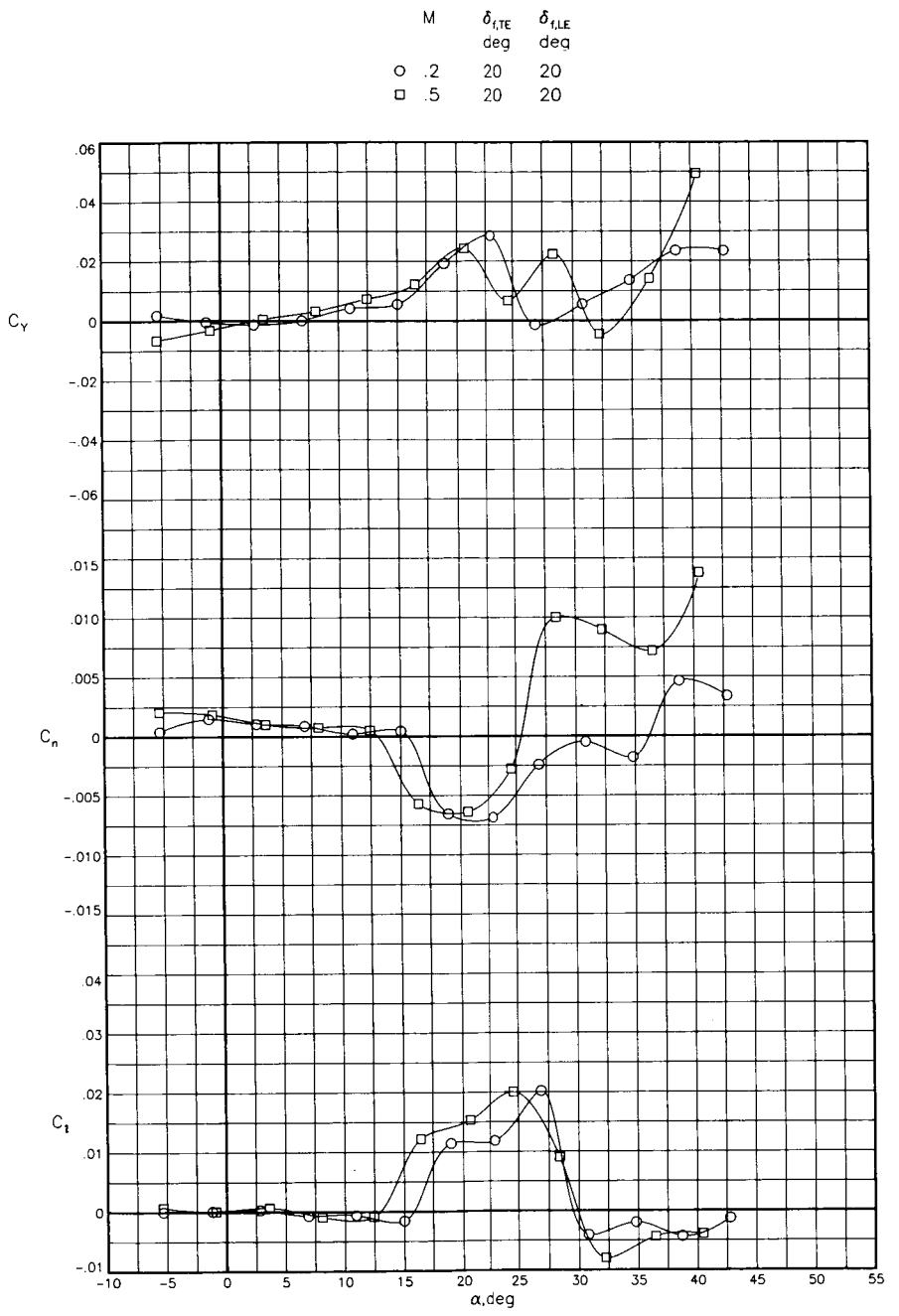


(b) Effect of Mach number on lateral-directional characteristics. $\beta = 0°$.

Figure 3. Continued.

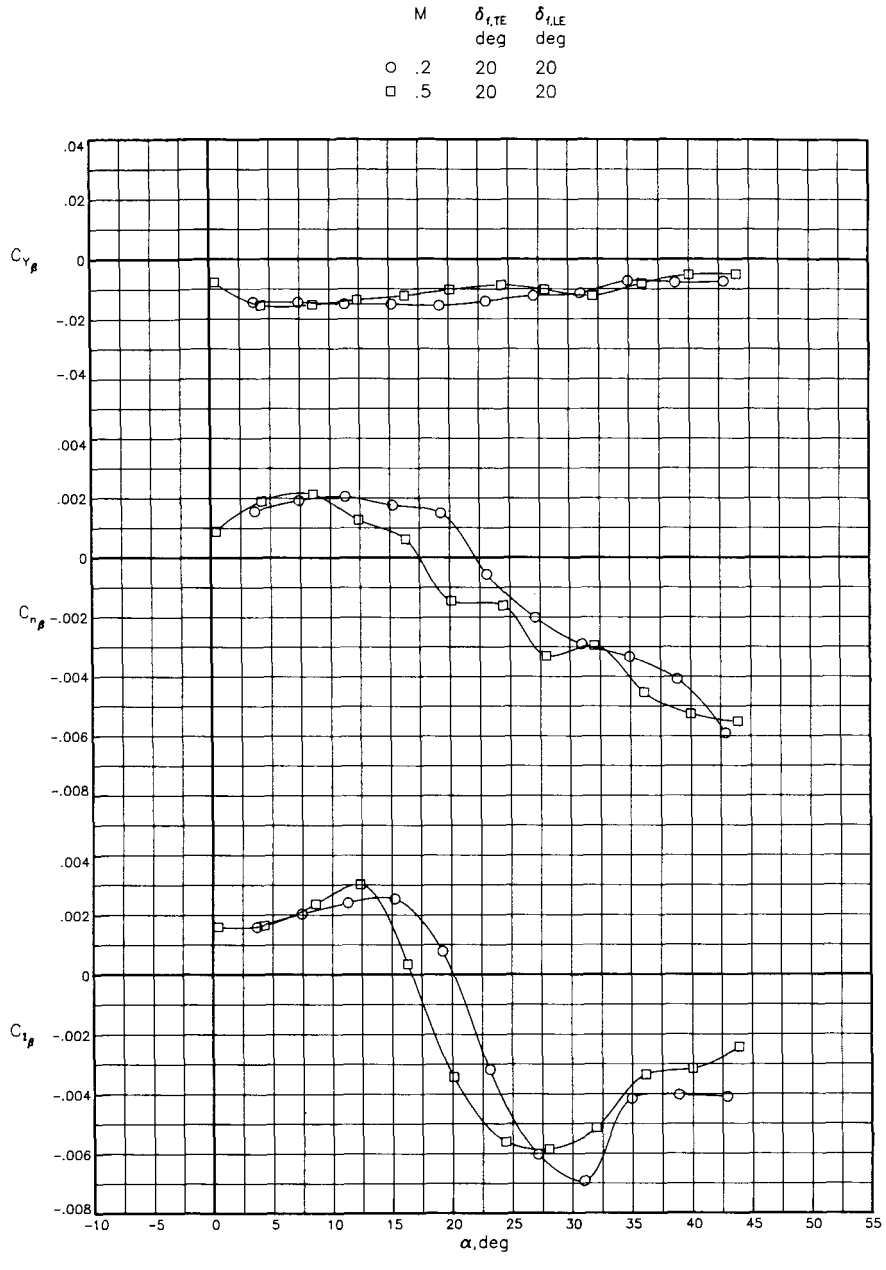


(c) Effect of Mach number on lateral-directional stability.

Figure 3. Continued.

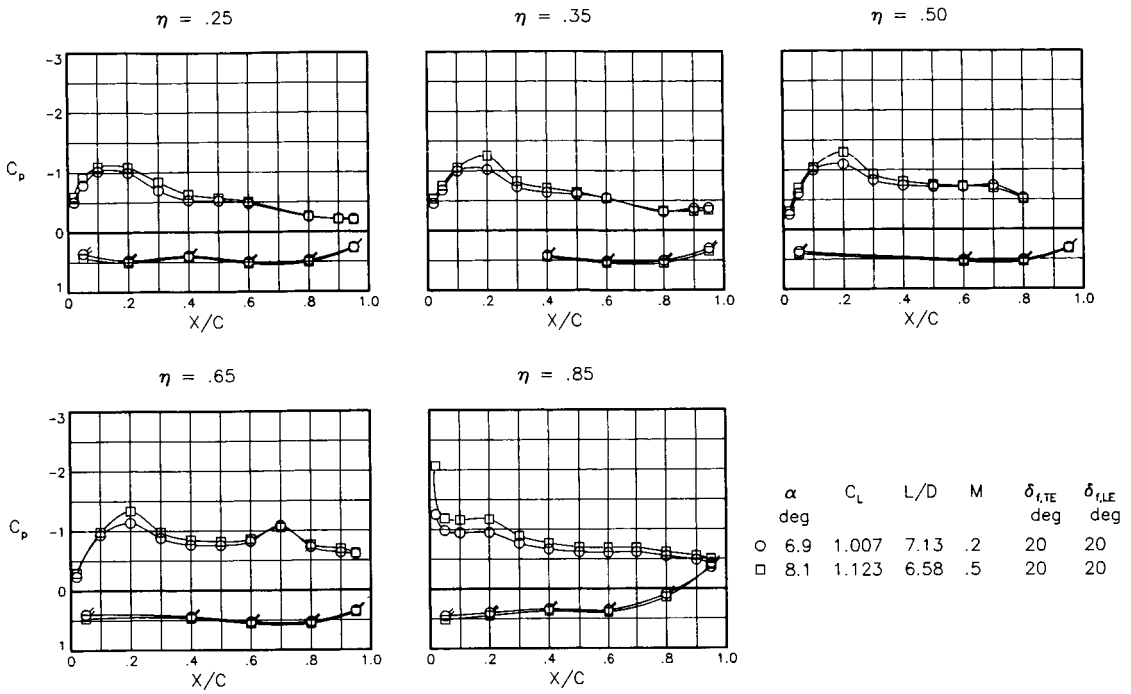


(d) Effect of Mach number on wing pressure distribution for lift coefficient near 1.0. $\beta = 0°$.

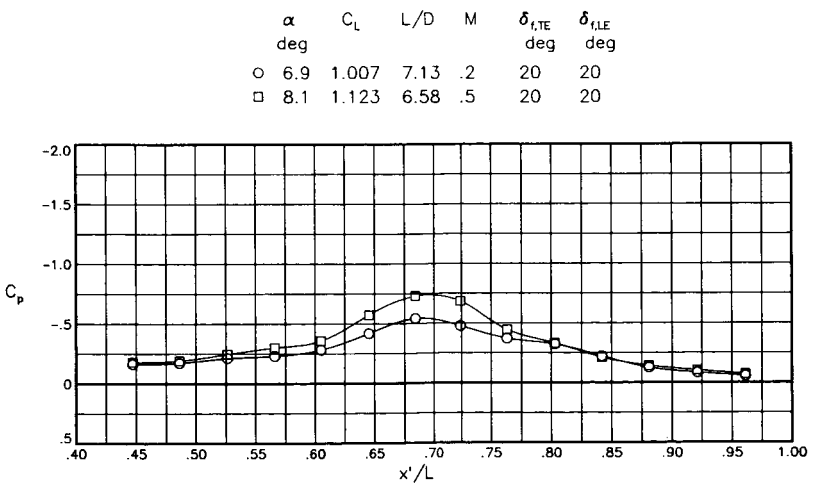


(e) Effect of Mach number on fuselage pressure distribution for lift coefficient near 1.0. $\beta = 0°$.

Figure 3. Continued.

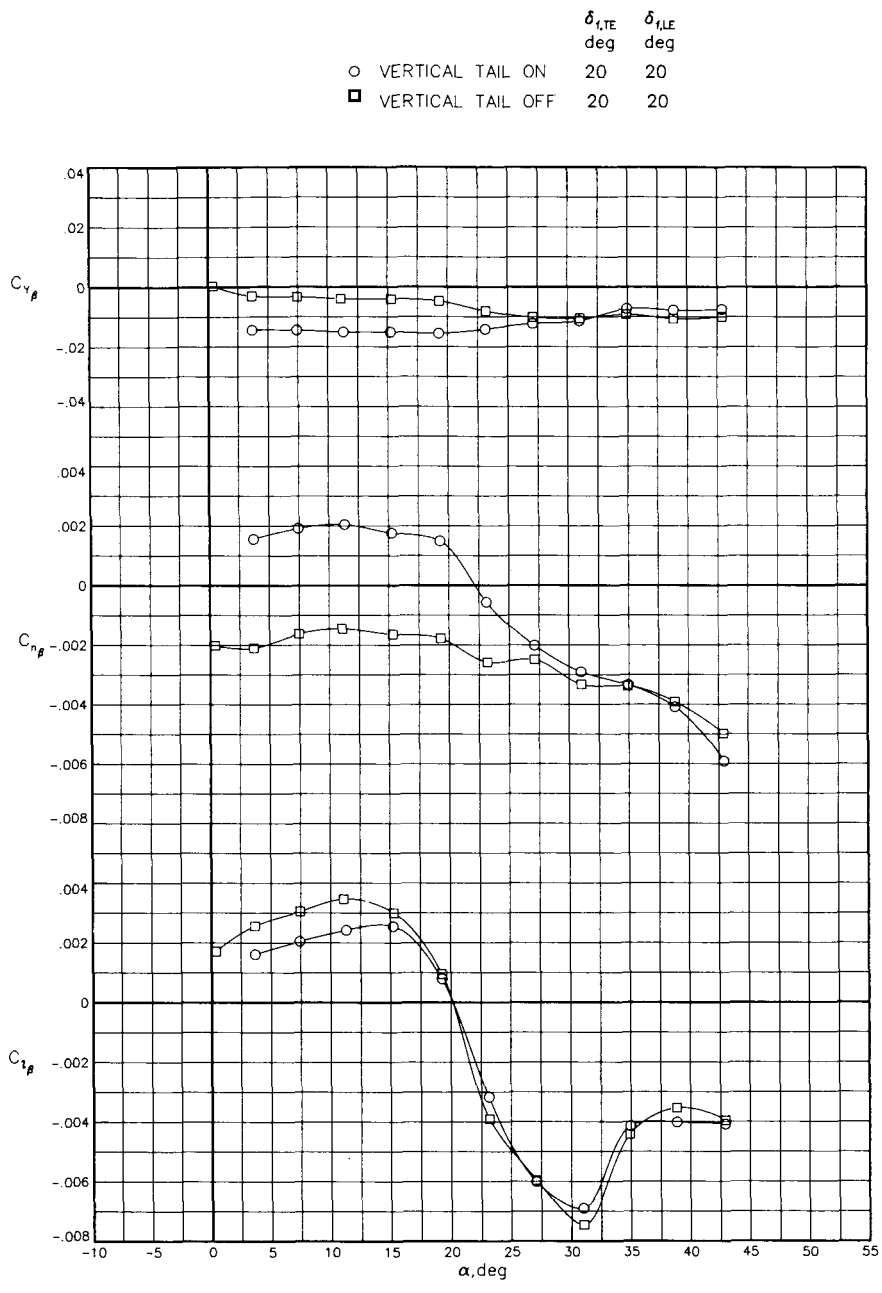


(f) Effect of vertical tail on lateral-directional stability. $M = 0.2$.

Figure 3. Continued.

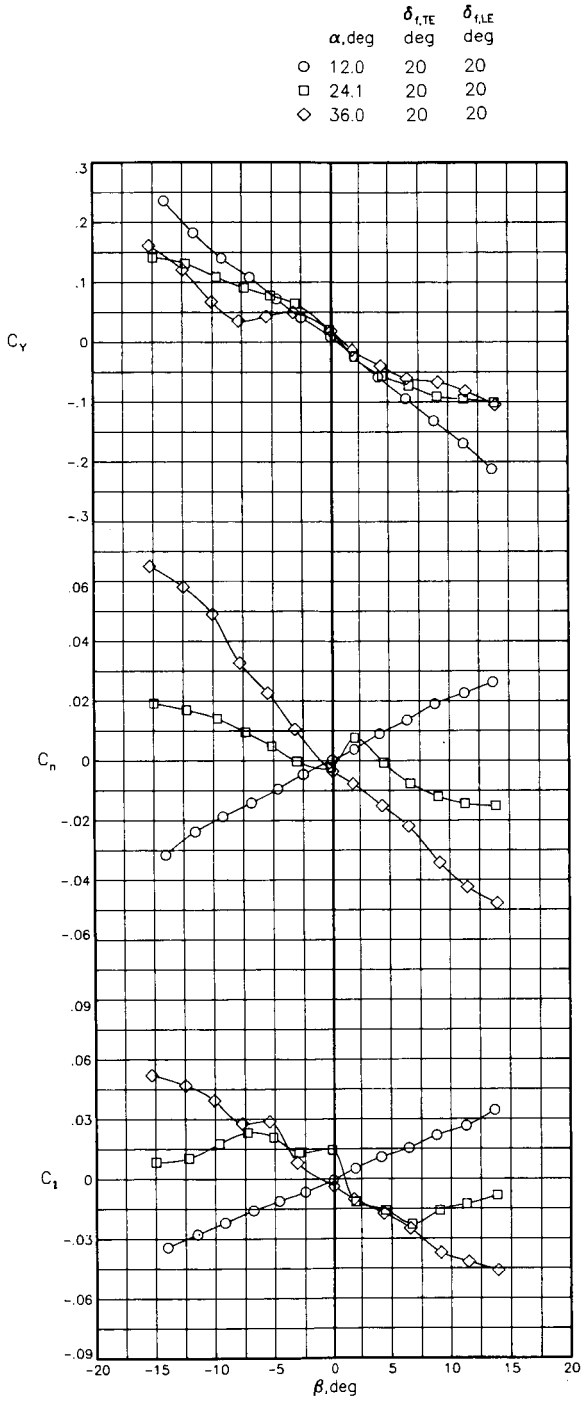


(g) Effect of angle of sideslip on lateral-directional characteristics. $M = 0.2$.

Figure 3. Concluded.

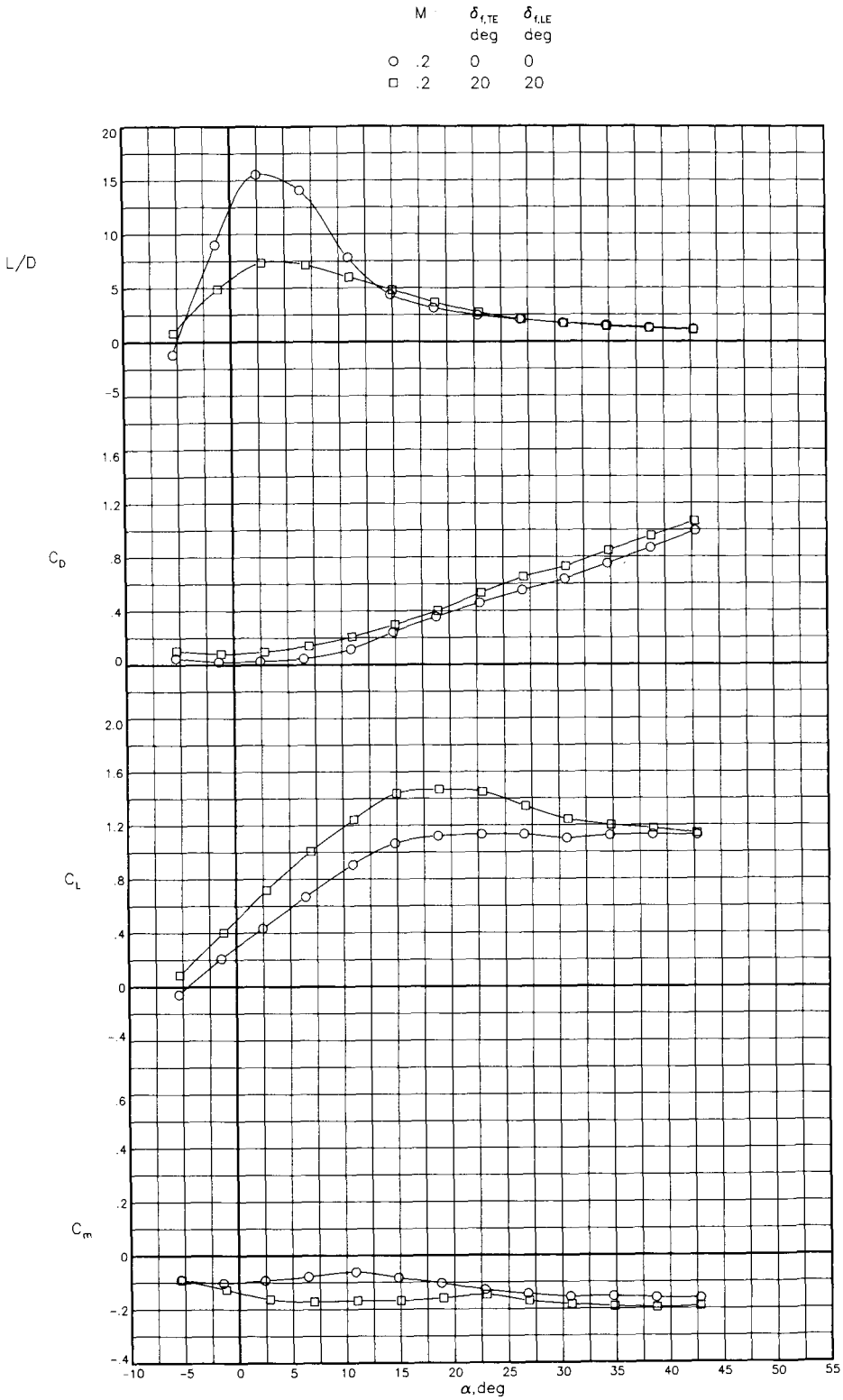


(a) Longitudinal characteristics. $\beta = 0°$.

Figure 4. Effects of leading- and trailing-edge flaps on wing-body configuration with canard and strake off. $M = 0.2$.

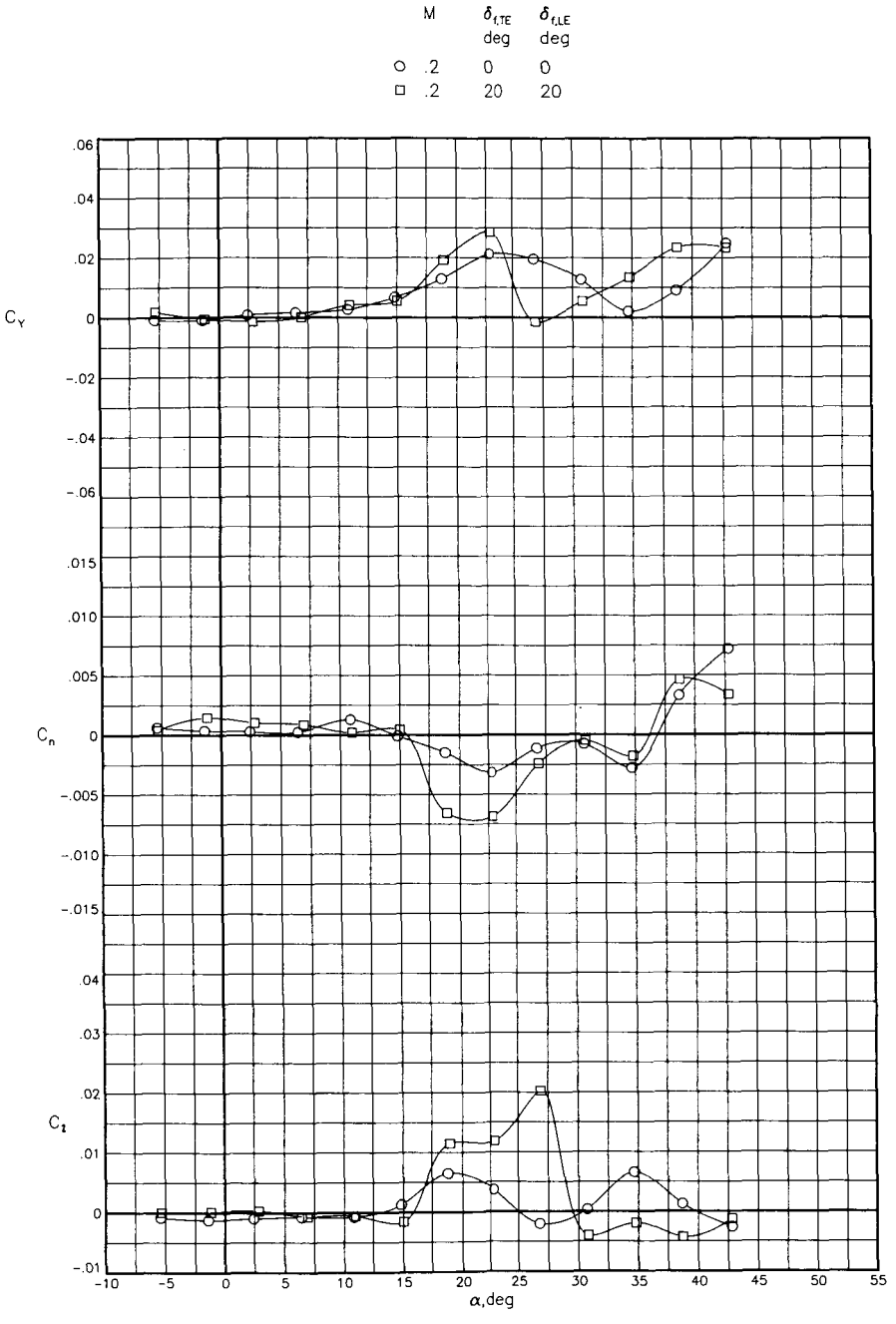


(b) Lateral-directional characteristics. $\beta = 0°$.

Figure 4. Continued.

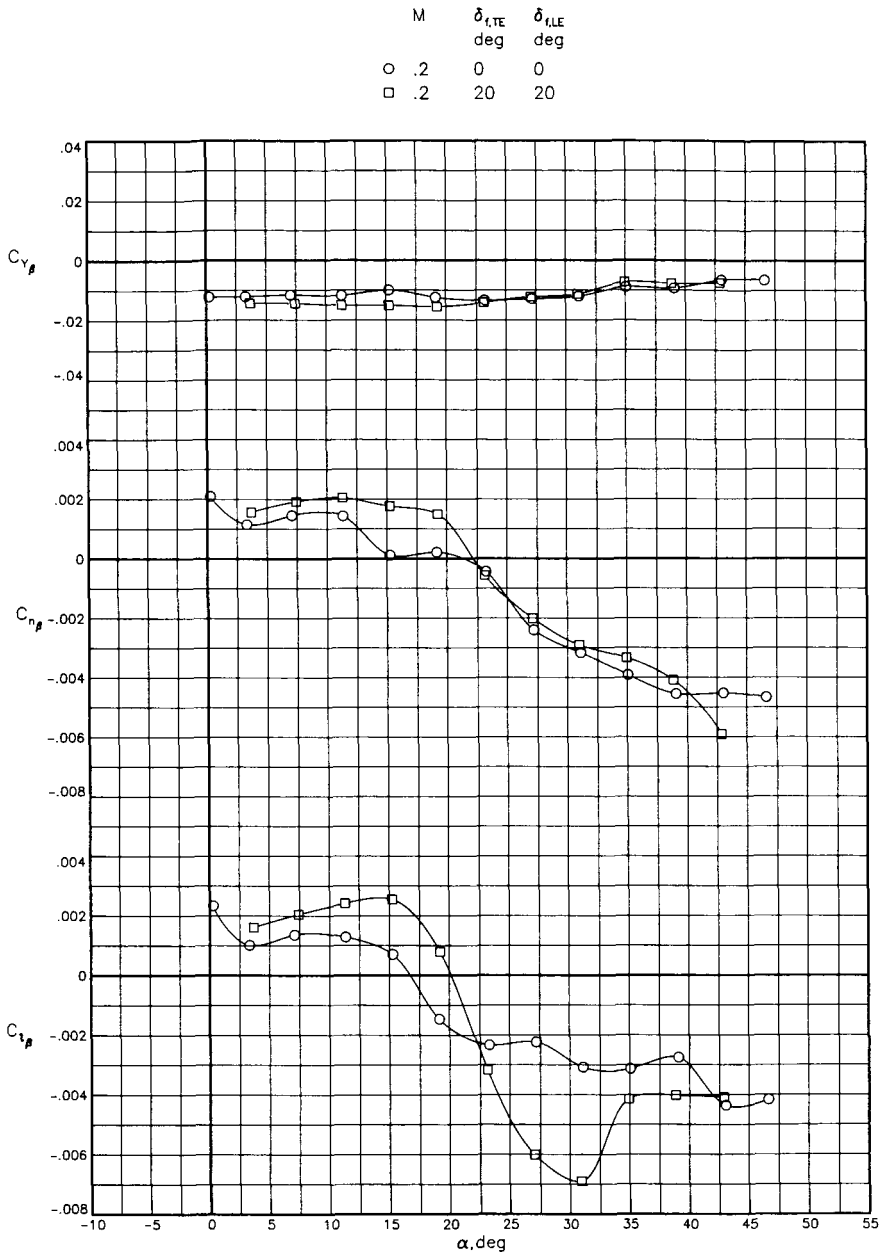


(c) Lateral-directional stability.

Figure 4. Continued.

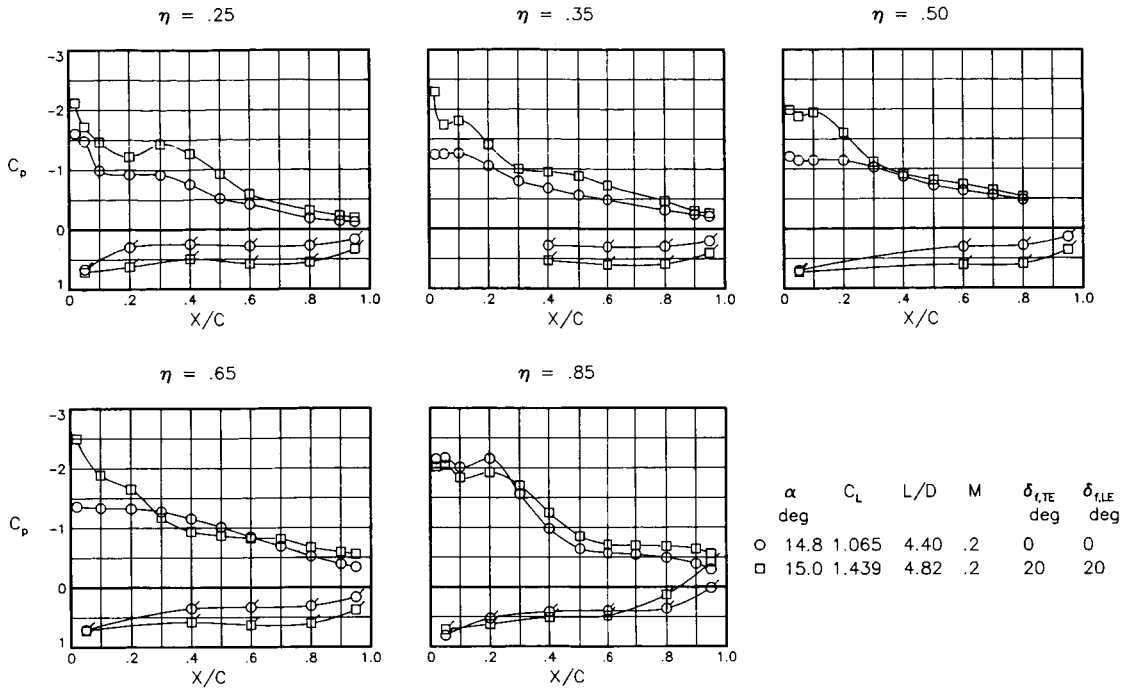


(d) Wing pressure distributions. $\alpha = 15°; \beta = 0°$.

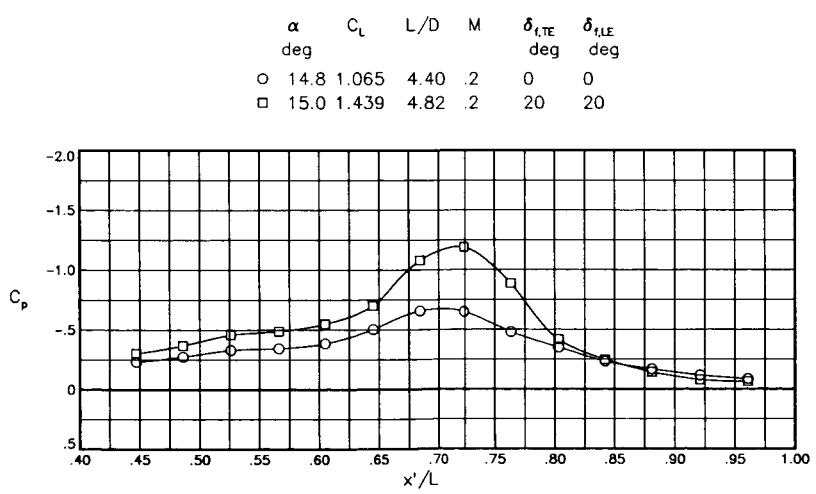


(e) Fuselage pressure distributions. $\alpha = 15°; \beta = 0°$.

Figure 4. Concluded.

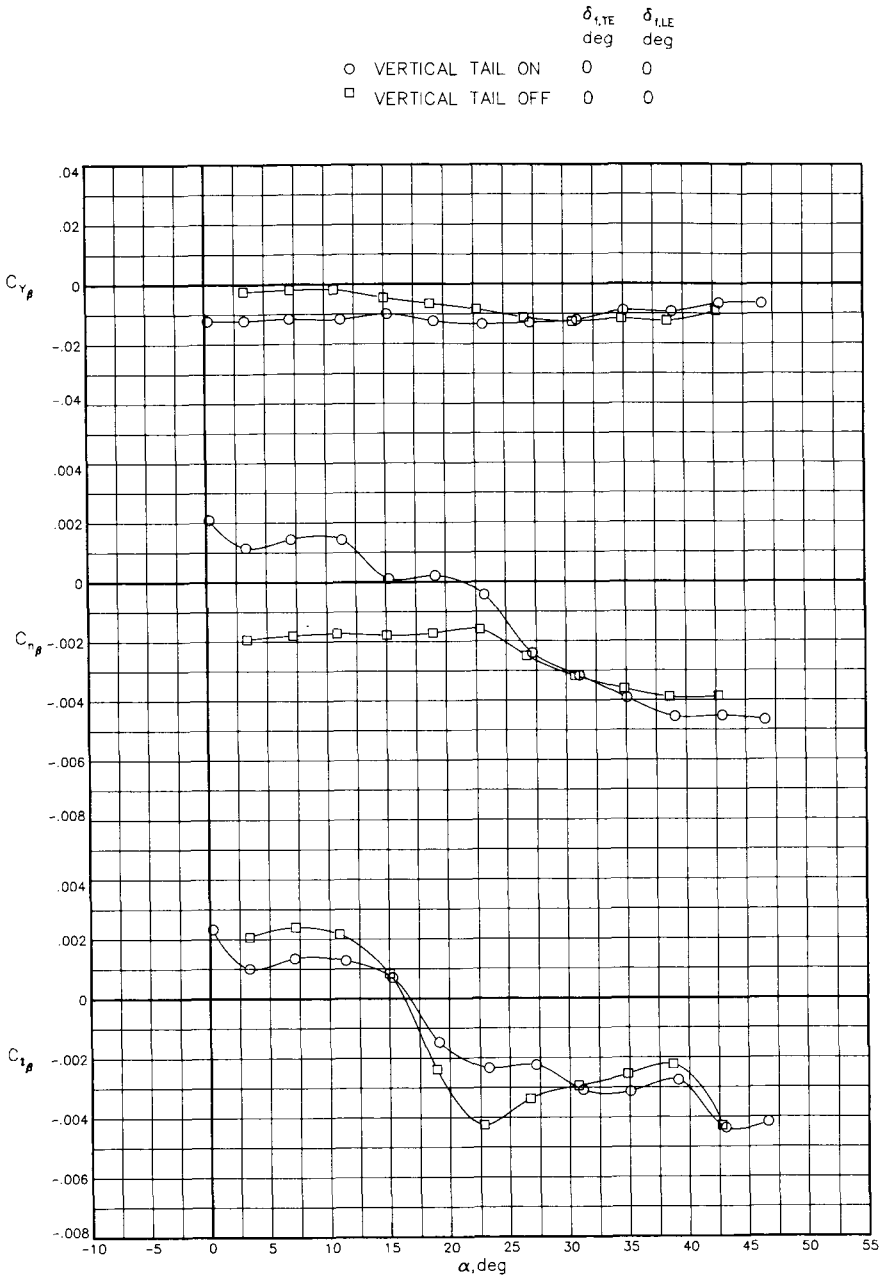


Figure 5. Effects of vertical tail on lateral-directional stability for wing-body configuration with canard and strake off. $\delta_{f,\mathrm{LE}} = \delta_{f,\mathrm{TE}} = 0°$; $M = 0.2$.

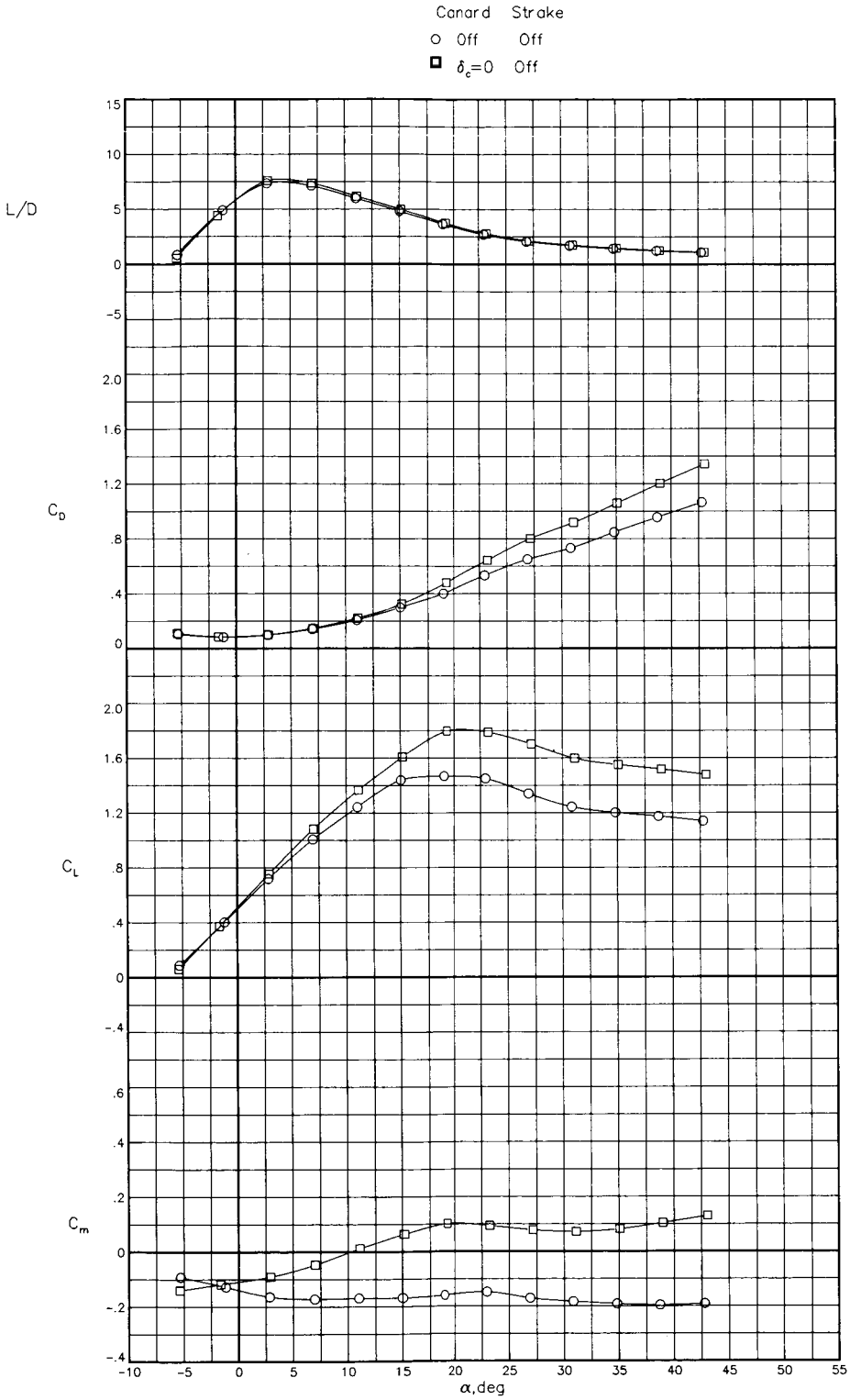


(a) Longitudinal characteristics for $M = 0.2$. $\beta = 0°$.

Figure 6. Effects of canard with strake off. $\delta_{f,\mathrm{LE}} = \delta_{f,\mathrm{TE}} = 20°$; $\delta_c = 0°$.

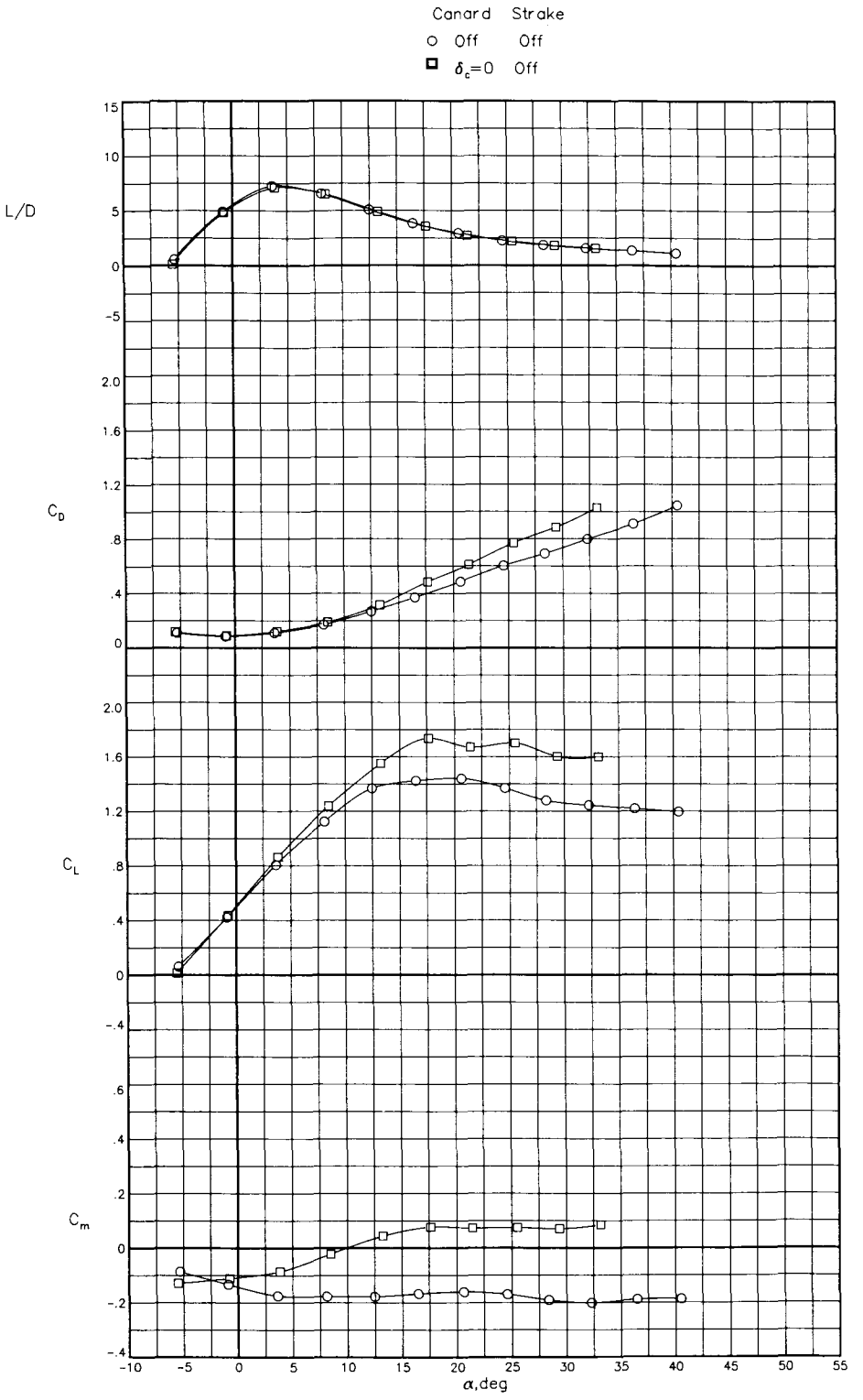


(b) Longitudinal characteristics for $M = 0.5$. $\beta = 0°$.

Figure 6. Continued.

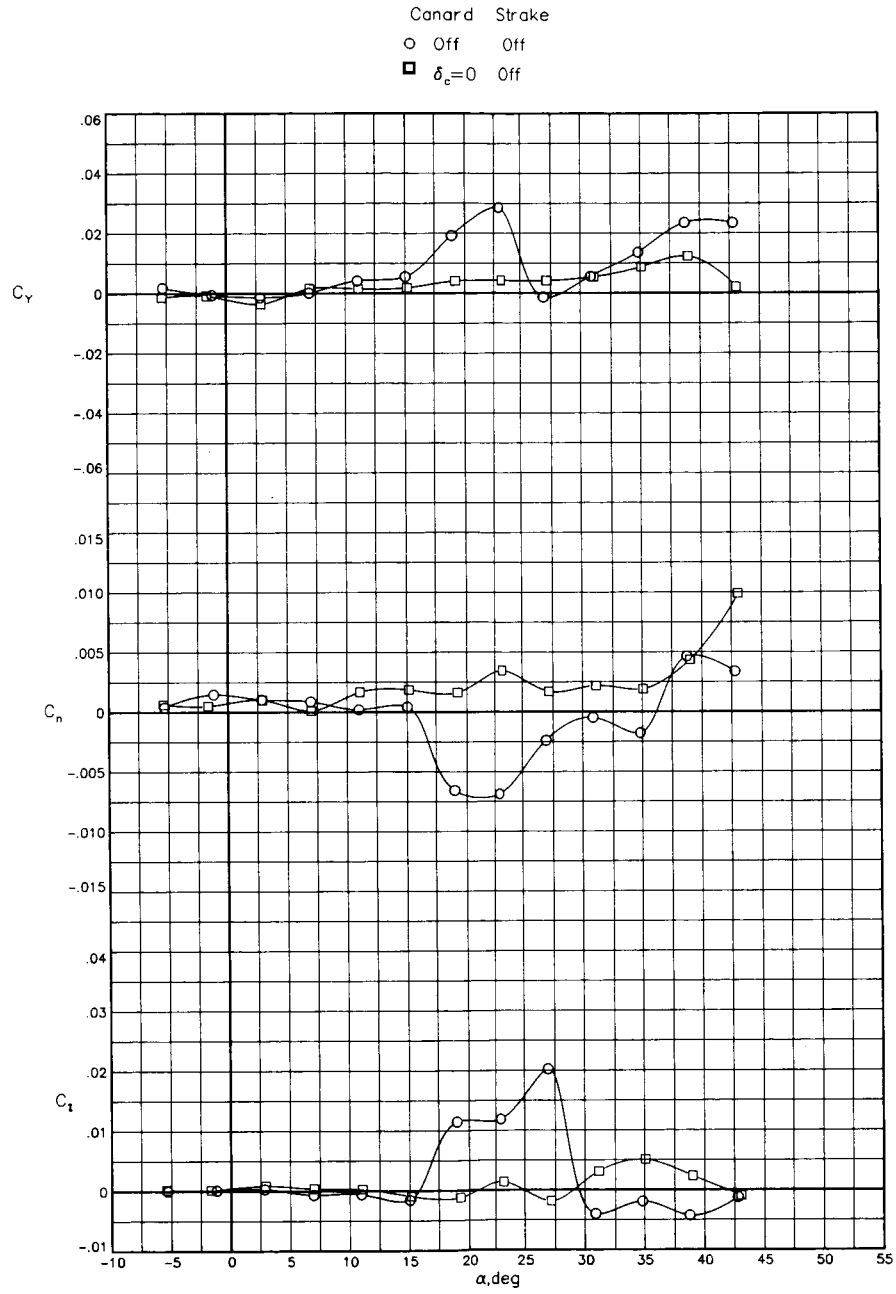


(c) Lateral-directional characteristics for $M = 0.2$. $\beta = 0°$.

Figure 6. Continued.

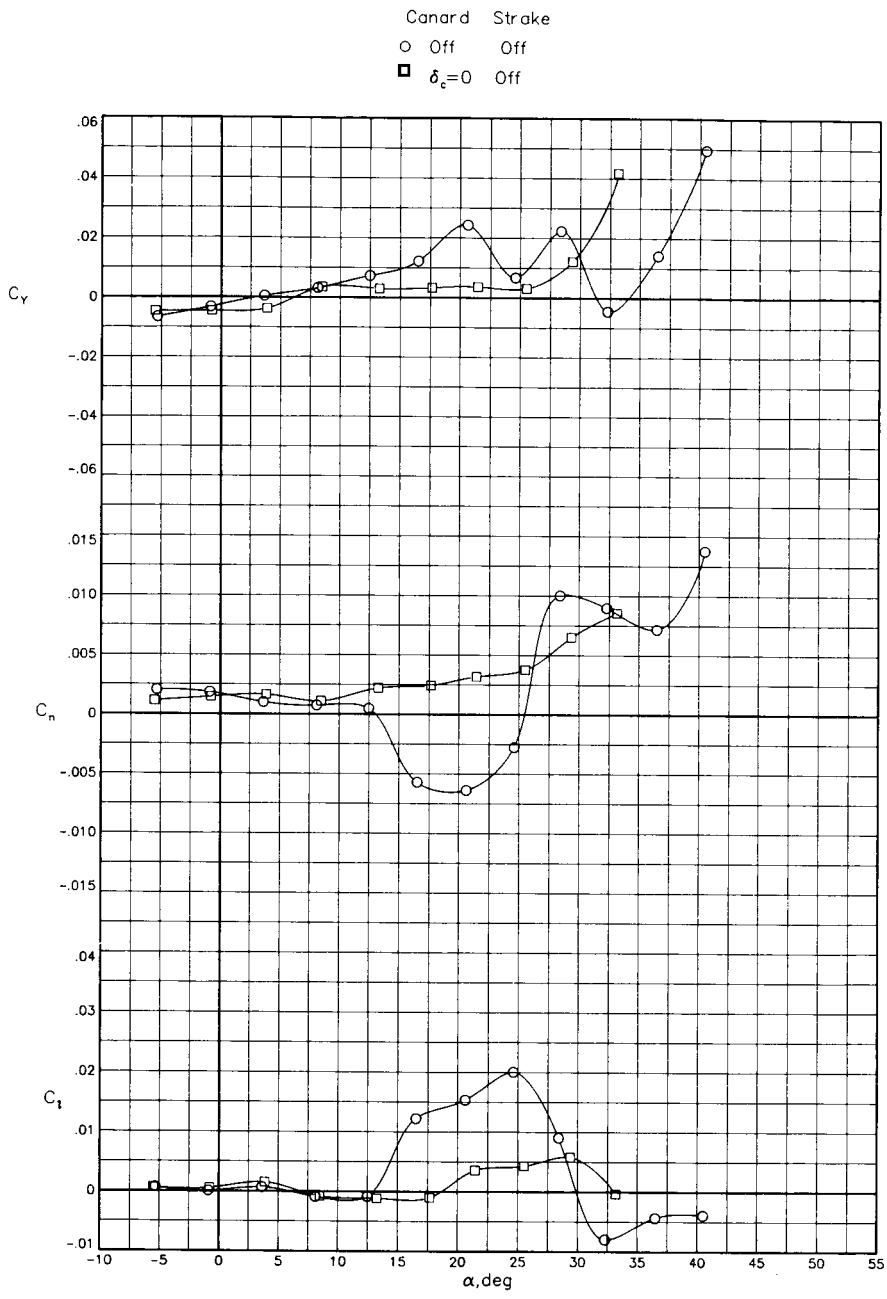


(d) Lateral-directional characteristics for $M = 0.5$. $\beta = 0°$.

Figure 6. Continued.

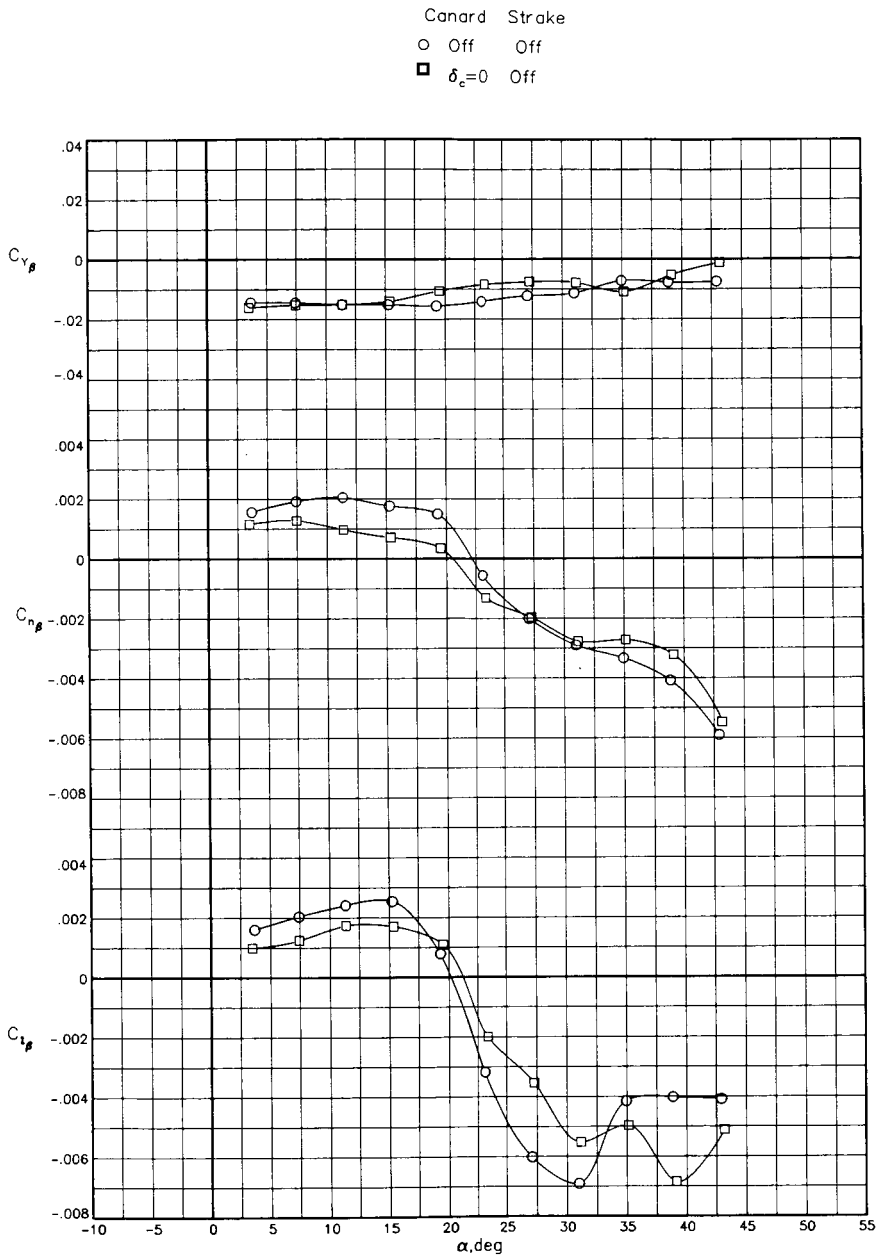


(e) Lateral-directional stability for $M = 0.2$.

Figure 6. Continued.

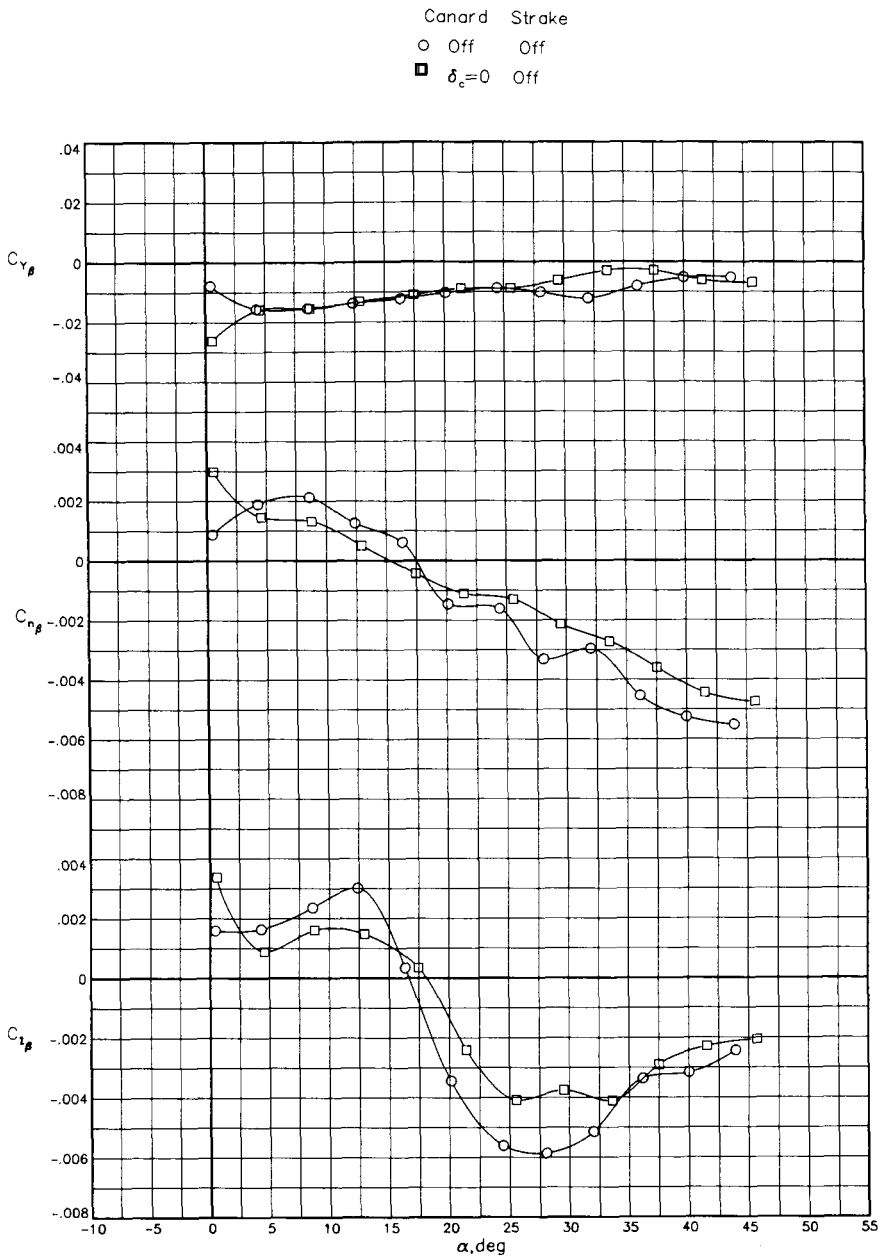


(f) Lateral-directional stability for $M = 0.5$.

Figure 6. Continued.

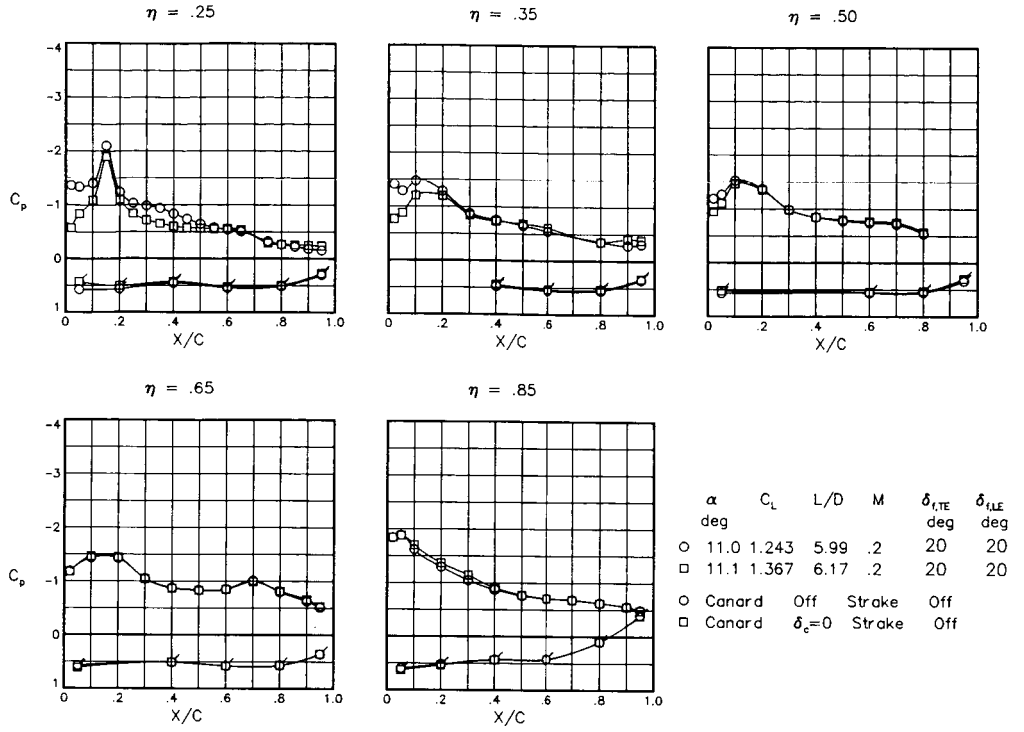


(g) Wing pressure distributions for $M = 0.2$. $\alpha \approx 11°; \beta = 0°$.

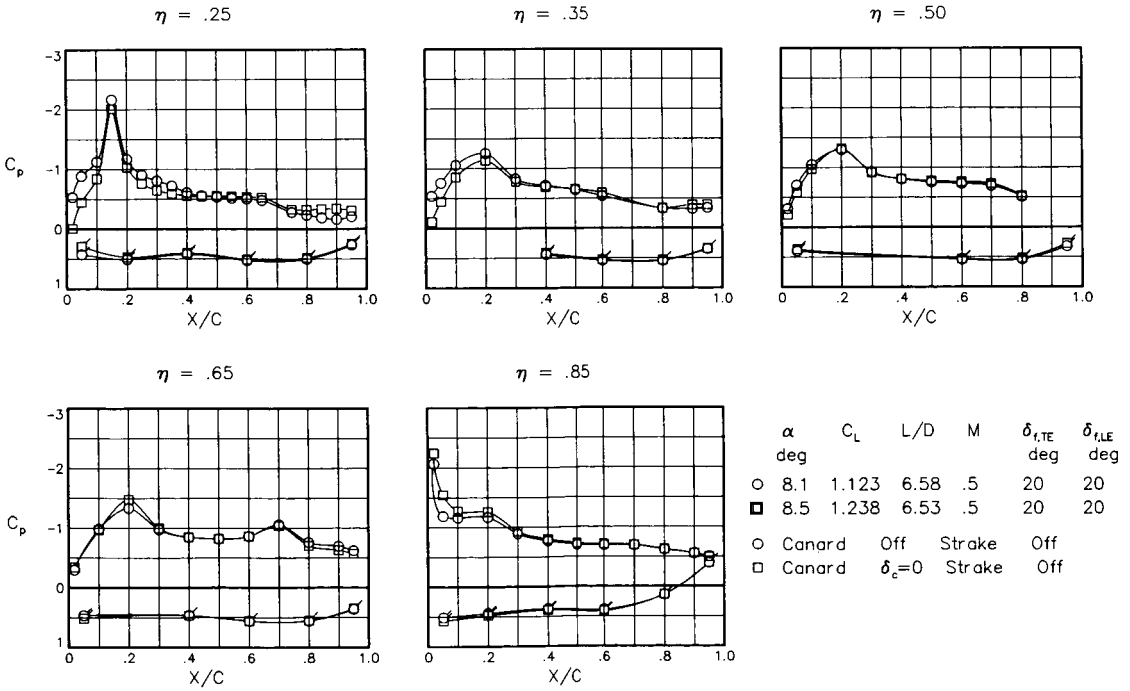


(h) Wing pressure distributions for $M = 0.5$. $\alpha \approx 8°; \beta = 0°$.

Figure 6. Continued.

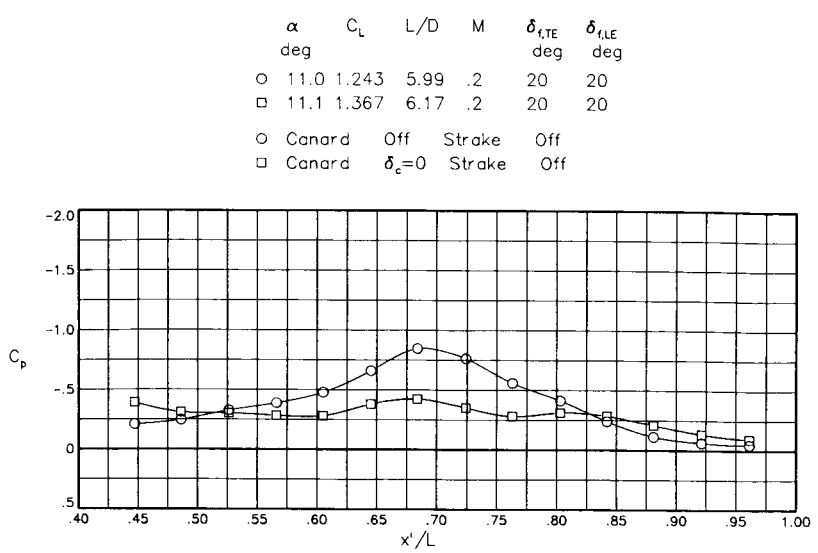


(i) Fuselage pressure distributions for $M = 0.2$. $\alpha \approx 11°; \beta = 0°$.

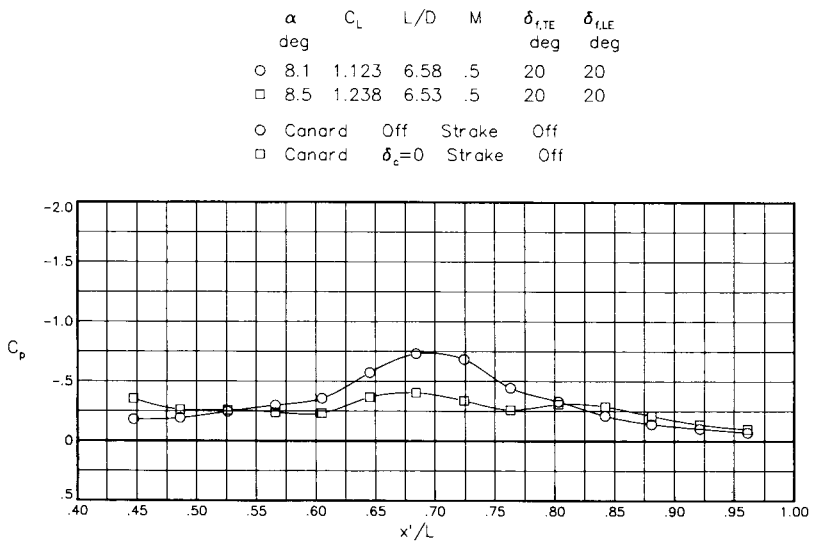


(j) Fuselage pressure distributions for $M = 0.5$. $\alpha \approx 8°; \beta = 0°$.

Figure 6. Continued.

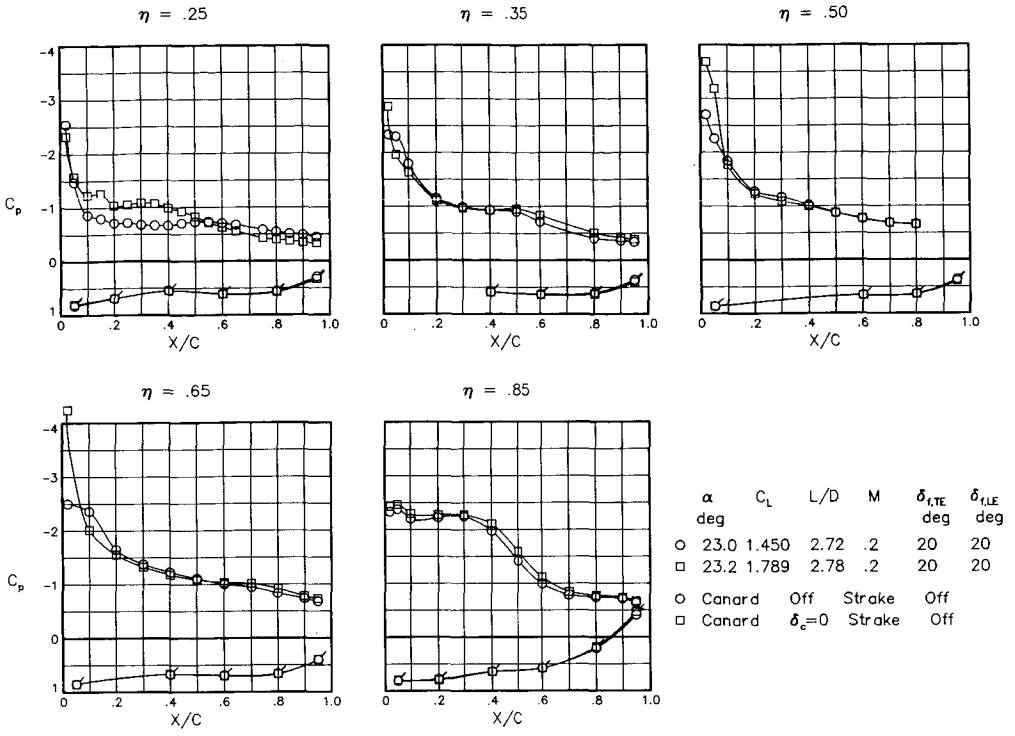


(k) Wing pressure distributions for $M = 0.2$. $\alpha \approx 23°; \beta = 0°$.

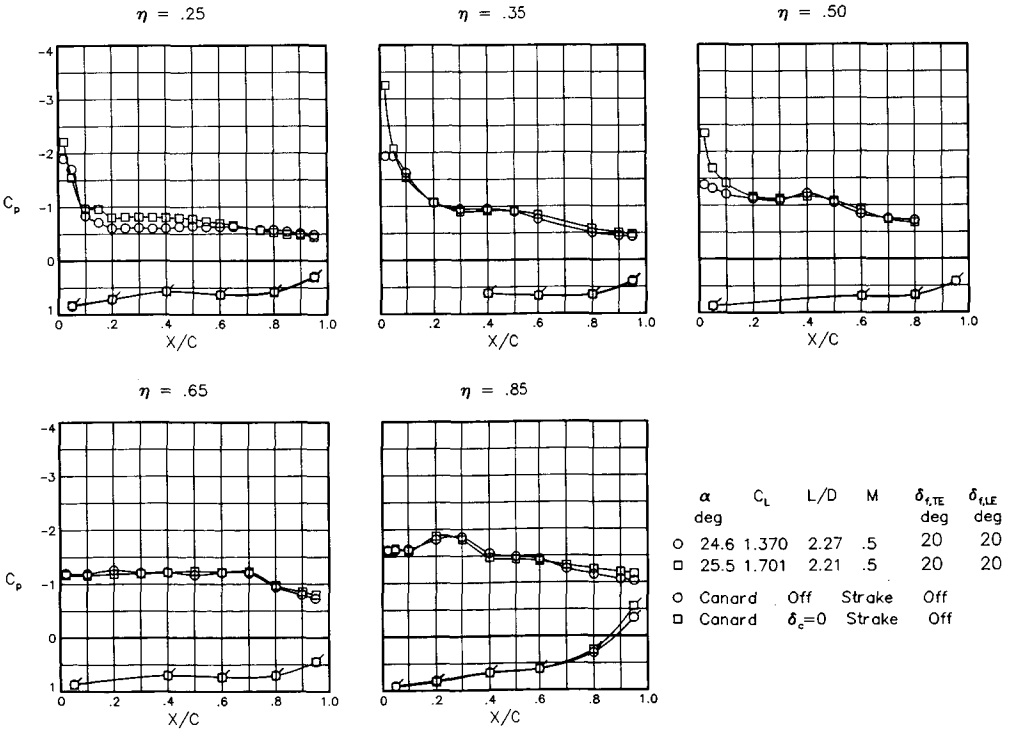


(l) Wing pressure distributions for $M = 0.5$. $\alpha \approx 25°; \beta = 0°$.

Figure 6. Continued.

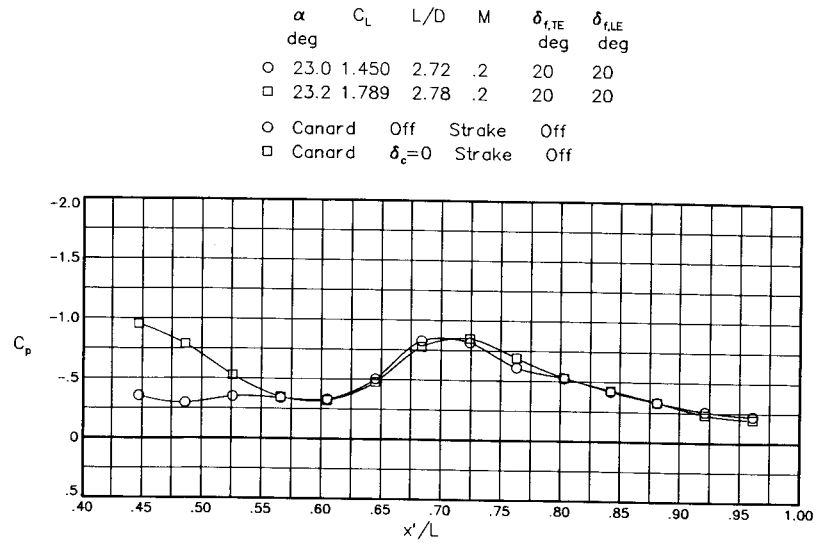


(m) Fuselage pressure distributions for $M = 0.2$. $\alpha \approx 23°; \beta = 0°$.

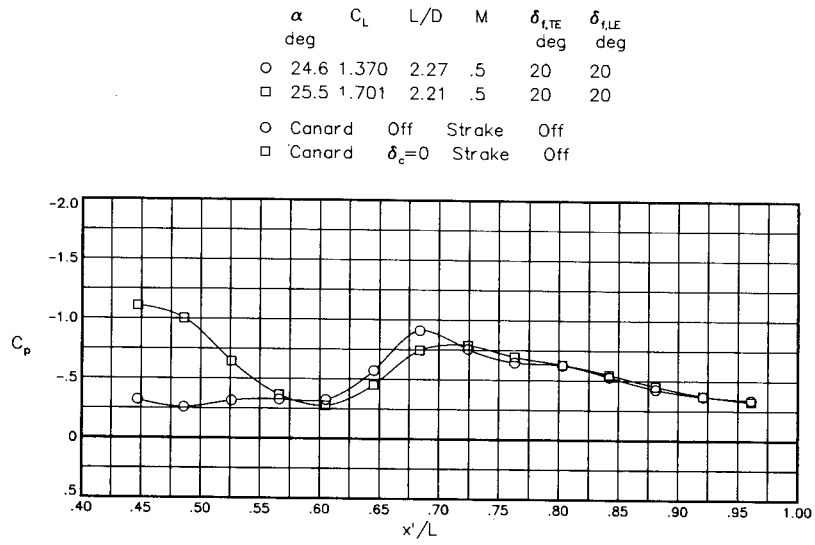


(n) Fuselage pressure distributions for $M = 0.5$. $\alpha \approx 25°; \beta = 0°$.

Figure 6. Continued.

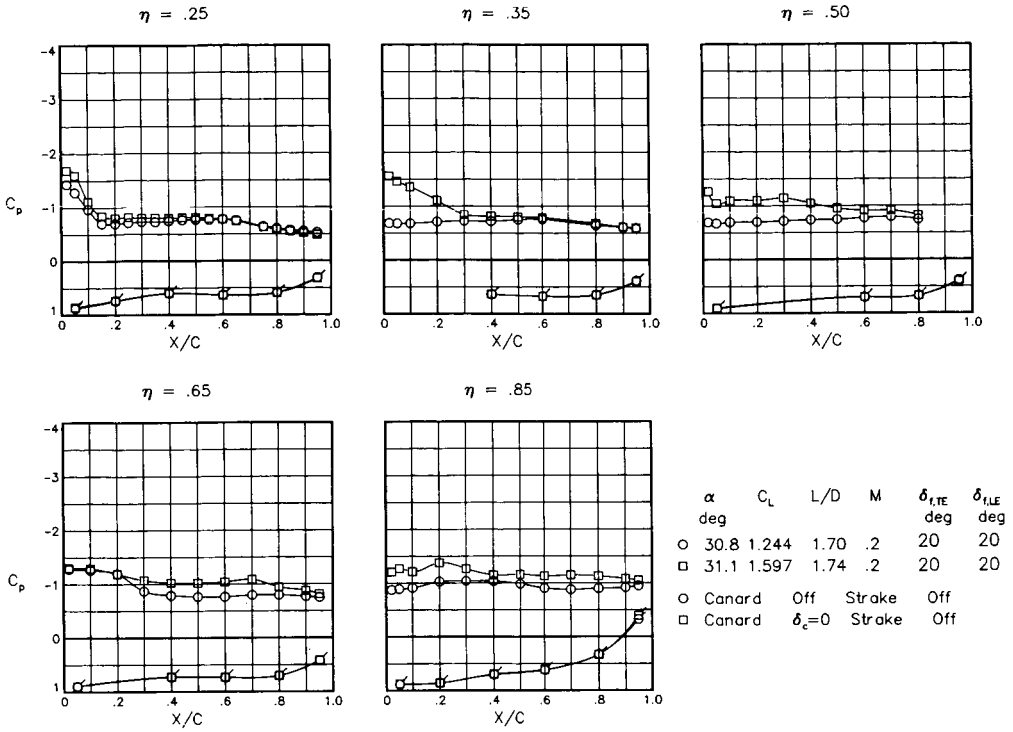


(o) Wing pressure distributions for $M = 0.2$. $\alpha \approx 31°; \beta = 0°$.

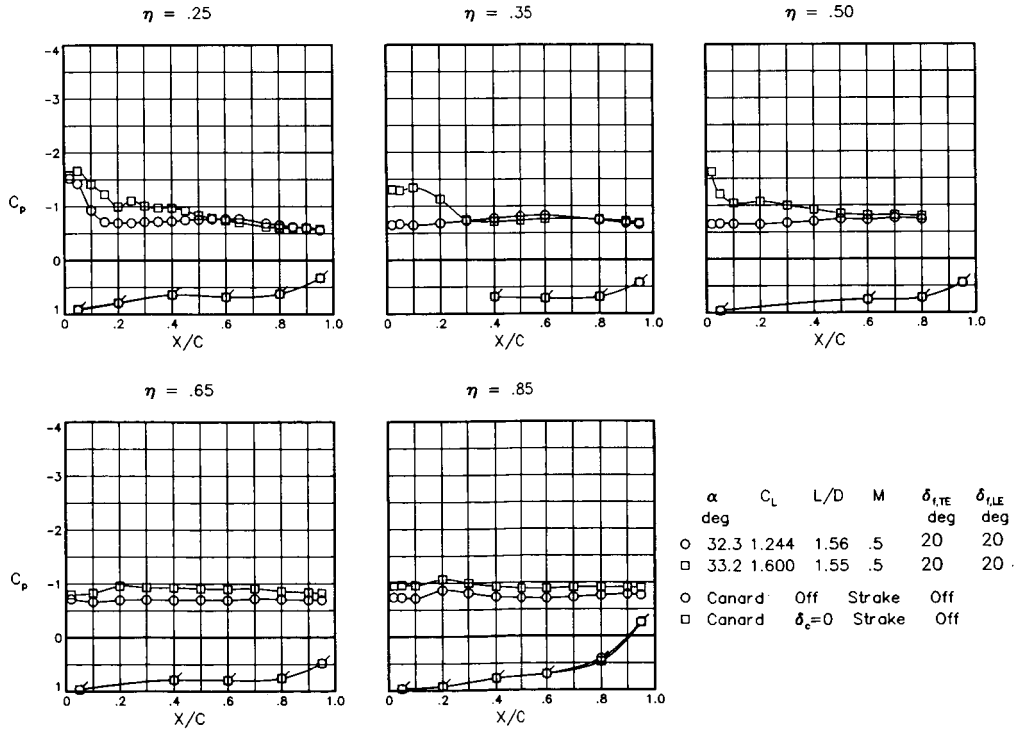


(p) Wing pressure distributions for $M = 0.5$. $\alpha \approx 32°; \beta = 0°$.

Figure 6. Continued.

| | $\alpha$ deg | $C_L$ | L/D | M | $\delta_{f,TE}$ deg | $\delta_{f,LE}$ deg |
|---|---|---|---|---|---|---|
| ○ | 30.8 | 1.244 | 1.70 | .2 | 20 | 20 |
| □ | 31.1 | 1.597 | 1.74 | .2 | 20 | 20 |

○ Canard Off Strake Off
□ Canard $\delta_c$=0 Strake Off

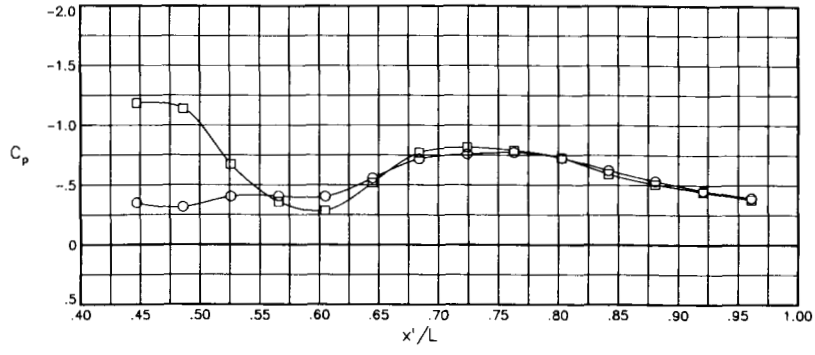


(q) Fuselage pressure distributions for $M = 0.2$. $\alpha \approx 31°; \beta = 0°$.

| | $\alpha$ deg | $C_L$ | L/D | M | $\delta_{f,TE}$ deg | $\delta_{f,LE}$ deg |
|---|---|---|---|---|---|---|
| ○ | 32.3 | 1.244 | 1.56 | .5 | 20 | 20 |
| □ | 33.2 | 1.600 | 1.55 | .5 | 20 | 20 |

○ Canard Off Strake Off
□ Canard $\delta_c$=0 Strake Off

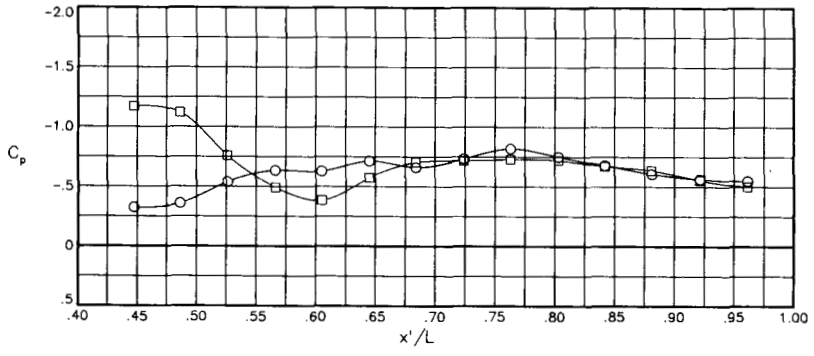


(r) Fuselage pressure distributions for $M = 0.5$. $\alpha \approx 32°; \beta = 0°$.

Figure 6. Continued.

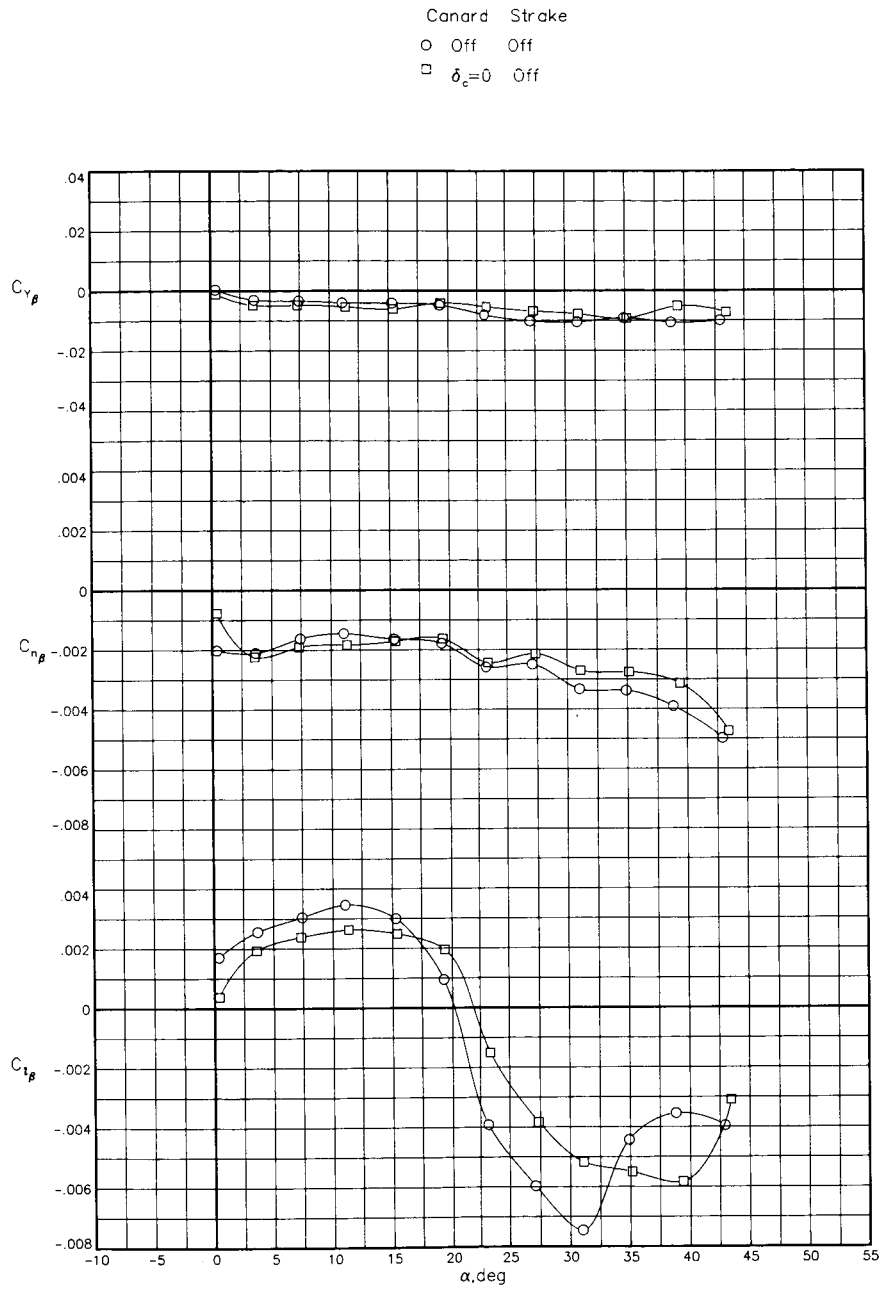


(s) Lateral-directional stability with vertical tail off. $M = 0.2$.

Figure 6. Concluded.

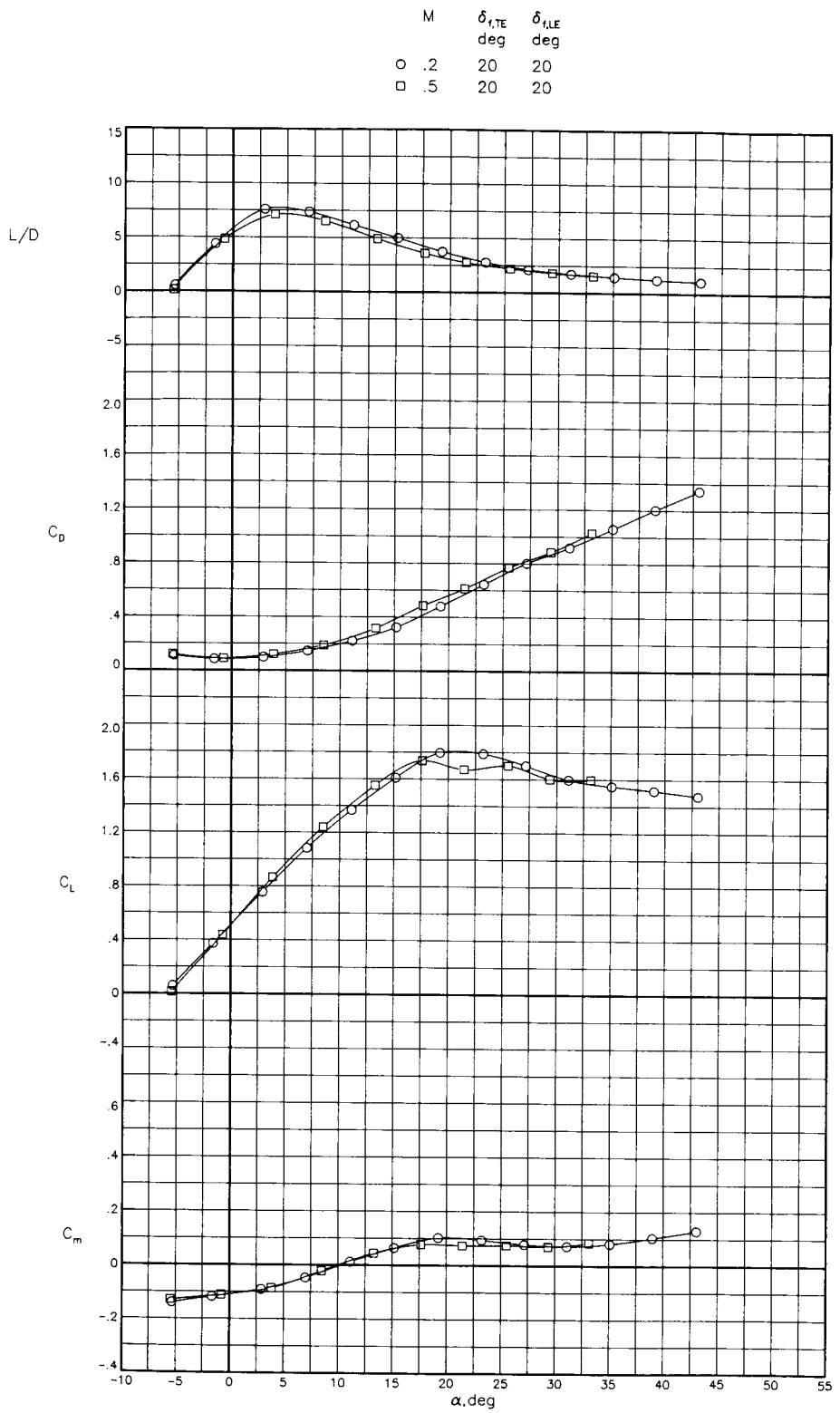


(a) Effect of Mach number on longitudinal characteristics. $\beta = 0°$.

Figure 7. Characteristics of canard-wing-body configuration with canard on at zero incidence and strake off. $\delta_{f,\mathrm{LE}} = \delta_{f,\mathrm{TE}} = 20°$.

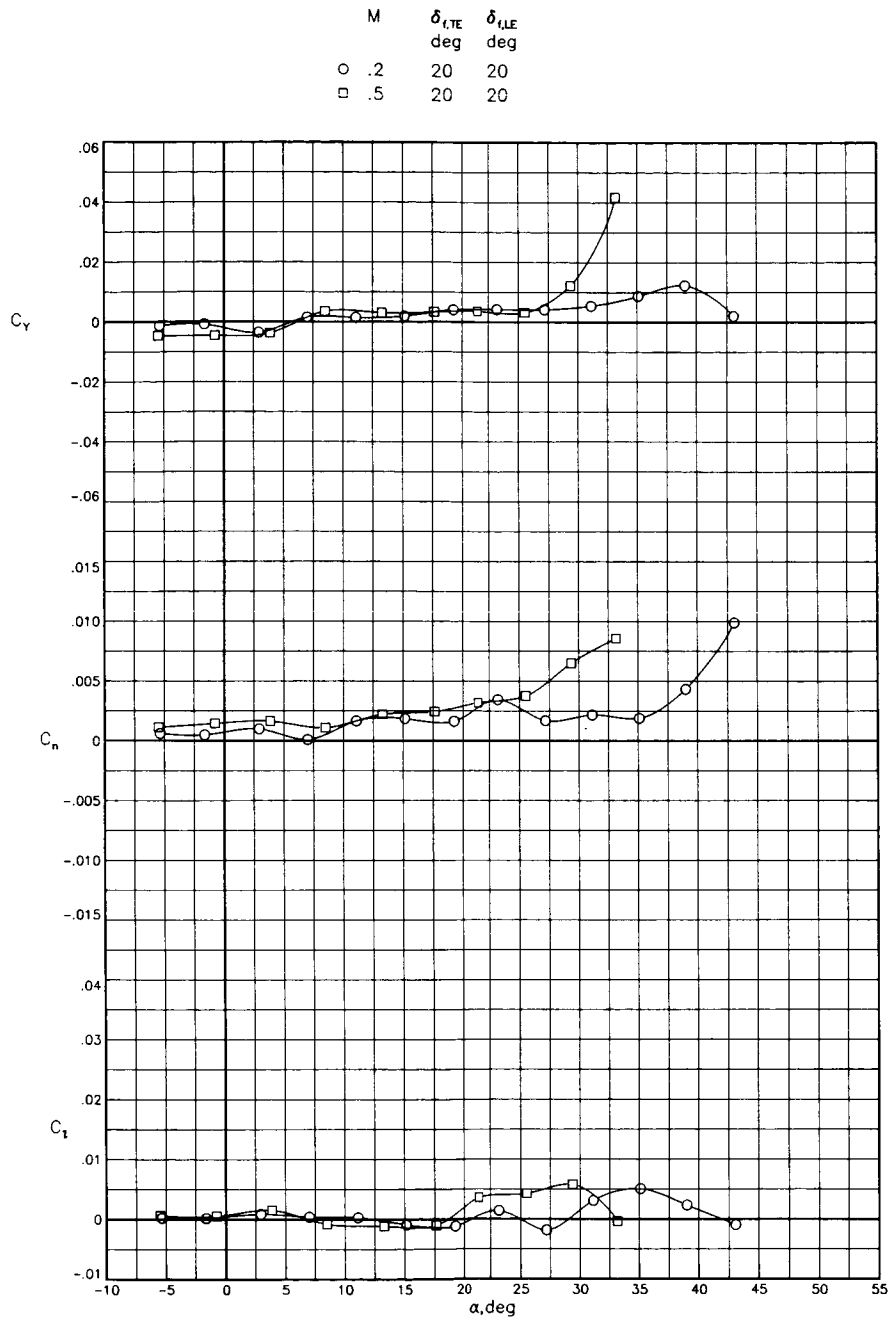


(b) Effect of Mach number on lateral-directional characteristics. $\beta = 0°$.

Figure 7. Continued.

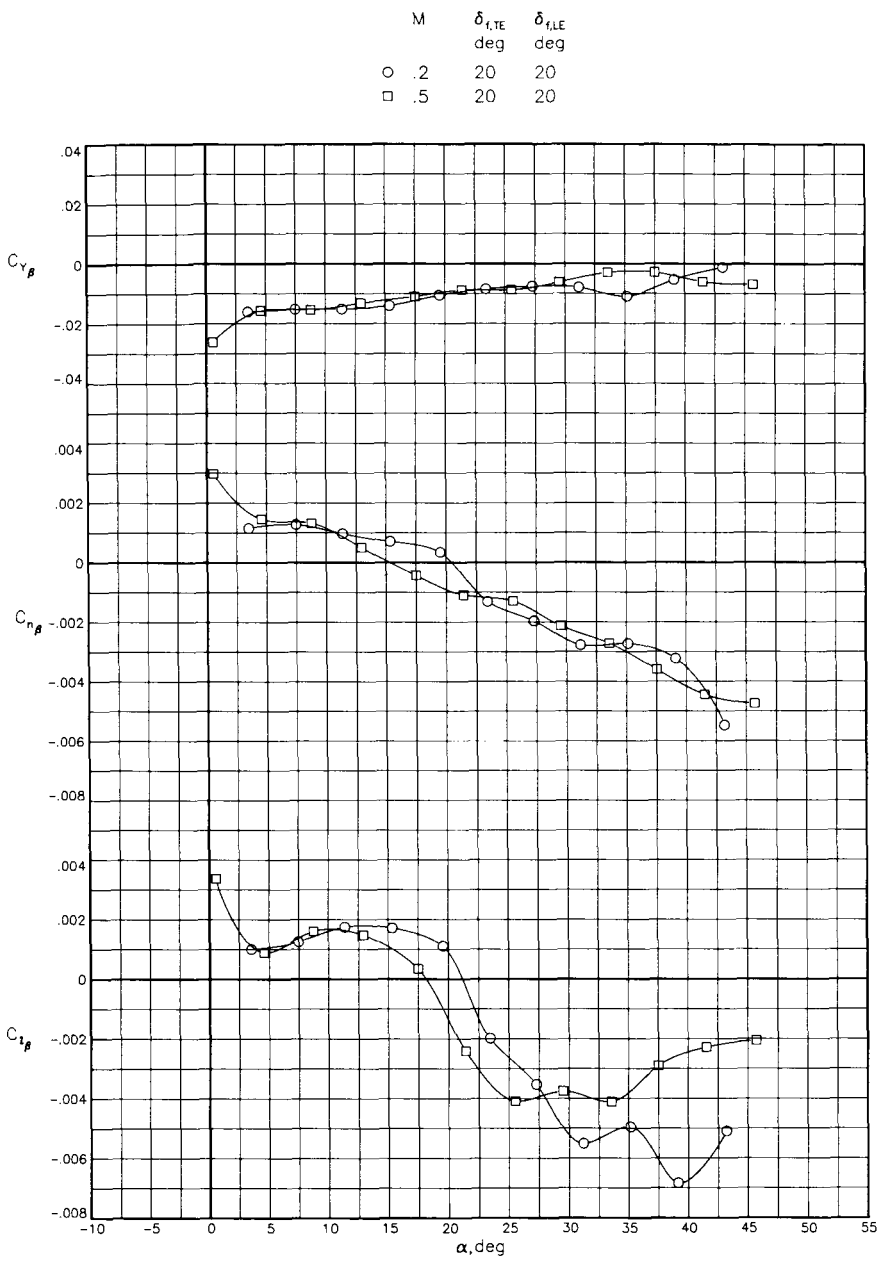


(c) Effect of Mach number on lateral-directional stability.

Figure 7. Continued.

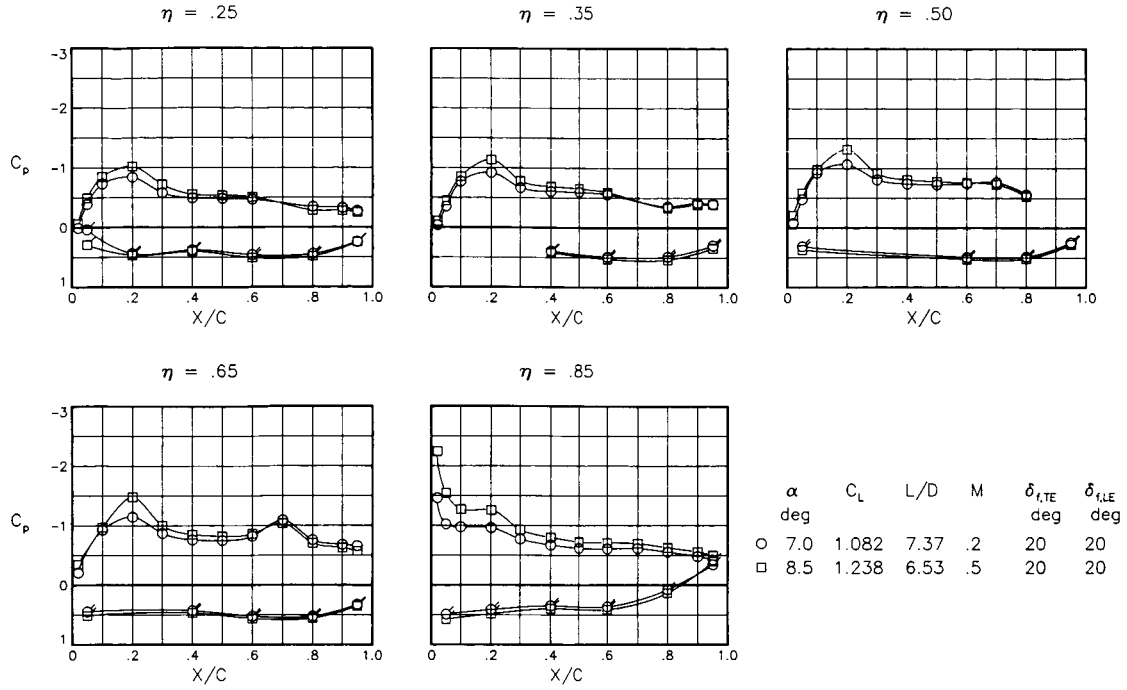


(d) Effect of Mach number on wing pressure distribution for a lift coefficient near 1.0. $\beta = 0°$.

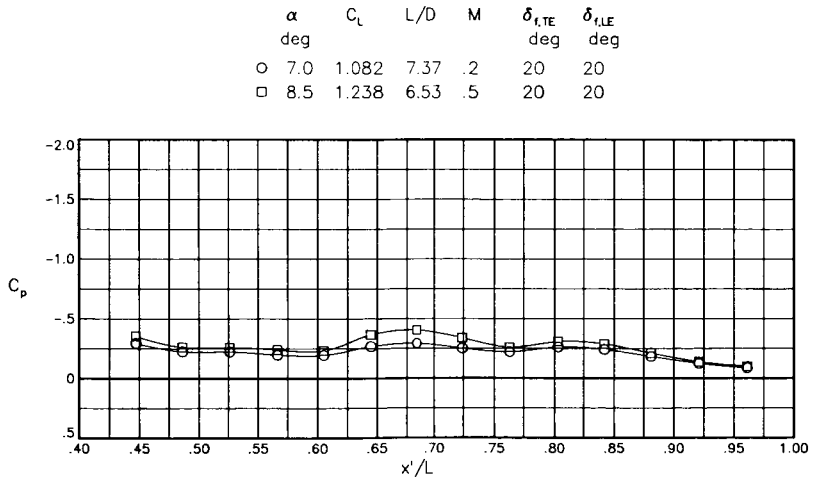


(e) Effect of Mach number on fuselage pressure distribution for a lift coefficient near 1.0. $\beta = 0°$.

Figure 7. Continued.

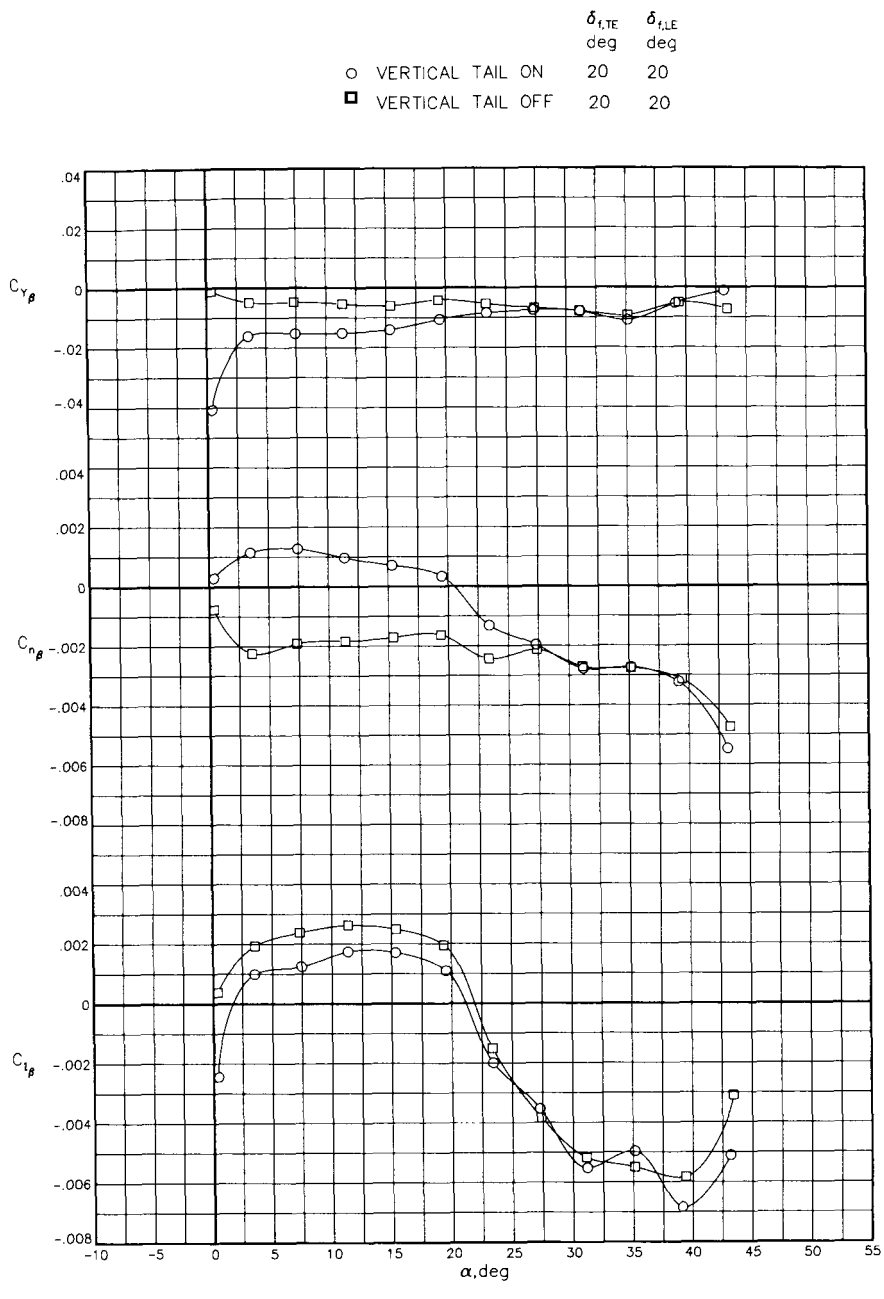


(f) Effect of vertical tail on lateral-directional stability. $M = 0.2$.

Figure 7. Continued.

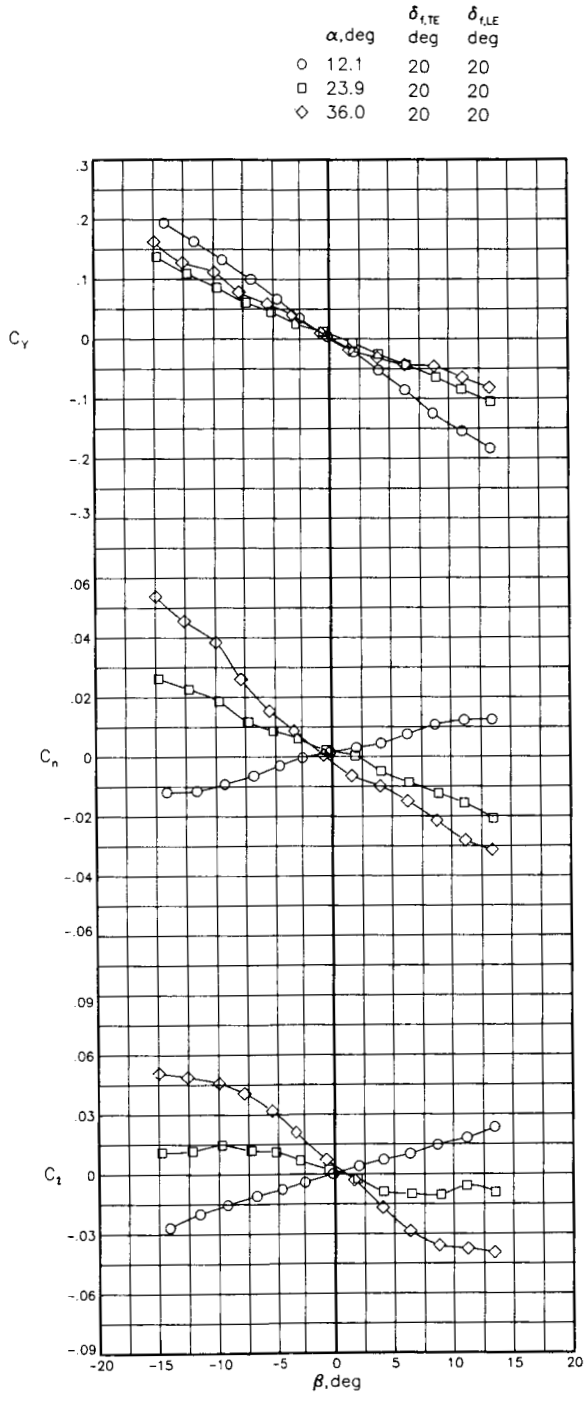


(g) Effect of angle of sideslip on lateral-directional characteristics. $M = 0.2$.

Figure 7. Concluded.

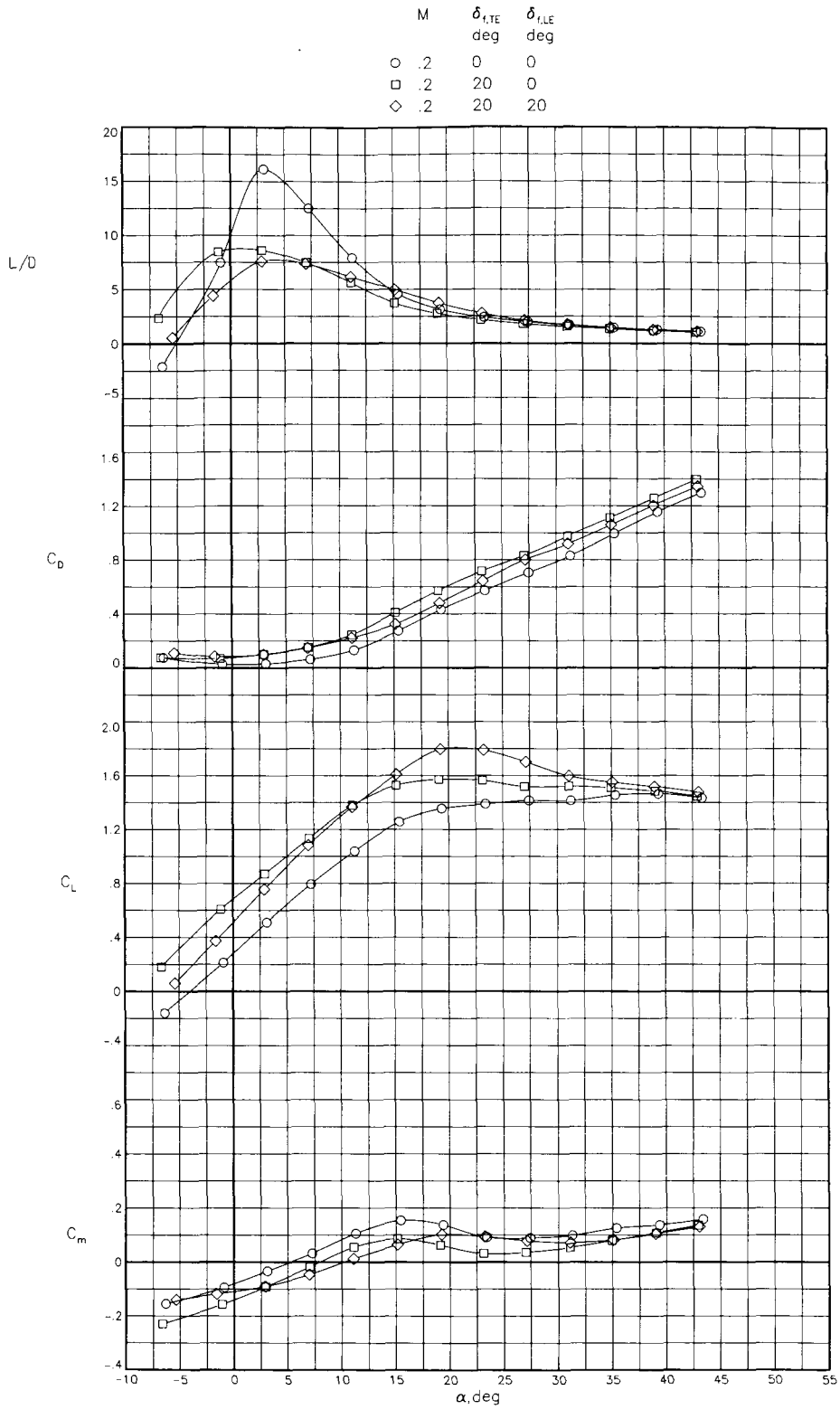


(a) Longitudinal characteristics. $\beta = 0°$.

Figure 8. Effects of leading- and trailing-edge flaps on canard-wing-body configuration with canard on at zero incidence and strake off. $M = 0.2$.

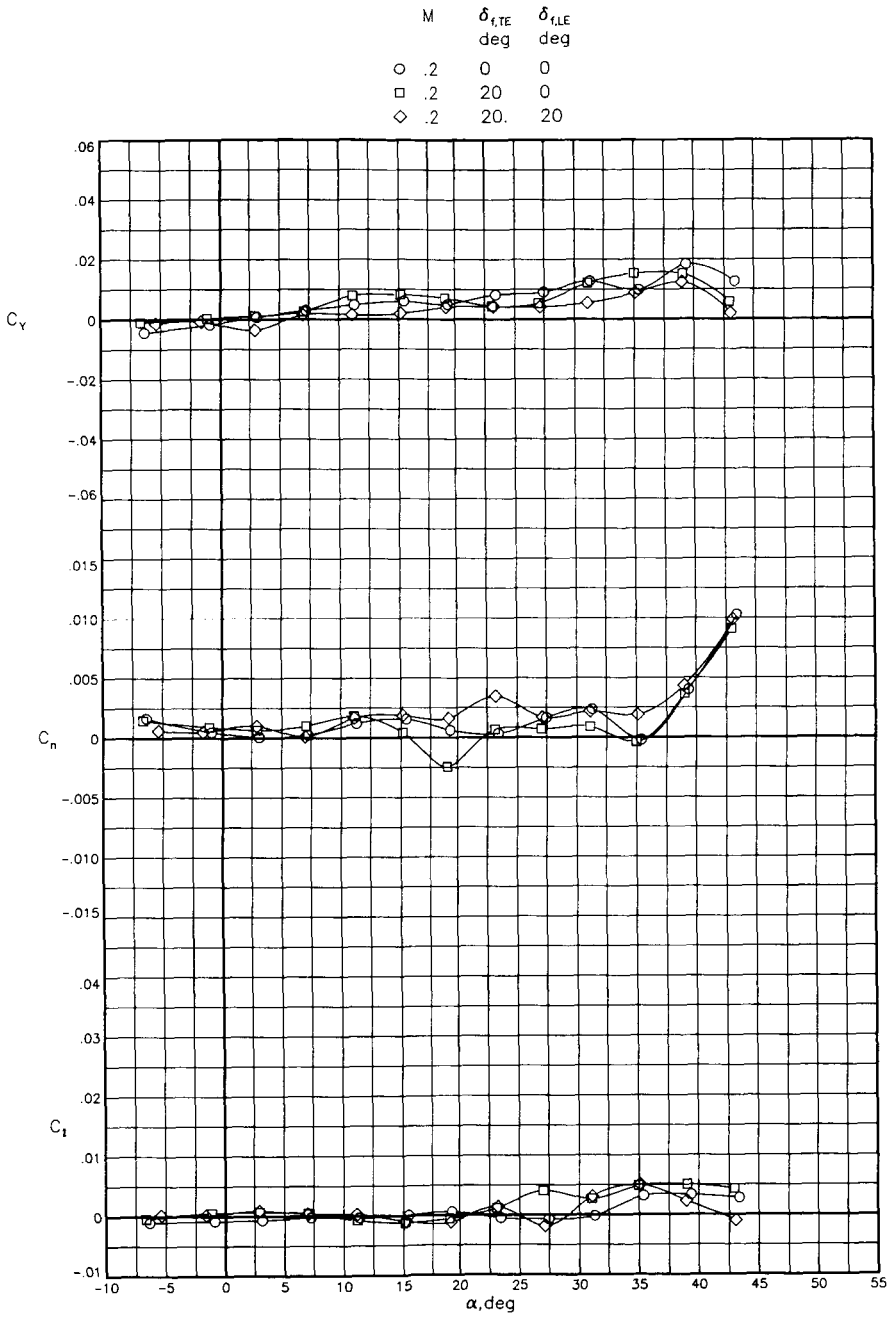


(b) Lateral-directional characteristics. $\beta = 0°$.

Figure 8. Continued.

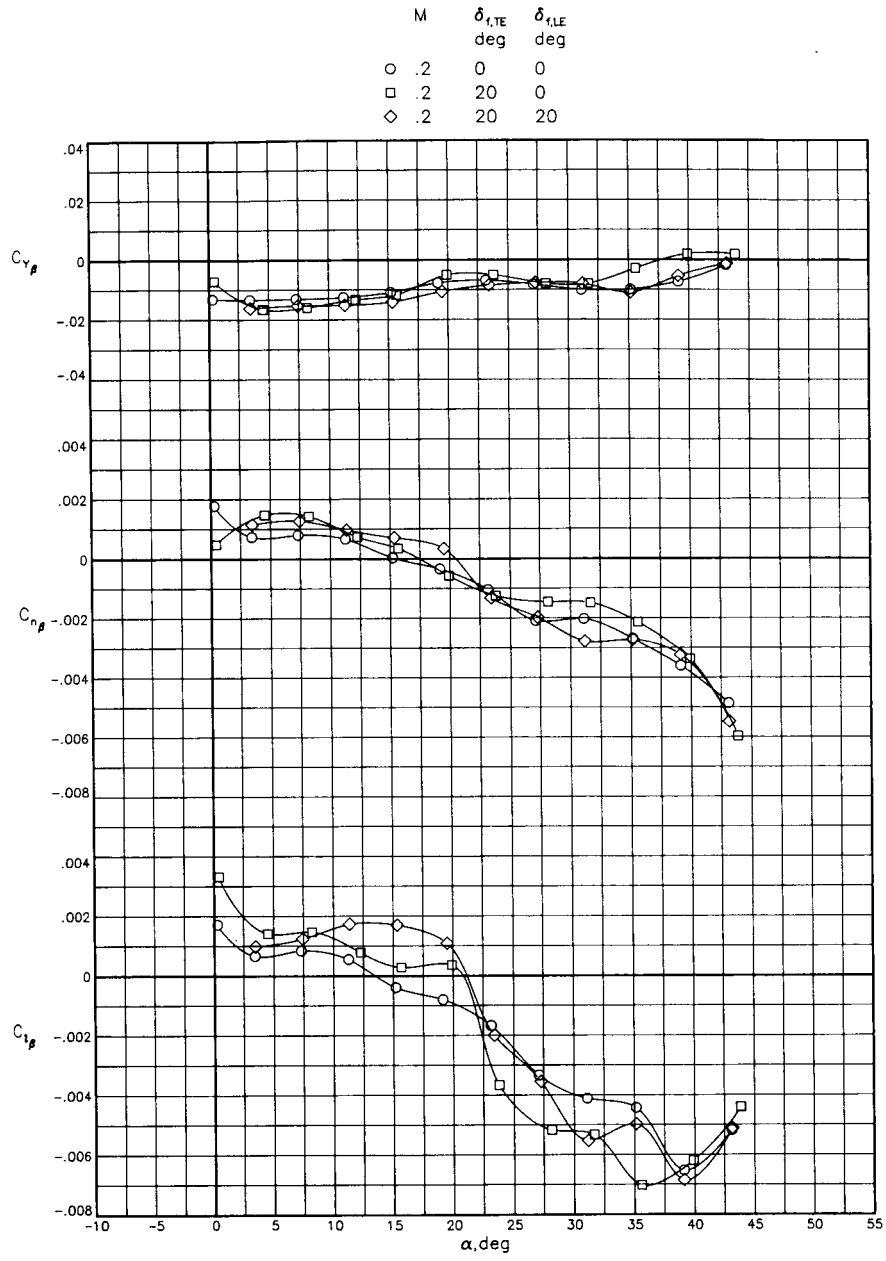


(c) Lateral-directional stability.

Figure 8. Continued.

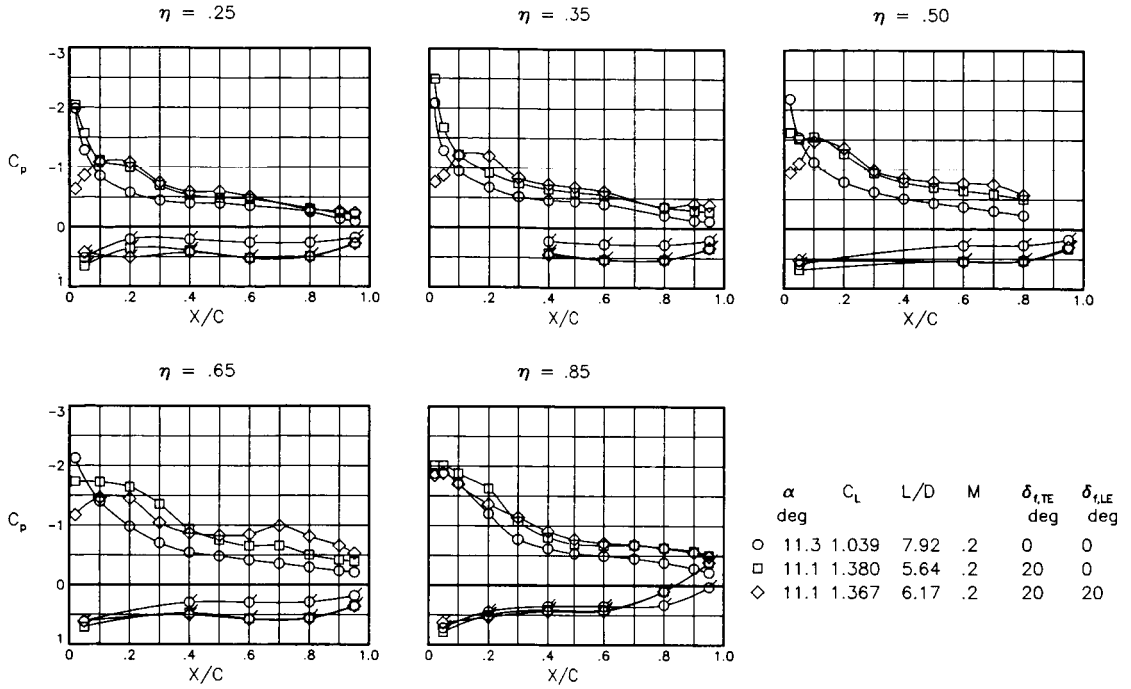


(d) Wing pressure distributions. $\alpha \approx 11°; \beta = 0°$.

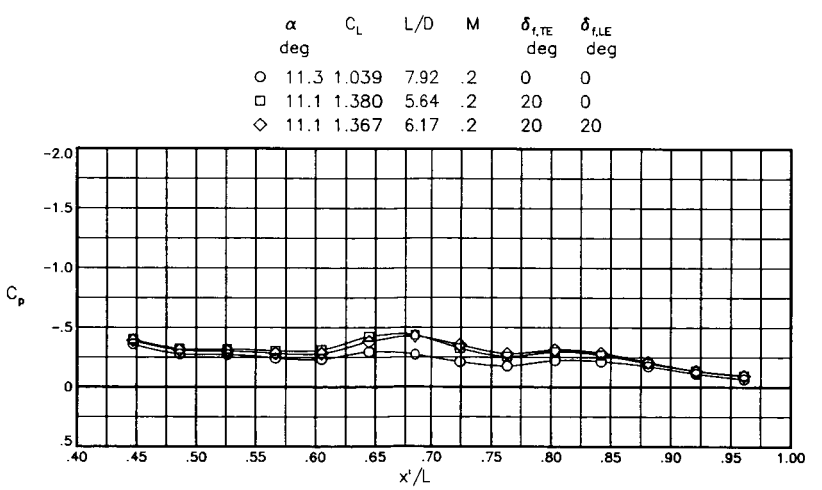


(e) Fuselage pressure distributions. $\alpha \approx 11°$; $\beta \approx 0°$.

Figure 8. Concluded.

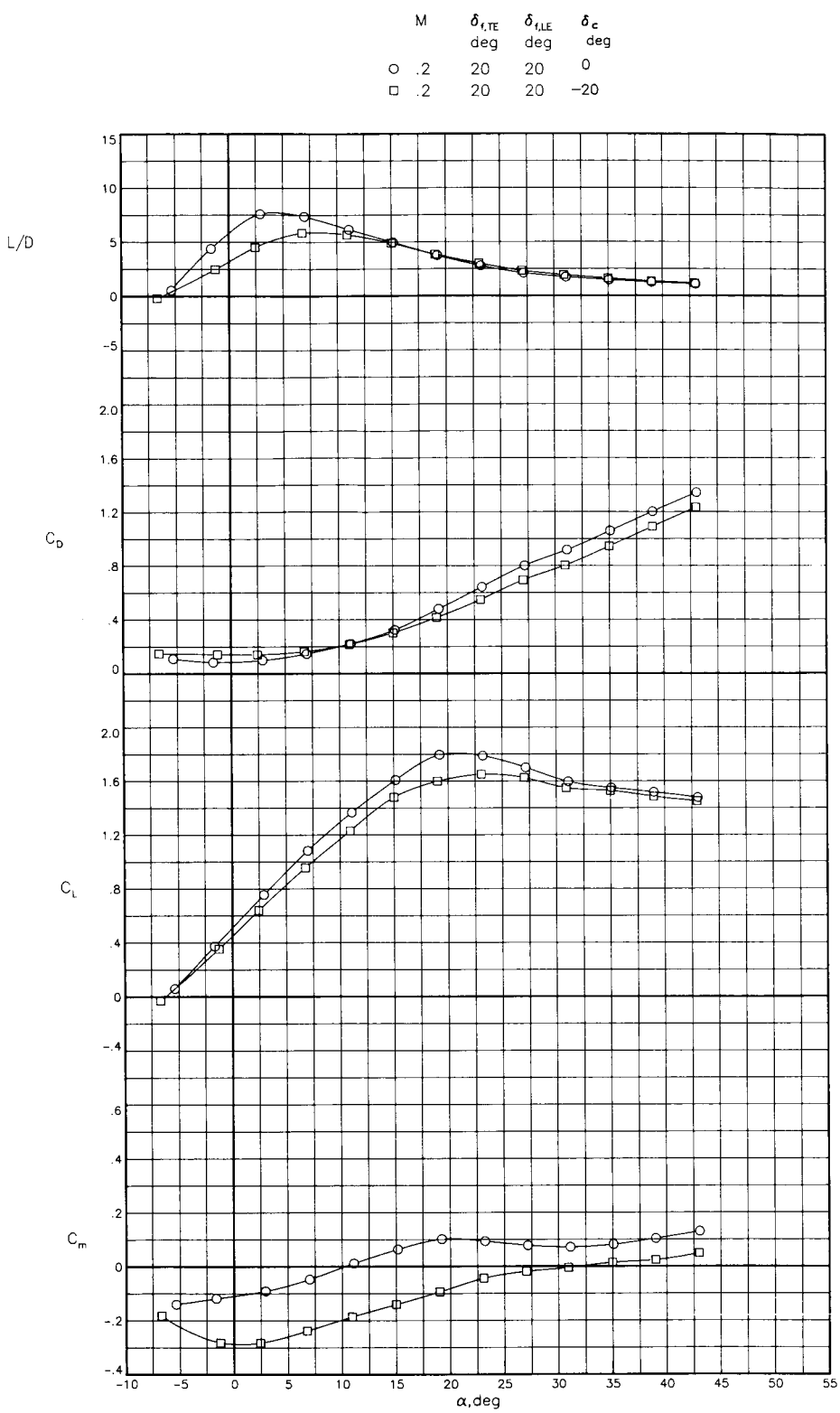


(a) Longitudinal characteristics. $\beta = 0°$.

Figure 9. Effects of canard incidence on canard-wing-body configuration with strakes off. $\delta_{f,\mathrm{LE}} = \delta_{f,\mathrm{TE}} = 20°$; $M = 0.2$.

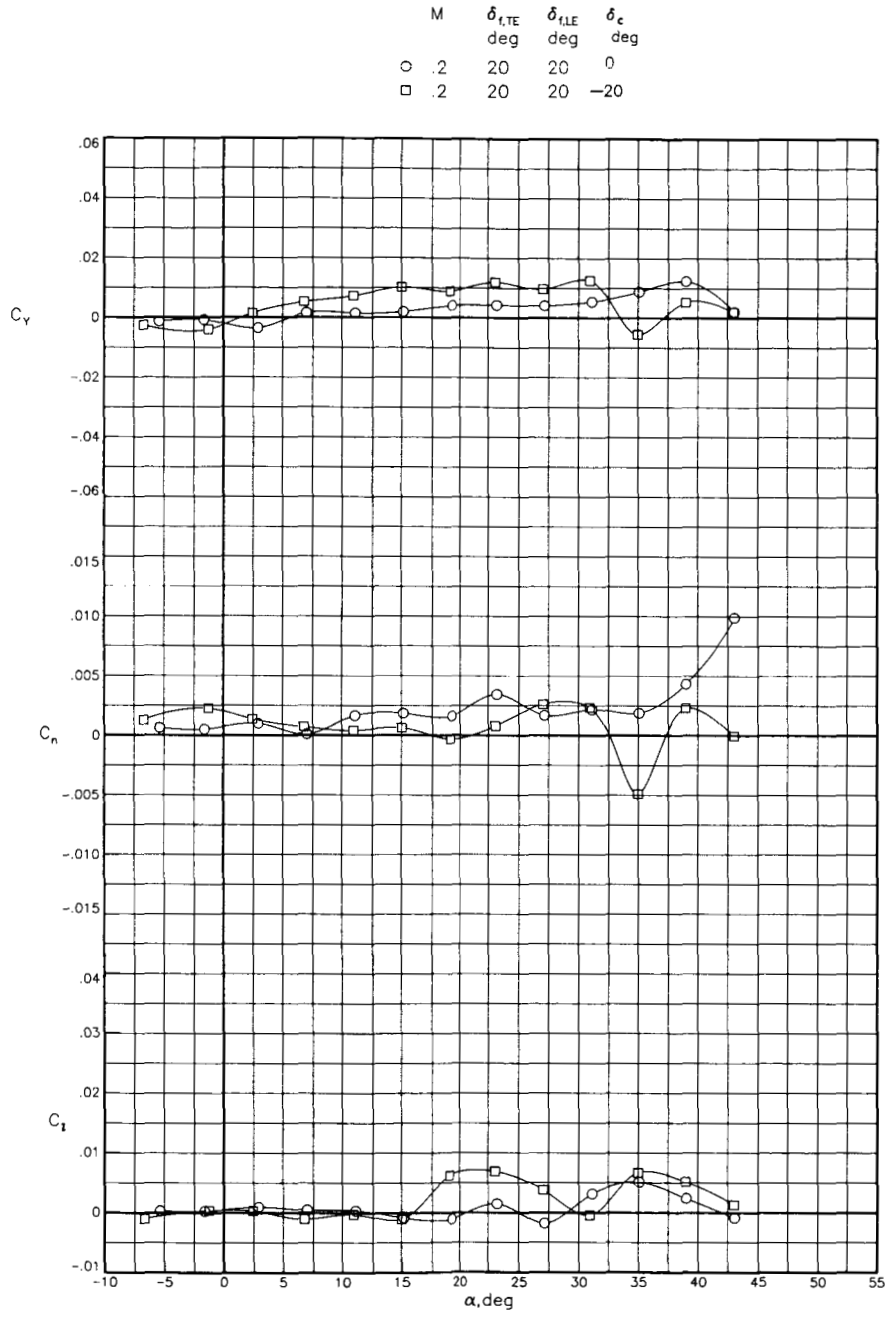


(b) Lateral-directional characteristics. $\beta = 0°$.

Figure 9. Continued.

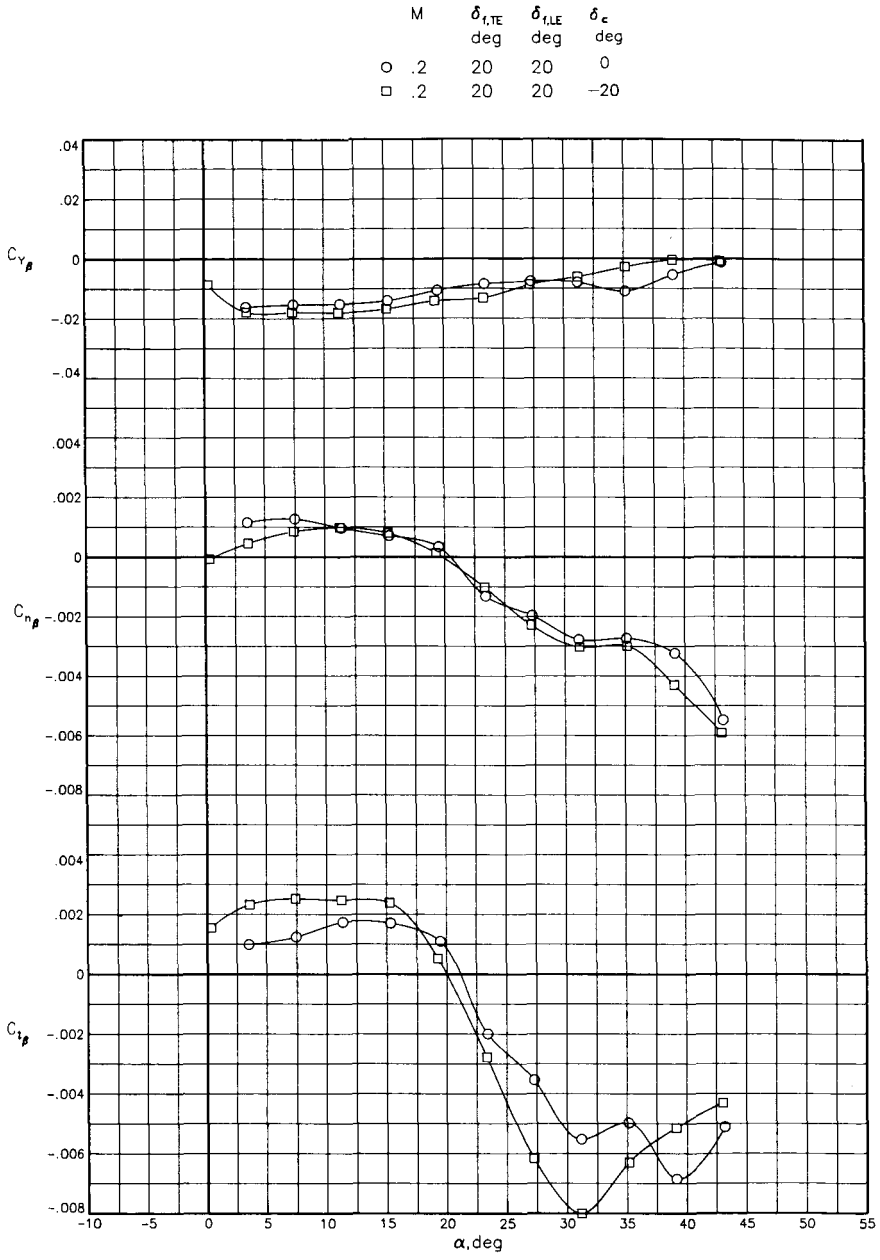


(c) Lateral-directional stability.

Figure 9. Concluded.

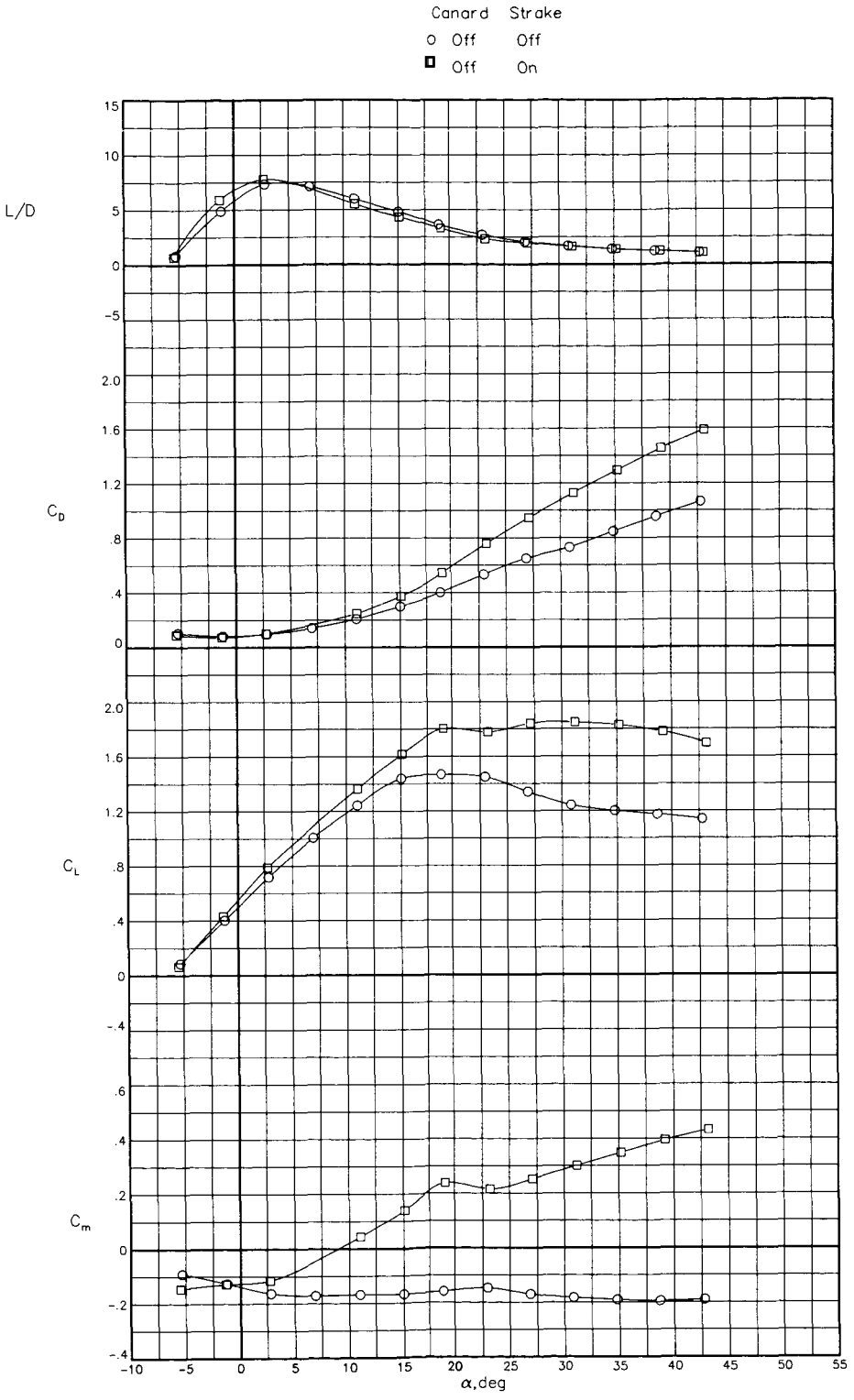


(a) Longitudinal characteristics for $M = 0.2$. $\beta = 0°$.

Figure 10. Effects of strake with canard off. $\delta_{f,\mathrm{LE}} = \delta_{f,\mathrm{TE}} = 20°$.

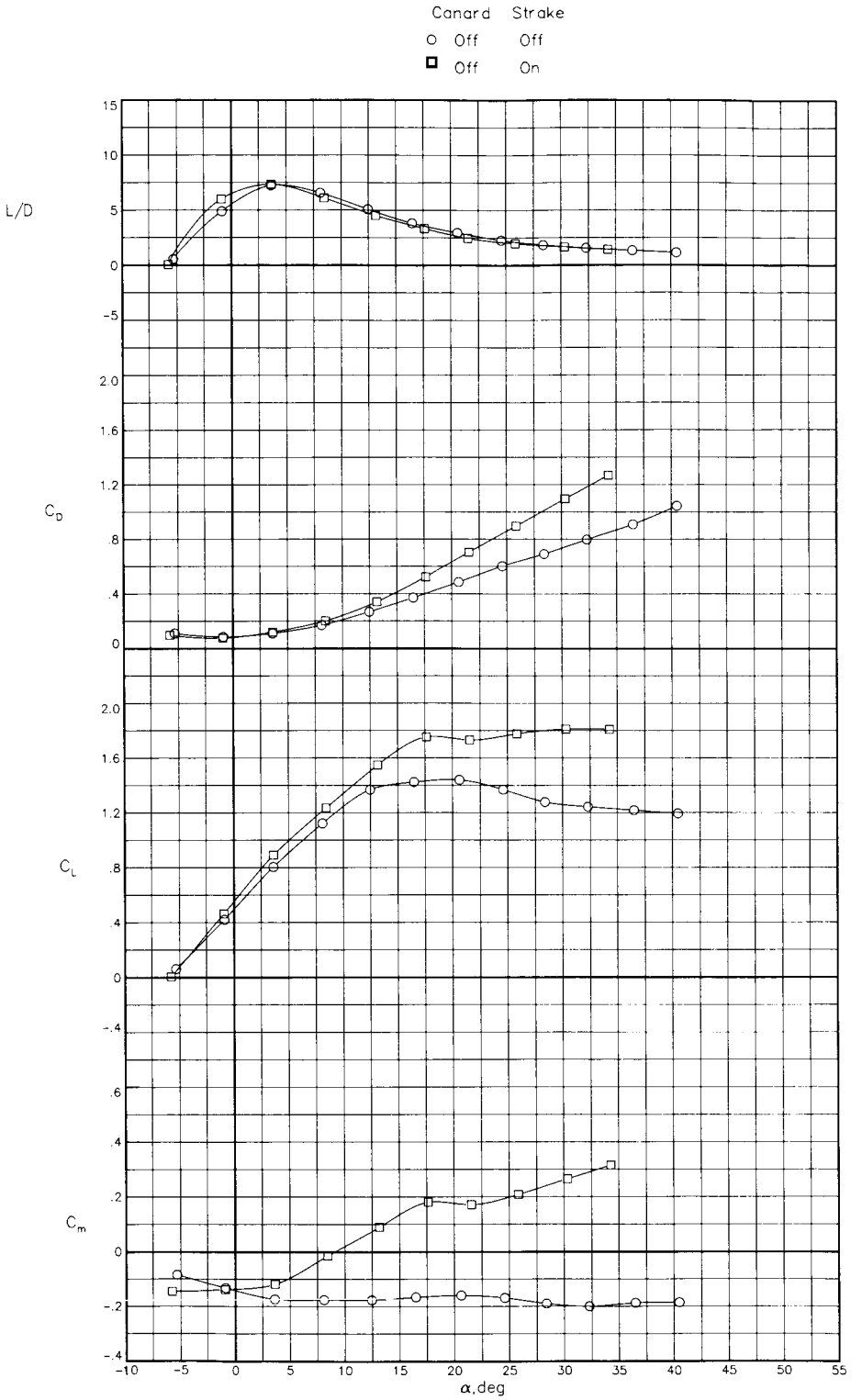


(b) Longitudinal characteristics for $M = 0.5$. $\beta = 0°$.

Figure 10. Continued.

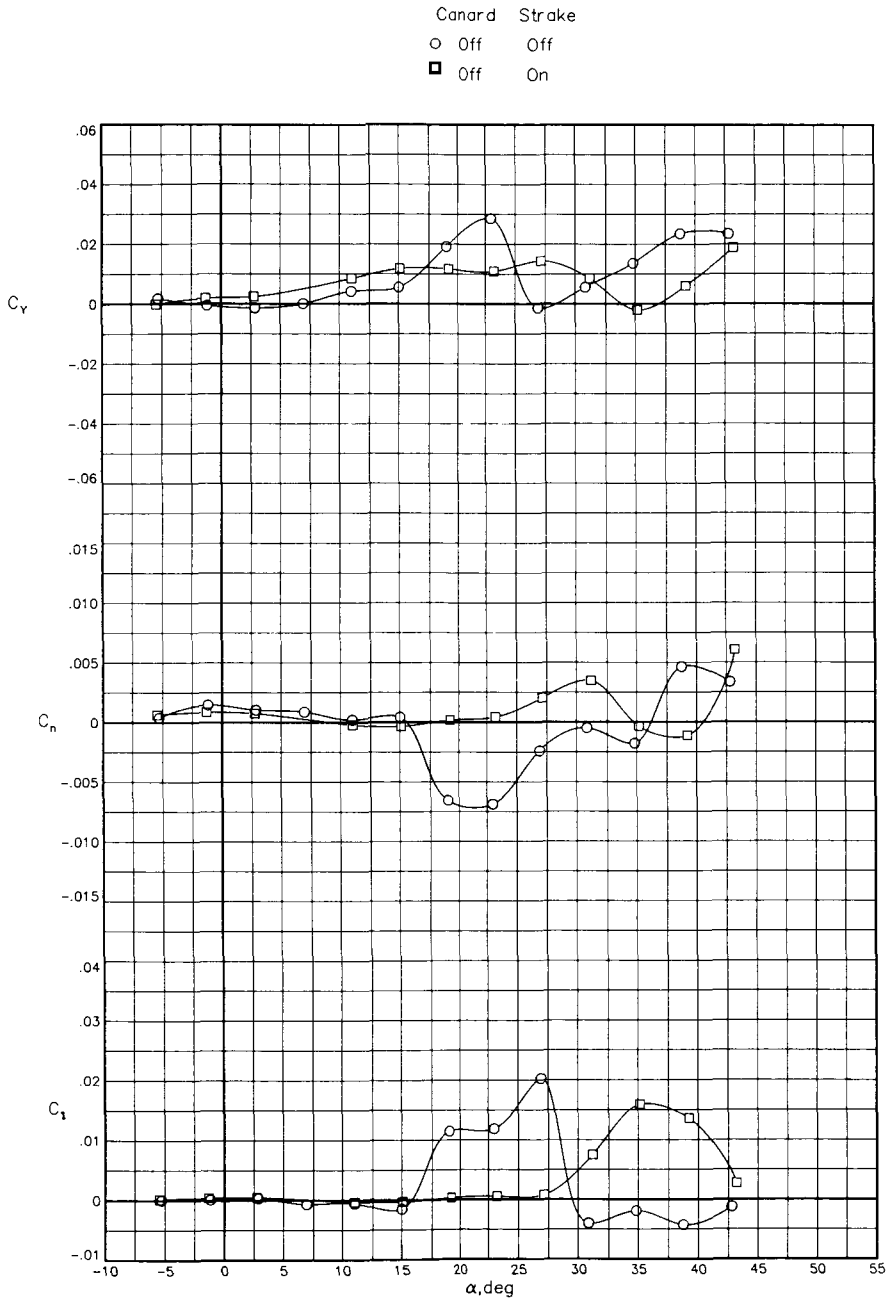


(c) Lateral-directional characteristics for $M = 0.2$. $\beta = 0°$.

Figure 10. Continued.

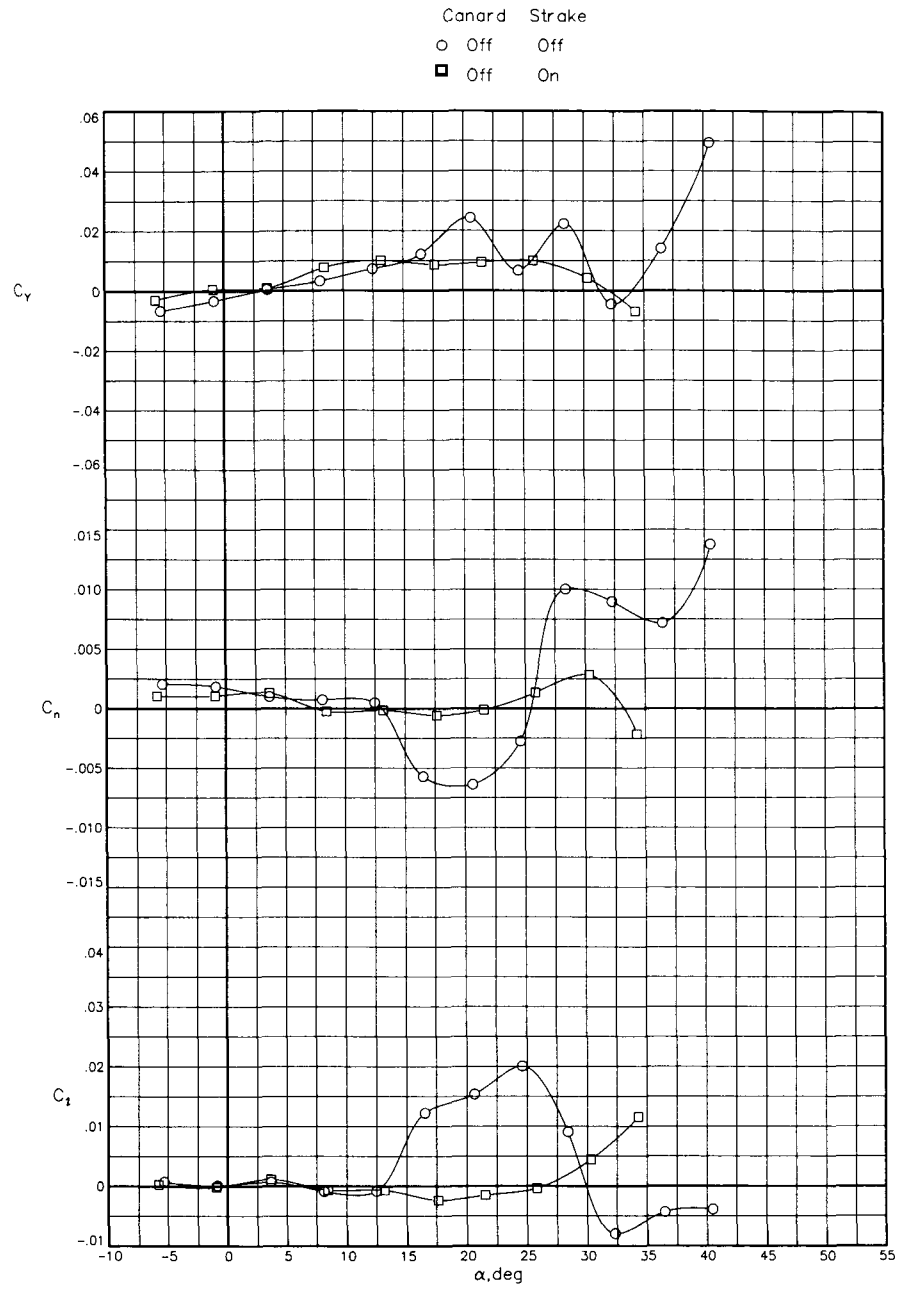


(d) Lateral-directional characteristics for $M = 0.5$. $\beta = 0°$.

Figure 10. Continued.

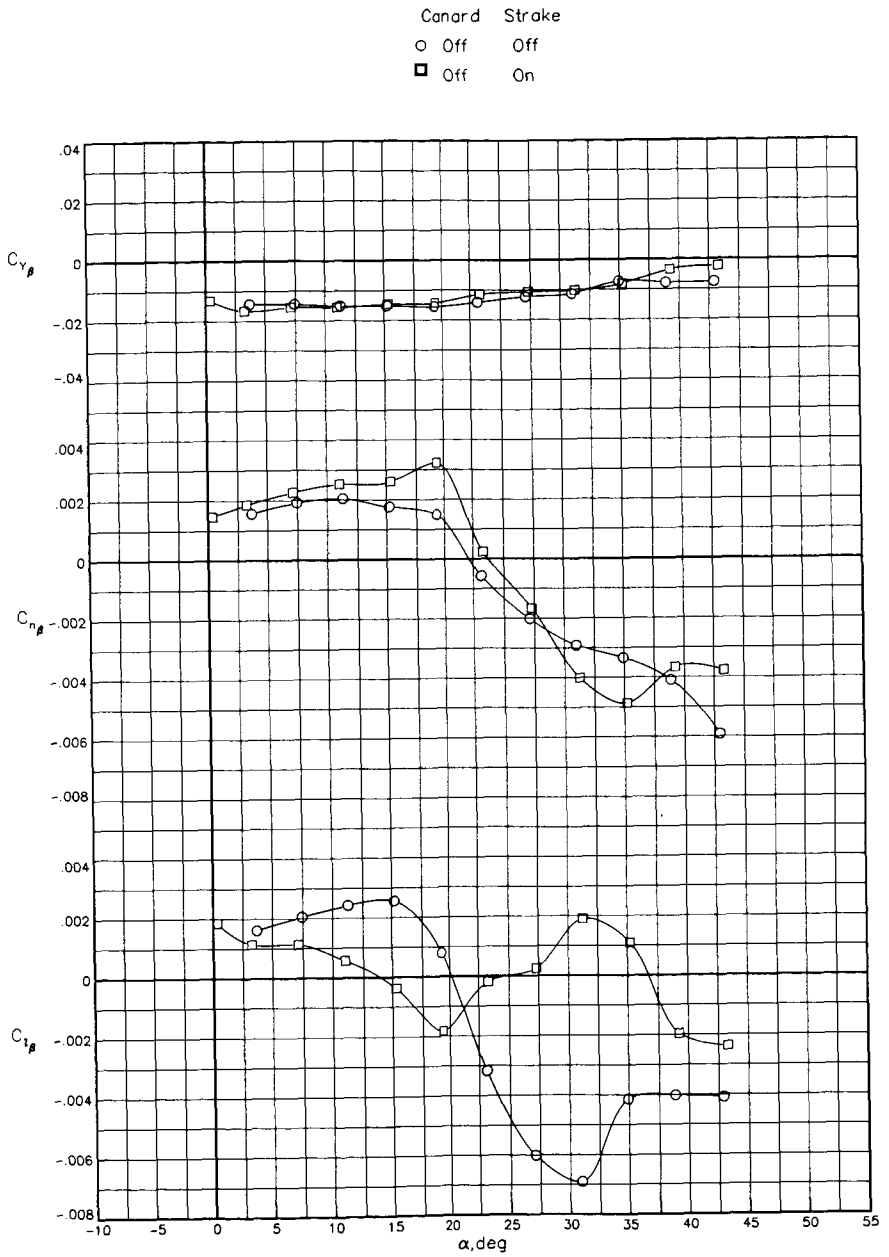


(e) Lateral-directional stability for $M = 0.2$.

Figure 10. Continued.

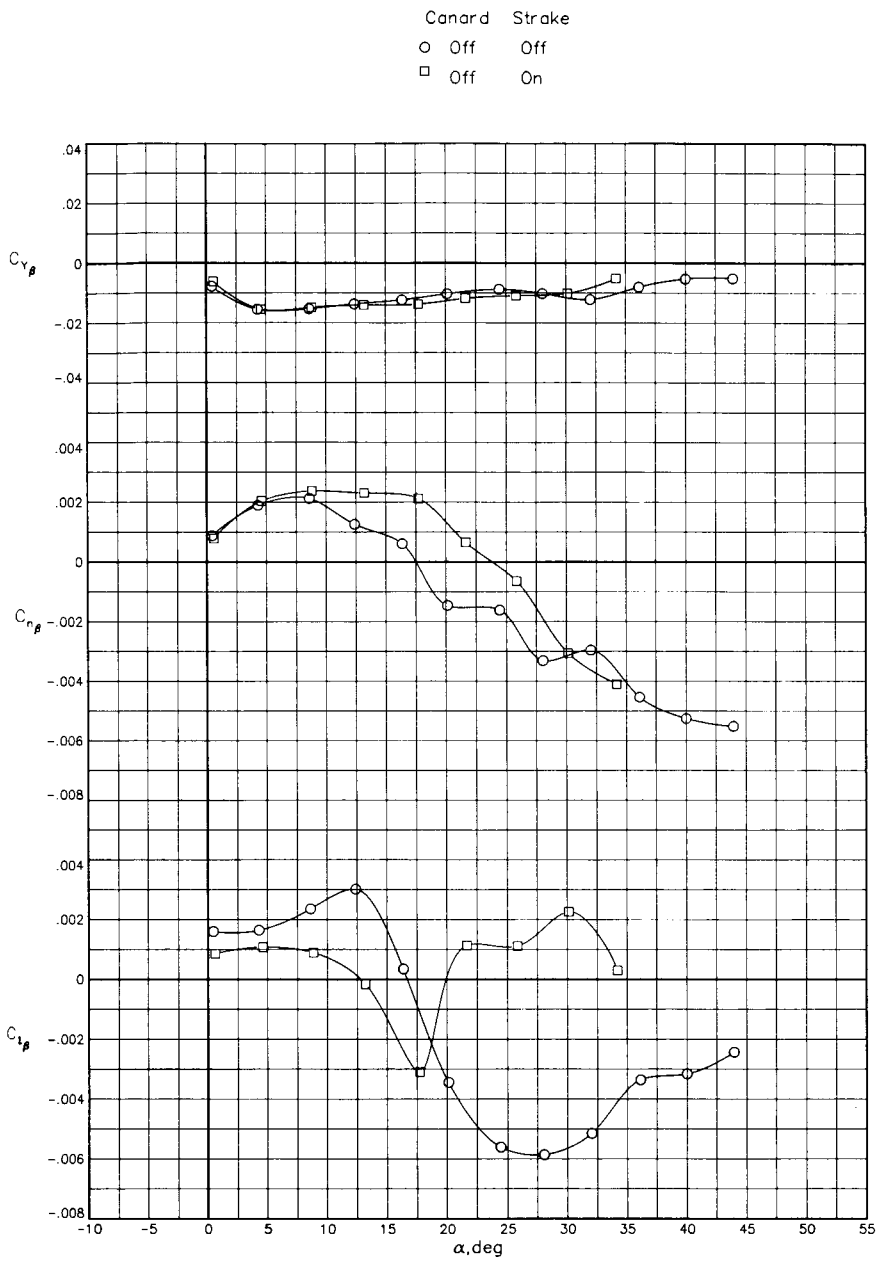


(f) Lateral-directional stability for $M = 0.5$.

Figure 10. Continued.

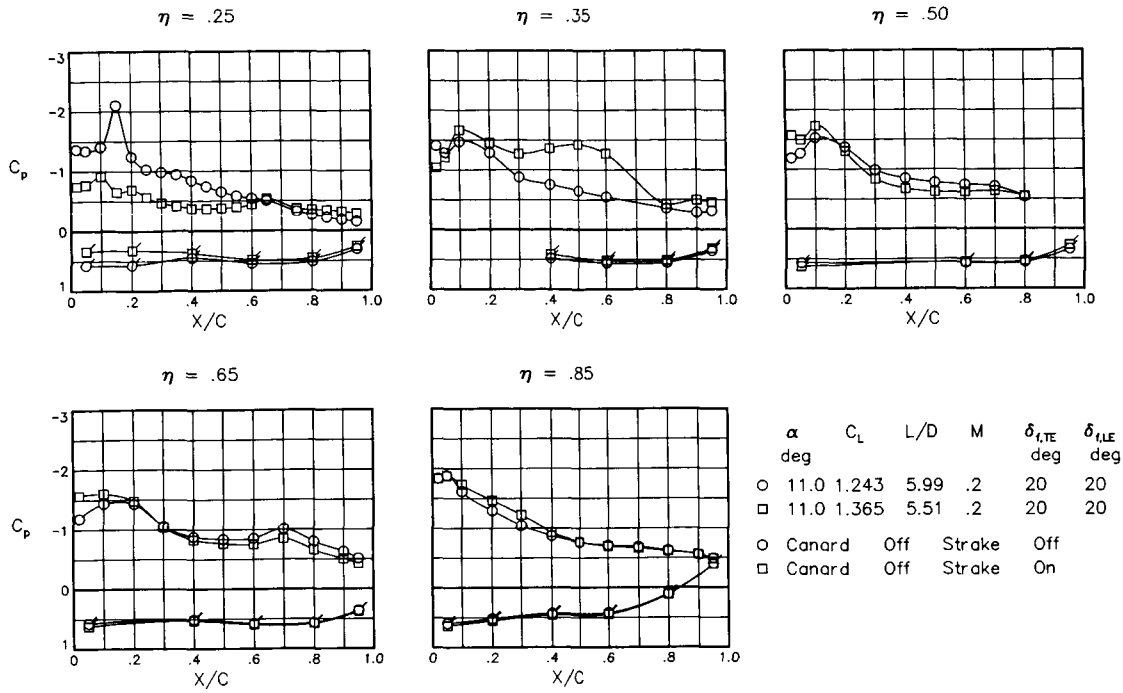


(g) Wing pressure distributions for $M = 0.2$. $\alpha \approx 11°$; $\beta = 0°$.

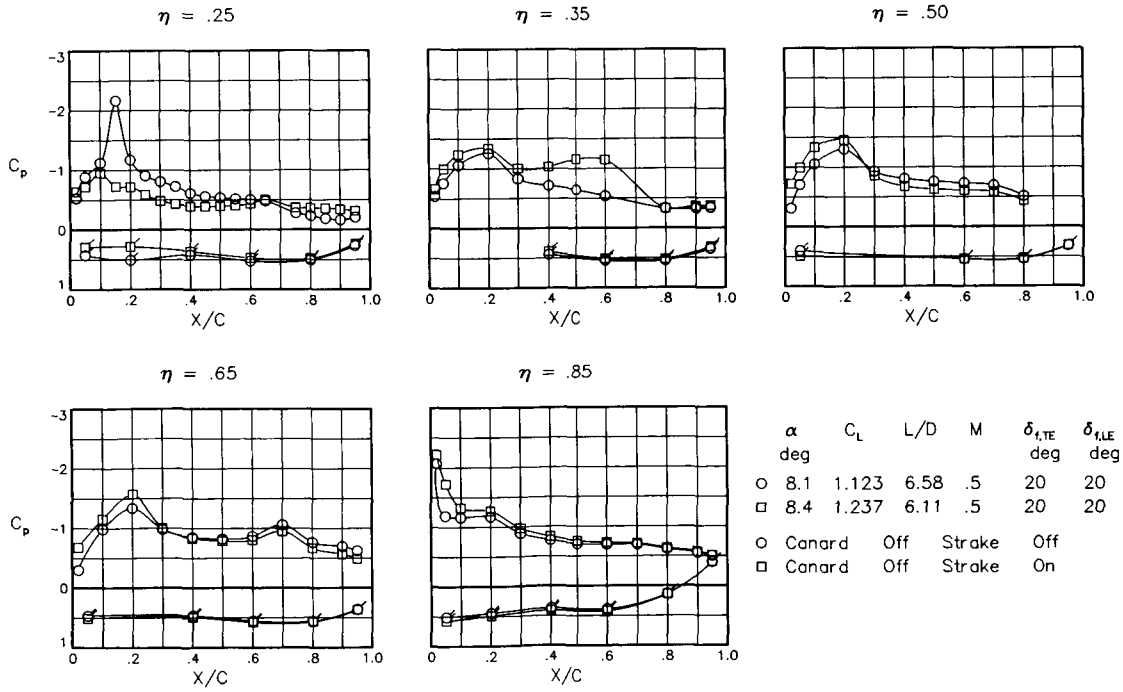


(h) Wing pressure distributions for $M = 0.5$. $\alpha \approx 8°$; $\beta = 0°$.

Figure 10. Continued.

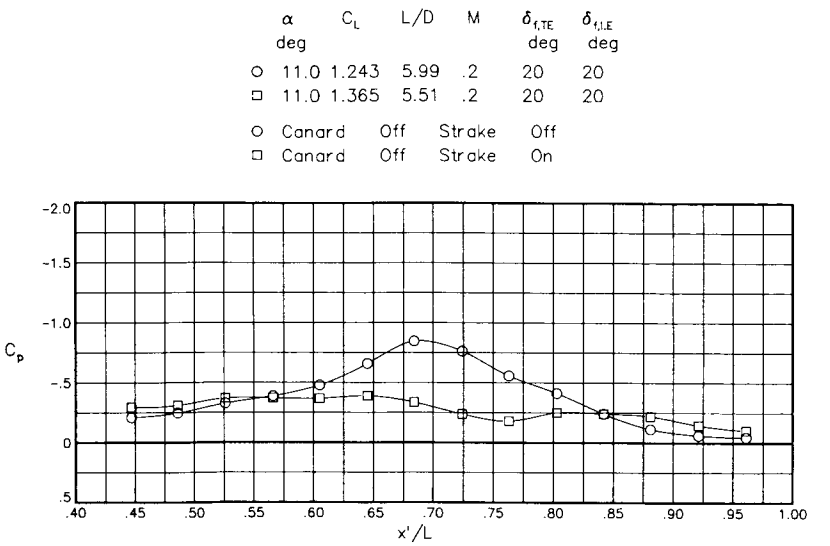


(i) Fuselage pressure distributions for $M = 0.2$. $\alpha \approx 11°$; $\beta = 0°$.

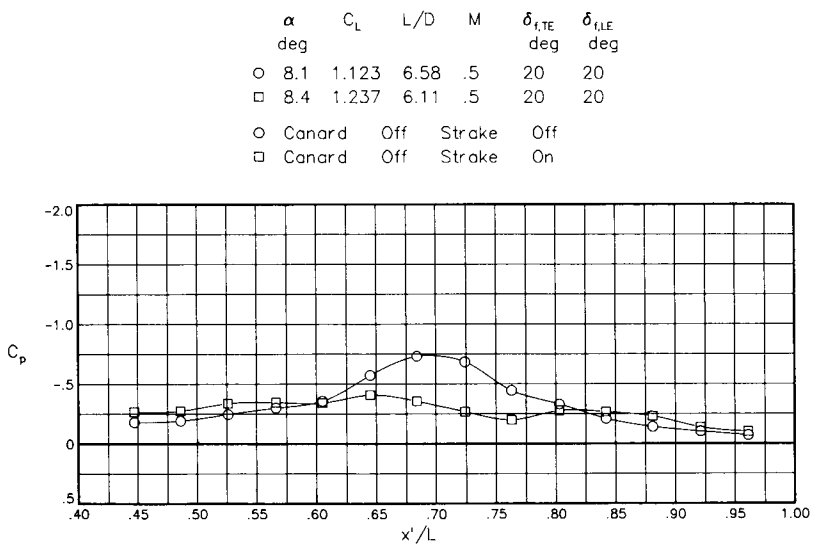


(j) Fuselage pressure distributions for $M = 0.5$. $\alpha \approx 8°$; $\beta = 0°$.

Figure 10. Continued.

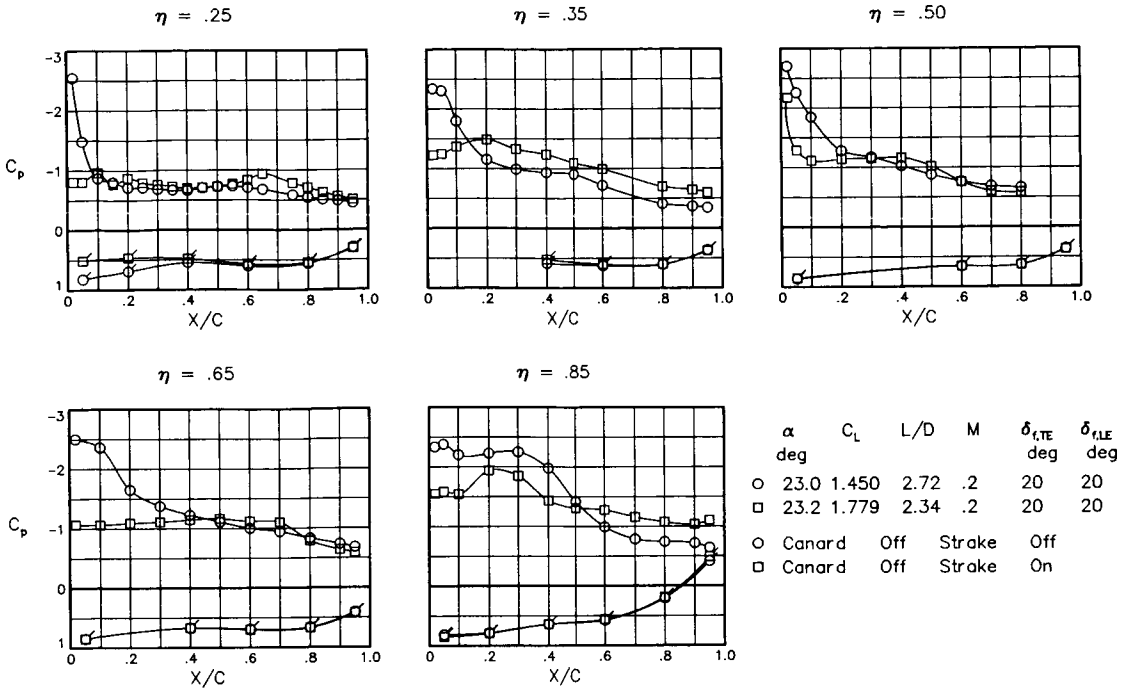


(k) Wing pressure distributions for $M = 0.2$. $\alpha \approx 23°$; $\beta = 0°$.

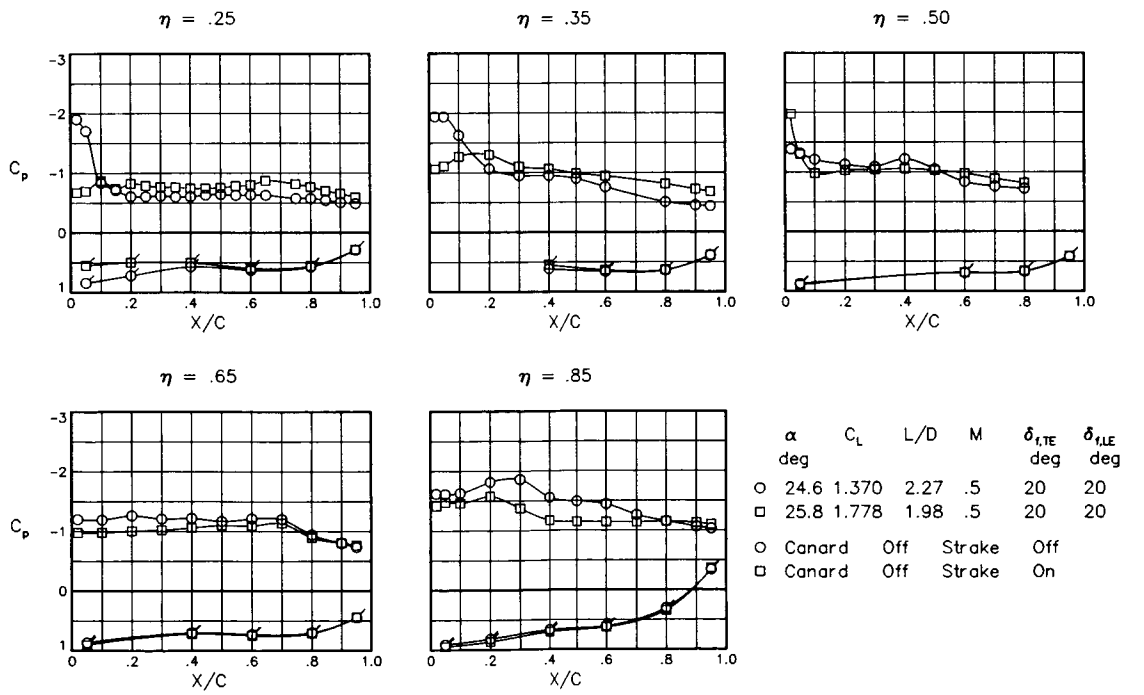


(l) Wing pressure distributions for $M = 0.5$. $\alpha \approx 25°$; $\beta = 0°$.

Figure 10. Continued.

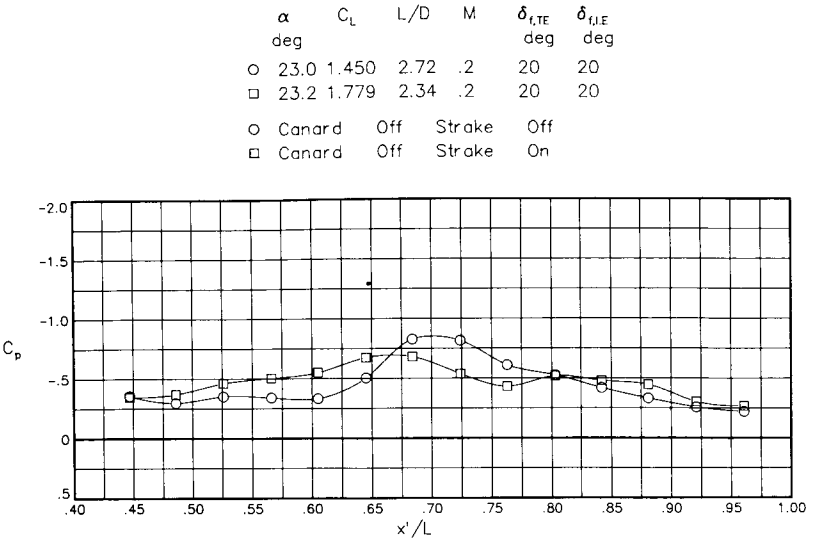


(m) Fuselage pressure distributions for $M = 0.2$. $\alpha \approx 23°$; $\beta = 0°$.

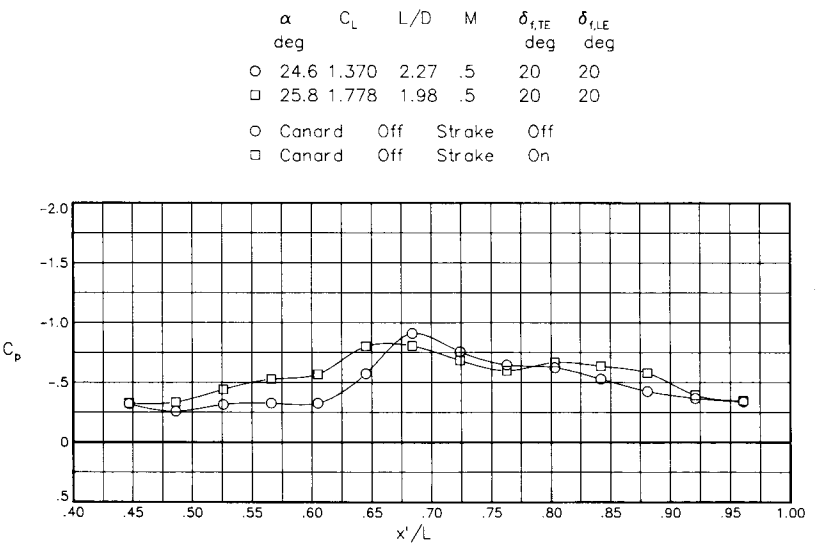


(n) Fuselage pressure distributions for $M = 0.5$. $\alpha \approx 25°$; $\beta = 0°$.

Figure 10. Continued.

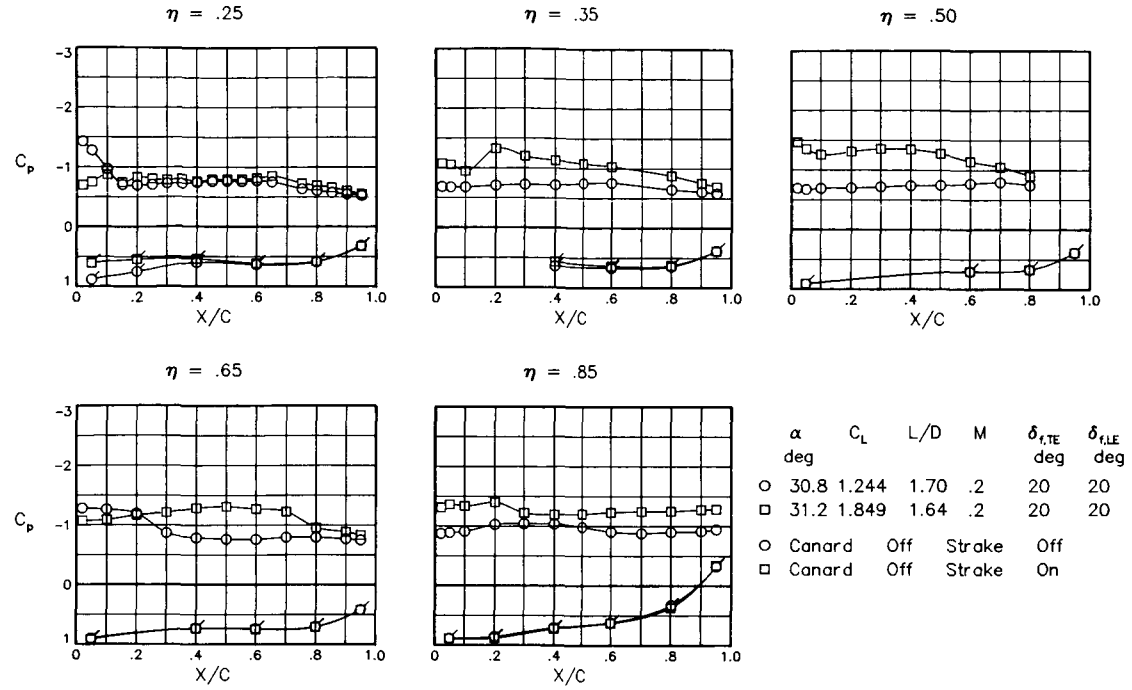


(o) Wing pressure distributions for $M = 0.2$. $\alpha \approx 31°$; $\beta = 0°$.

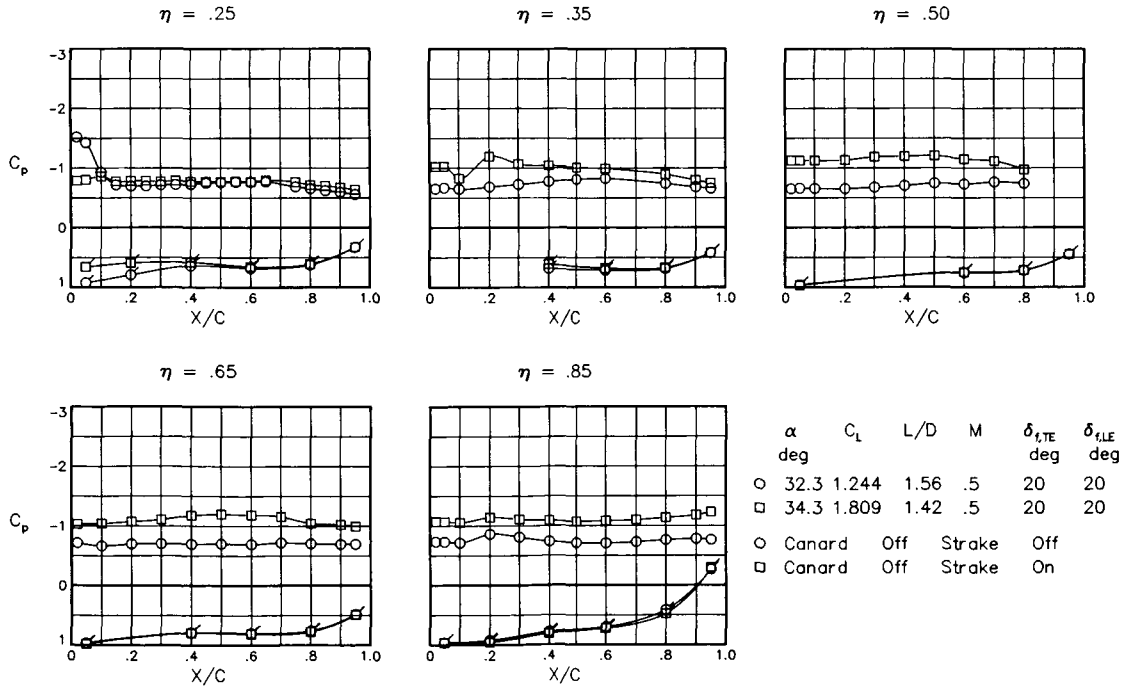


(p) Wing pressure distributions for $M = 0.5$. $\alpha \approx 33°$; $\beta = 0°$.

Figure 10. Continued.

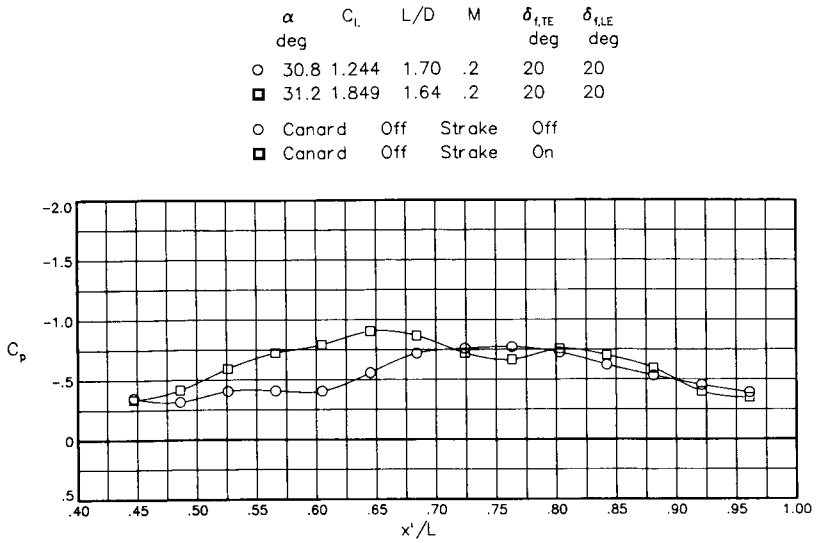


(q) Fuselage pressure distributions for $M = 0.2$. $\alpha \approx 31°$; $\beta = 0°$.

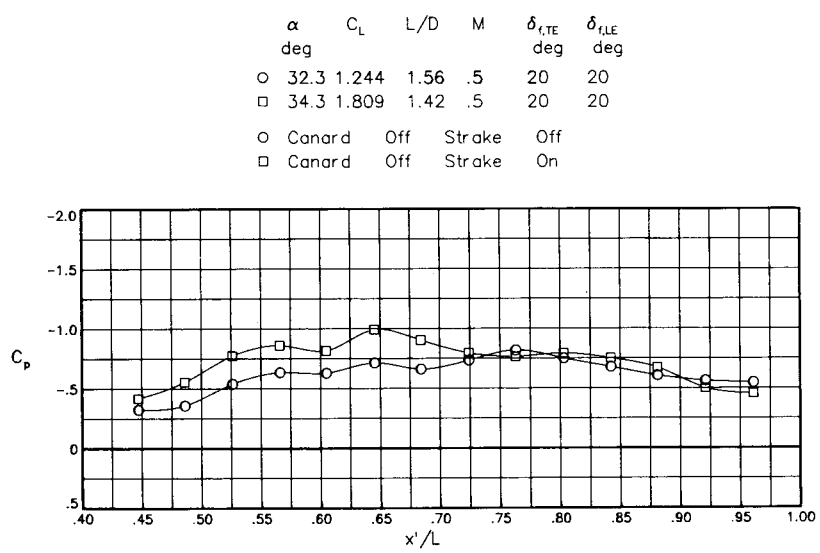


(r) Fuselage pressure distributions for $M = 0.5$. $\alpha \approx 33°$; $\beta = 0°$.

Figure 10. Continued.

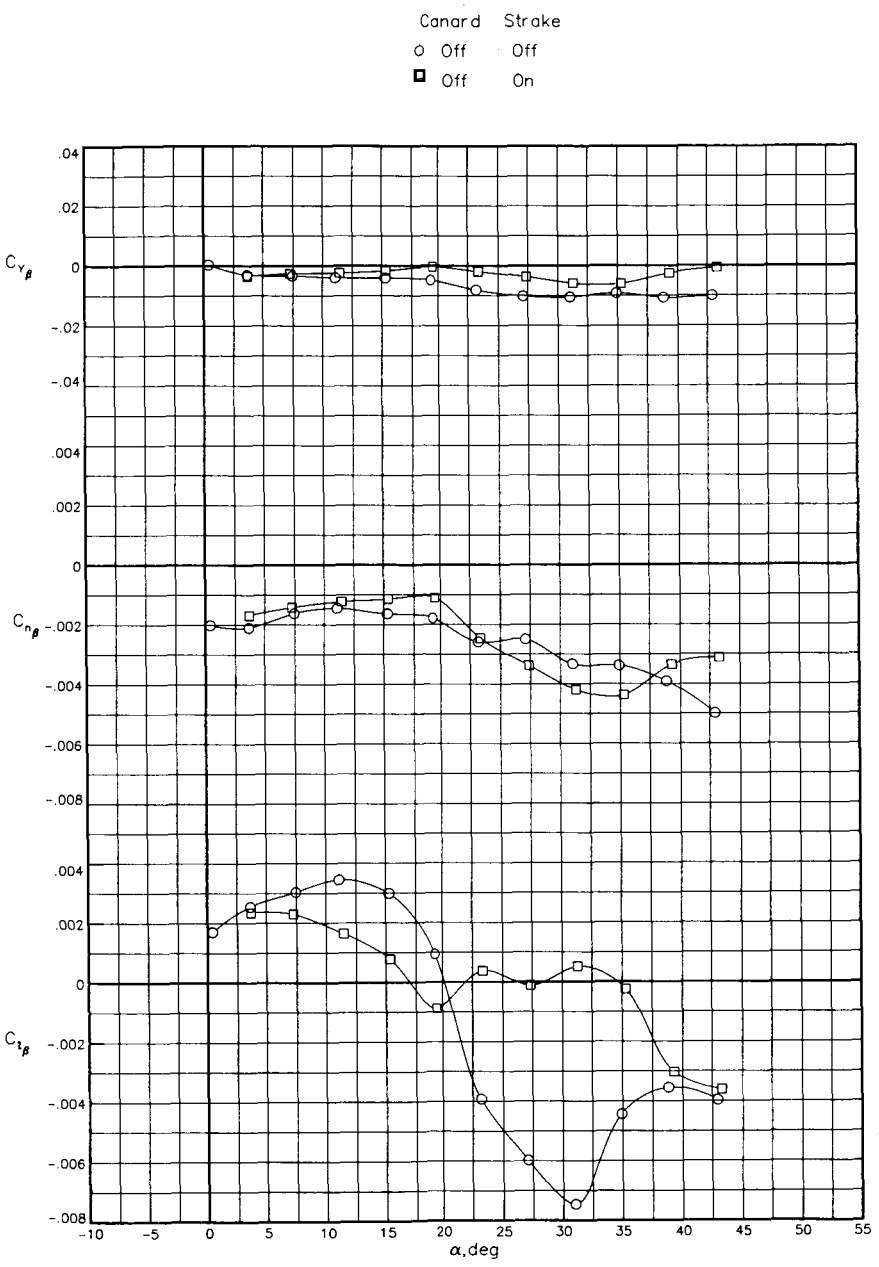


(s) Lateral-directional stability with vertical tail off. $M = 0.2$.

Figure 10. Concluded.

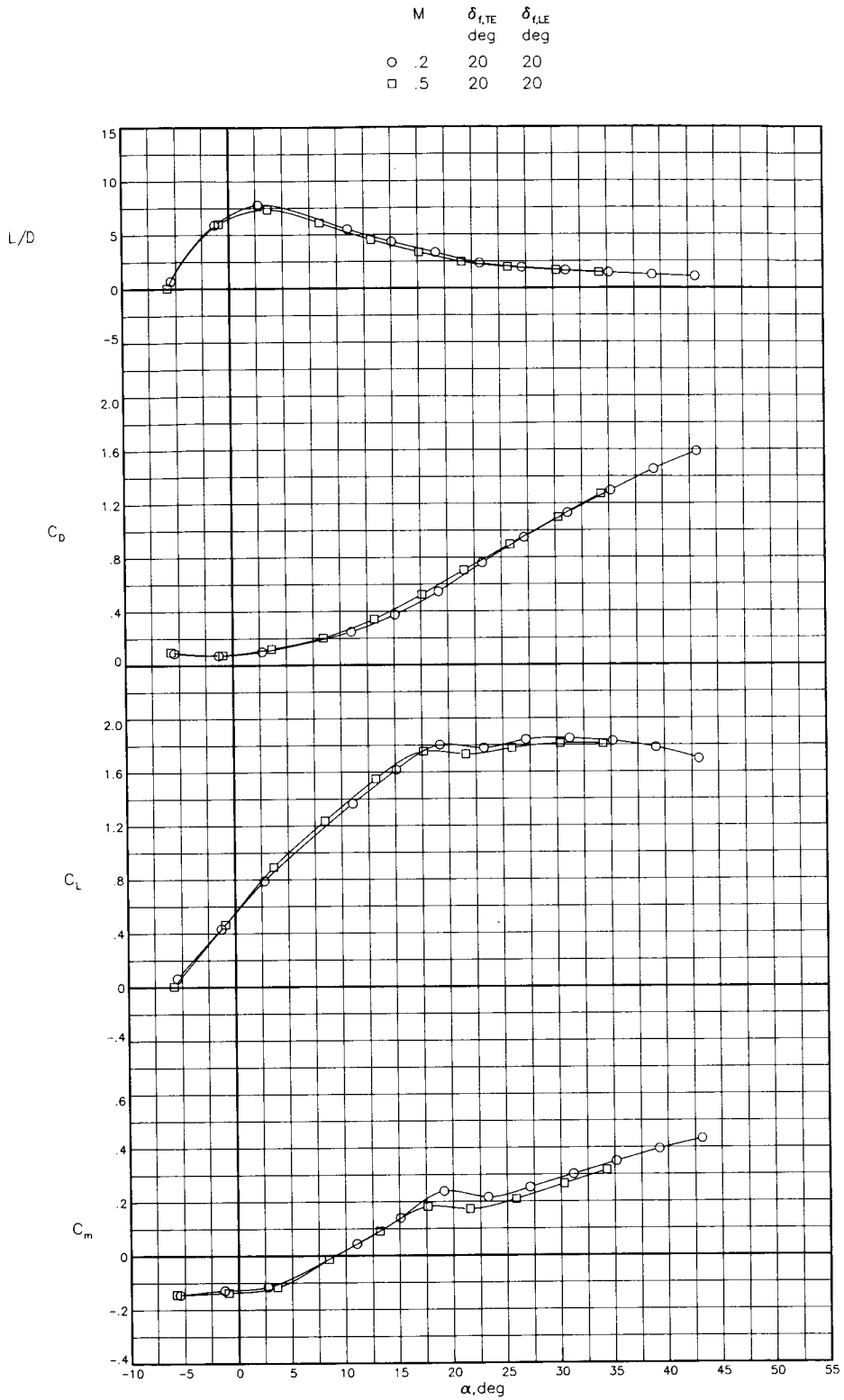


(a) Effect of Mach number on longitudinal characteristics. $\beta = 0°$.

Figure 11. Characteristics of strake-wing-body configuration with canard off and strake on. $\delta_{f,\mathrm{LE}} = \delta_{f,\mathrm{TE}} = 20°$.

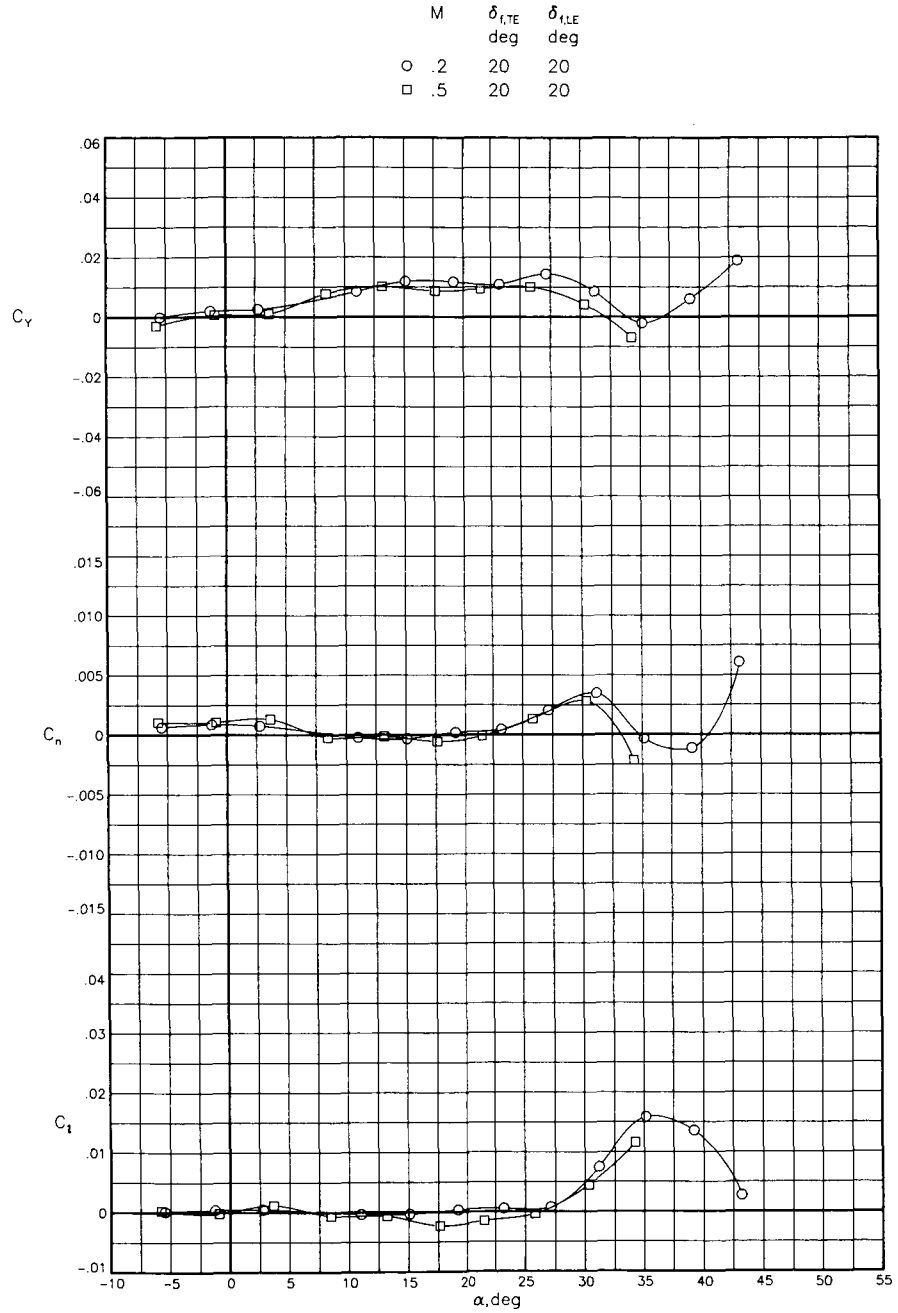


(b) Effect of Mach number on lateral-directional characteristics. $\beta = 0°$.

Figure 11. Continued.

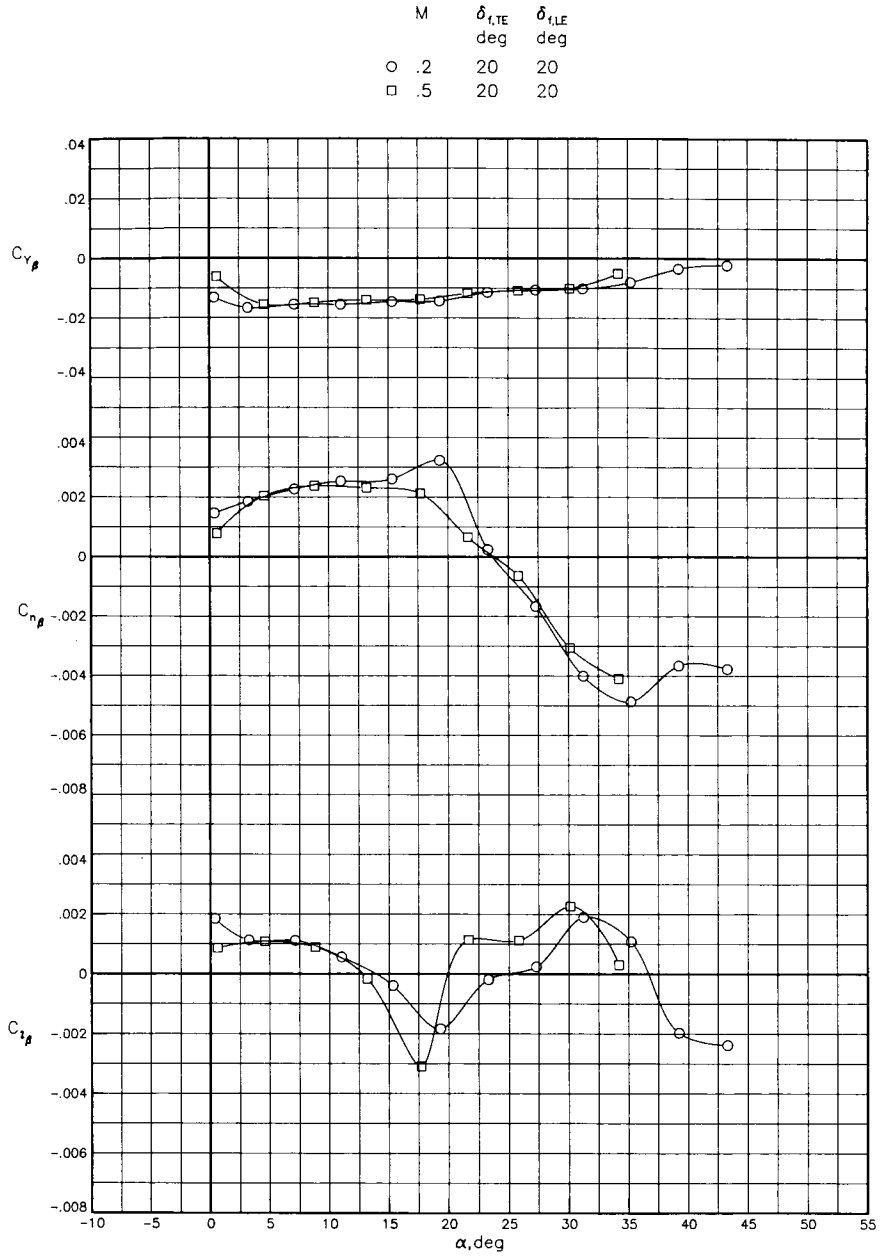


(c) Effect of Mach number on lateral-directional stability.

Figure 11. Continued.

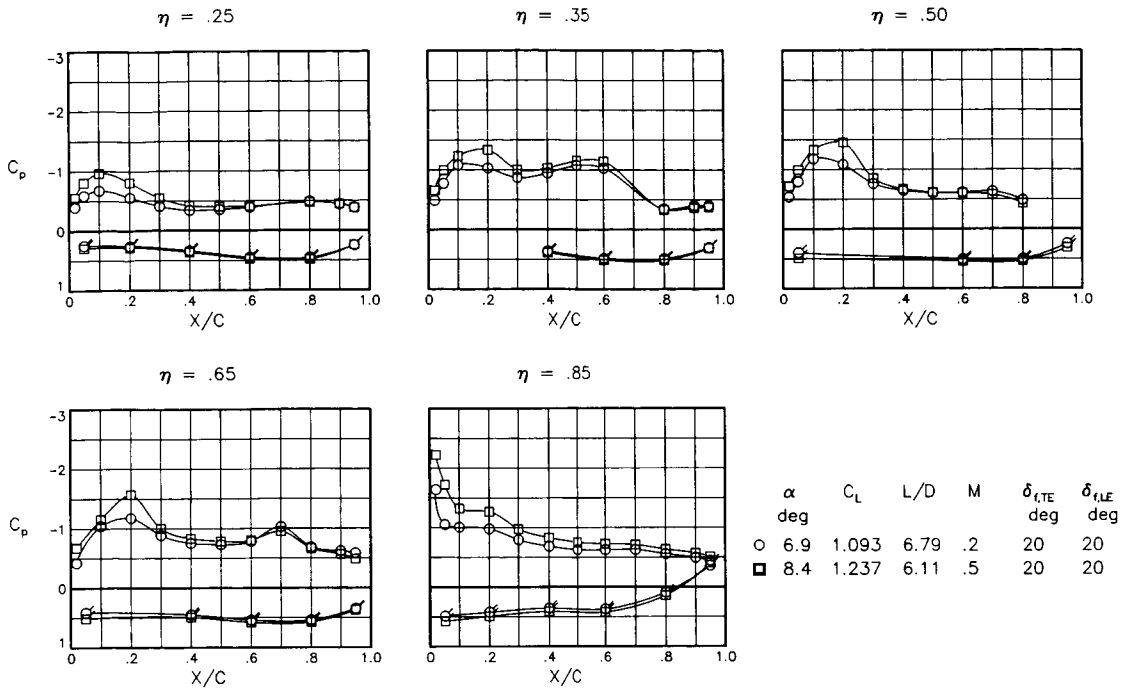


(d) Effect of Mach number on wing pressure distribution for lift coefficient near 1.0. $\beta = 0°$.

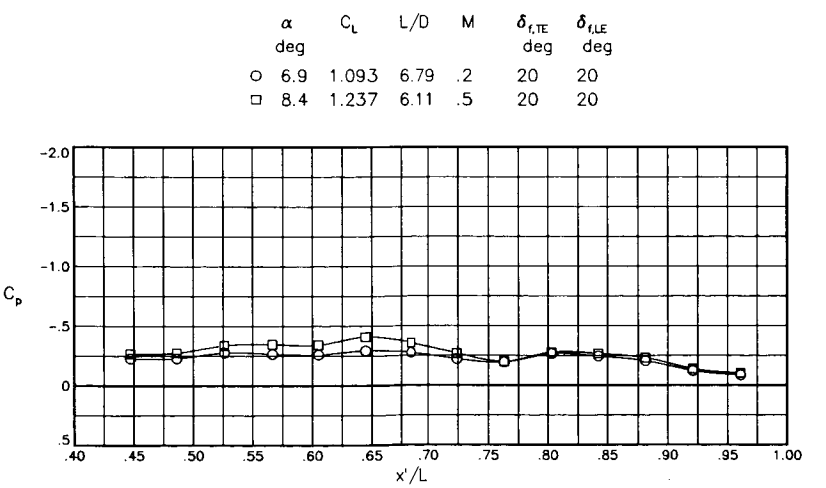


(e) Effect of Mach number on fuselage pressure distribution for lift coefficient near 1.0. $\beta = 0°$.

Figure 11. Continued.

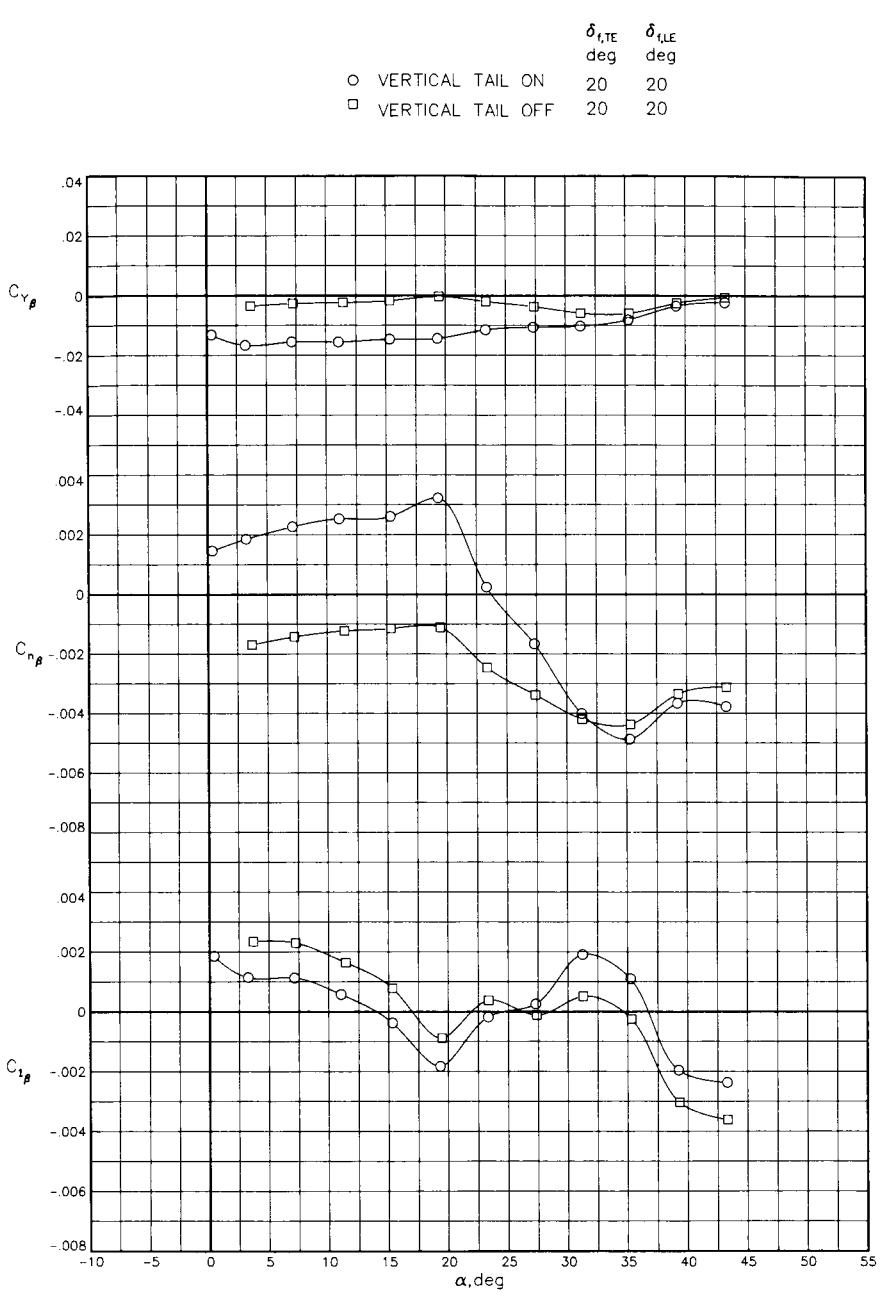


(f) Effect of vertical tail on lateral-directional stability. $M = 0.2$.

Figure 11. Continued.

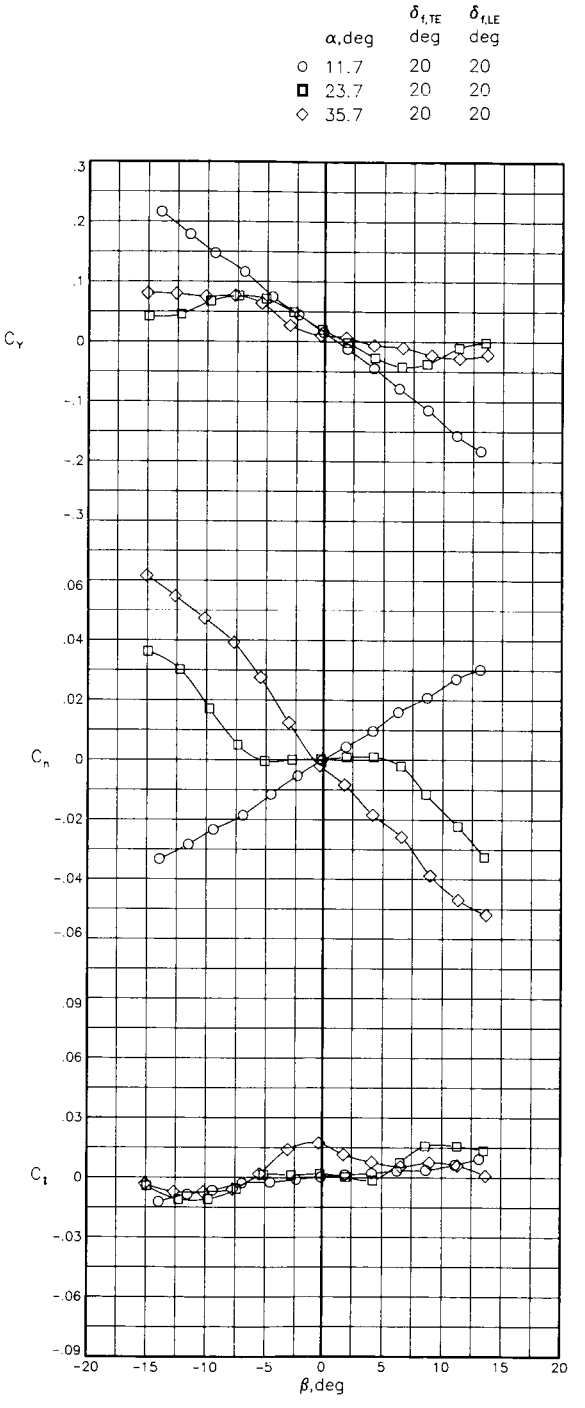


(g) Effect of angle of sideslip on lateral-directional characteristics. $M = 0.2$.

Figure 11. Concluded.

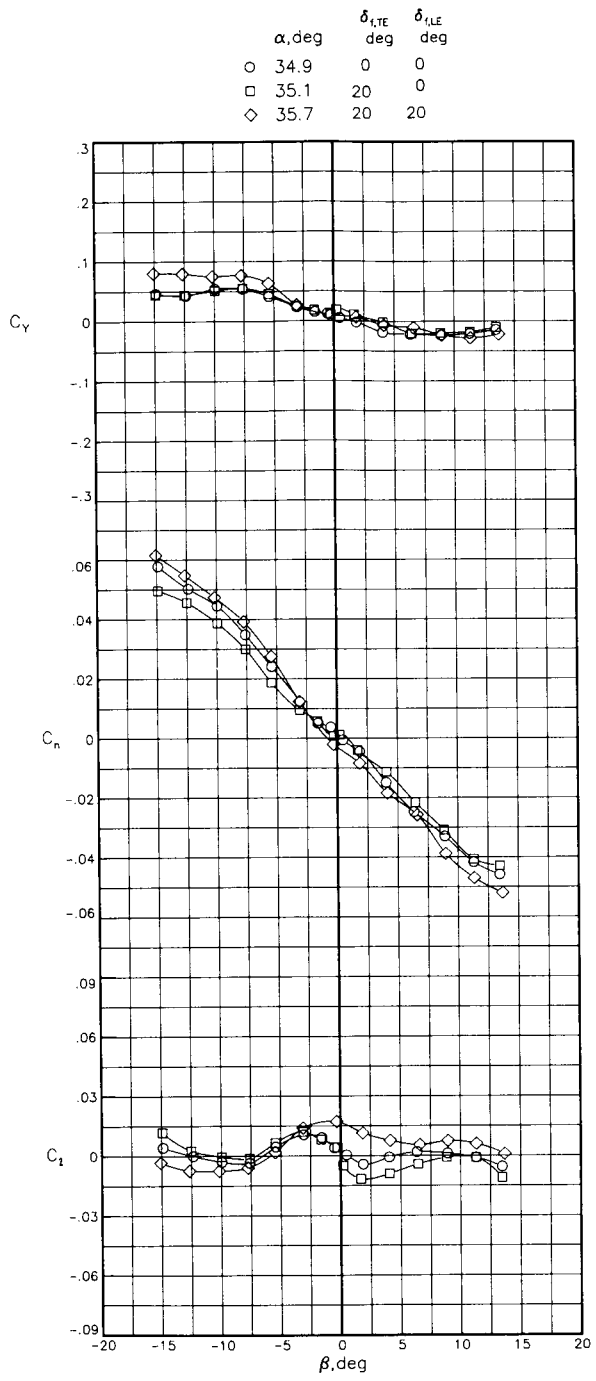


Figure 12. Effects of leading- and trailing-edge flaps on lateral-directional characteristics as function of sideslip angle for strake-wing-body configuration with canard off and strake on. $M = 0.2; \alpha \approx 36°$.

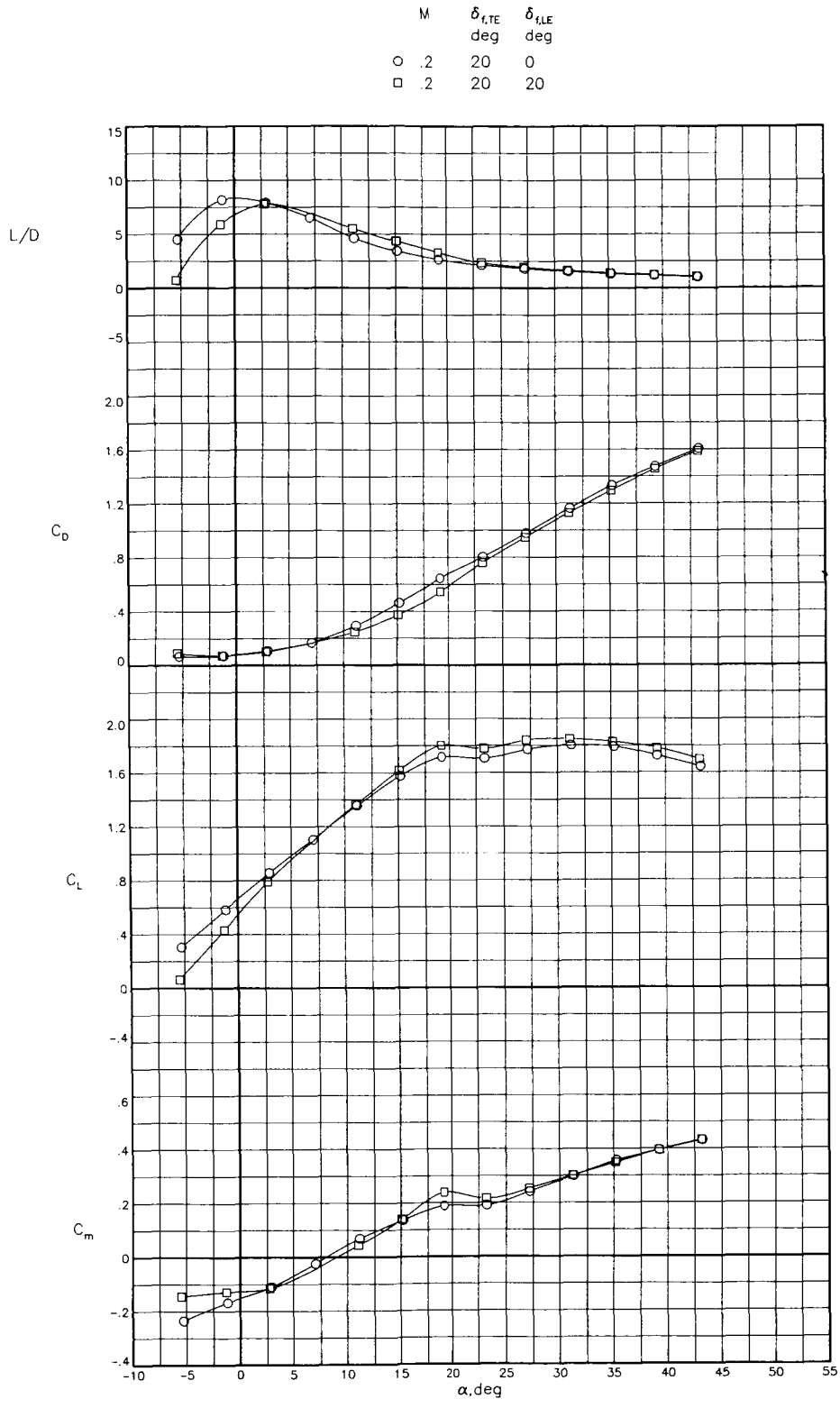


(a) Longitudinal characteristics. $\beta = 0°$.

Figure 13. Effects of leading-edge flap on strake-wing-body configuration with canard off and strake on. $\delta_{f,\mathrm{TE}} = 20°$; $M = 0.2$.

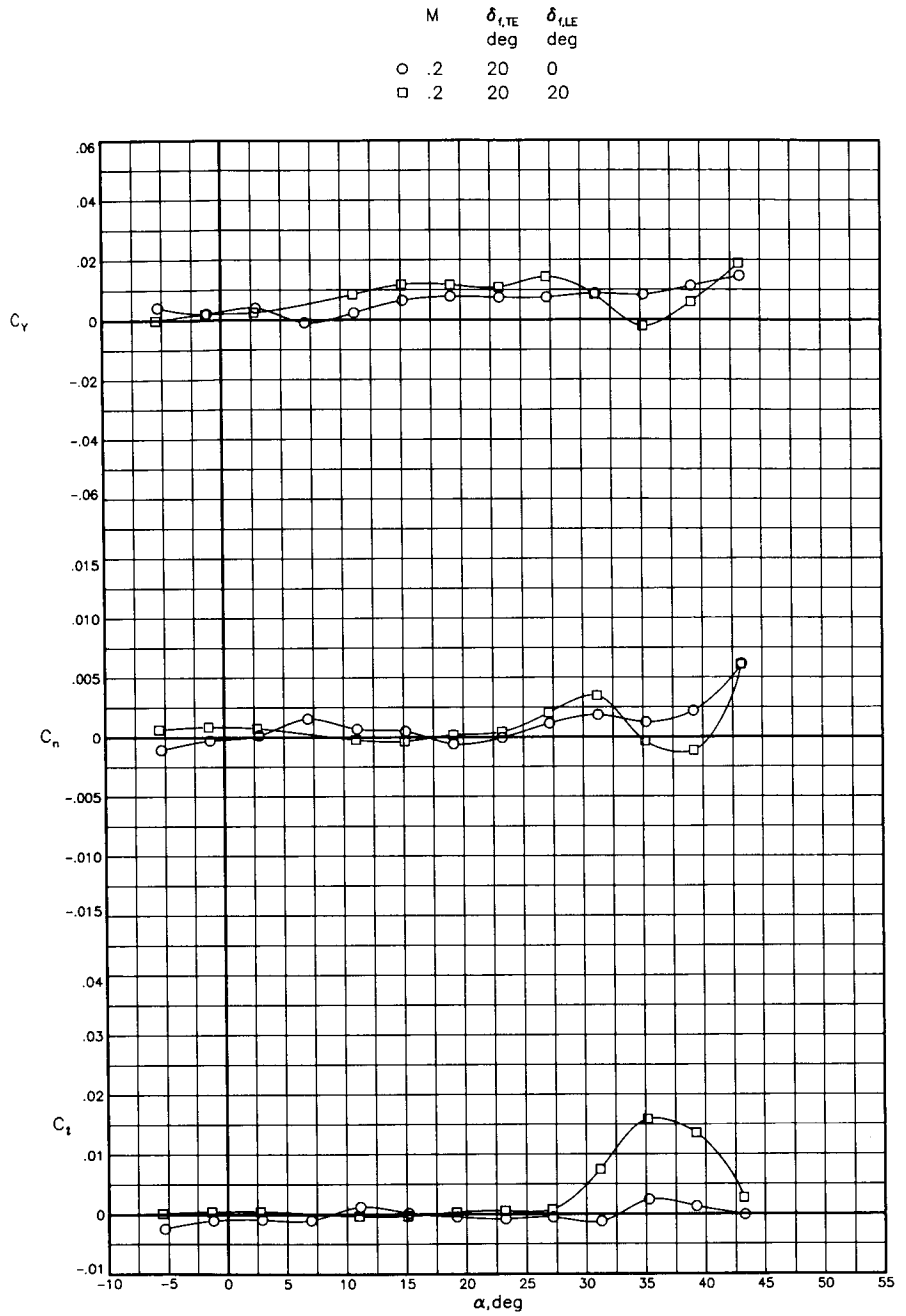


(b) Lateral-directional characteristics. $\beta = 0°$.

Figure 13. Continued.

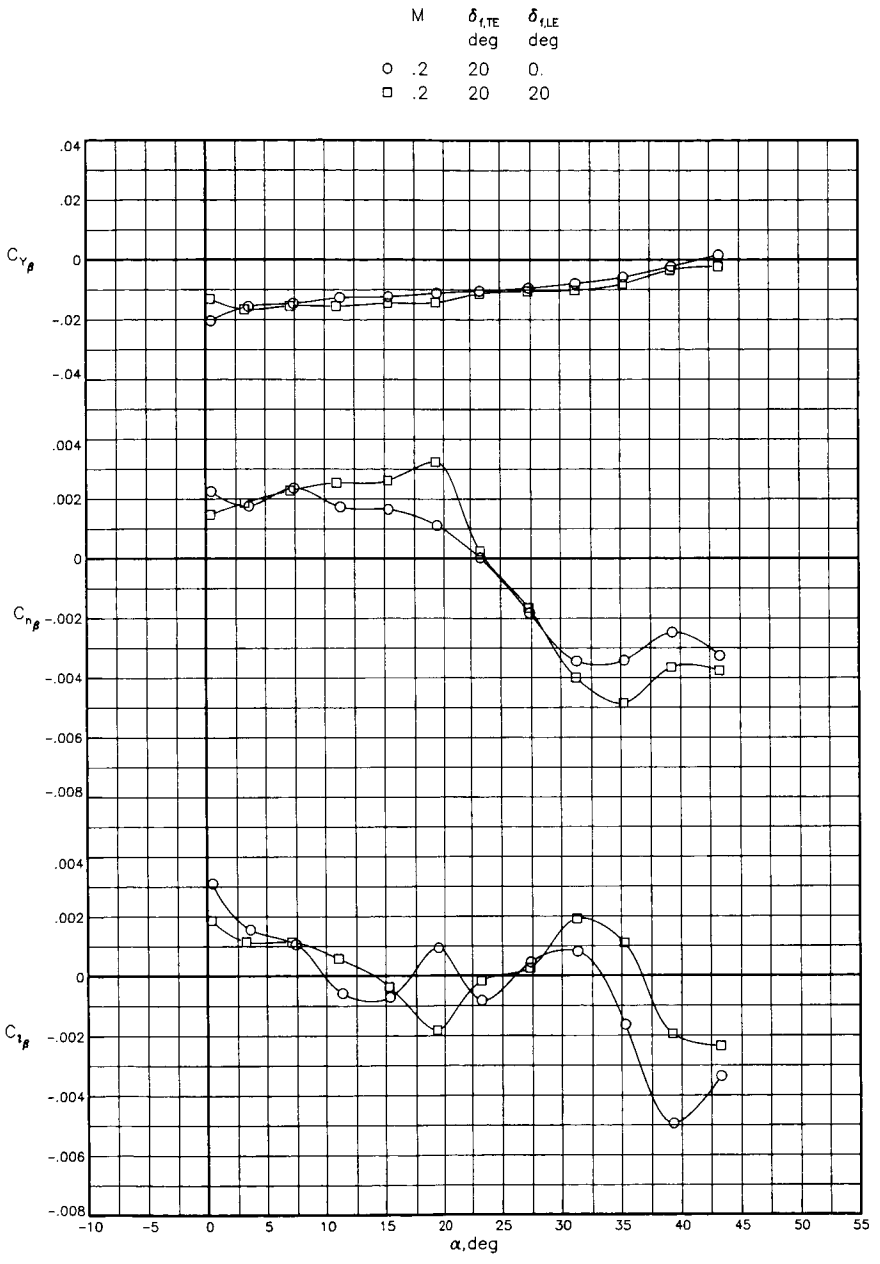


(c) Lateral-directional stability.

Figure 13. Continued.

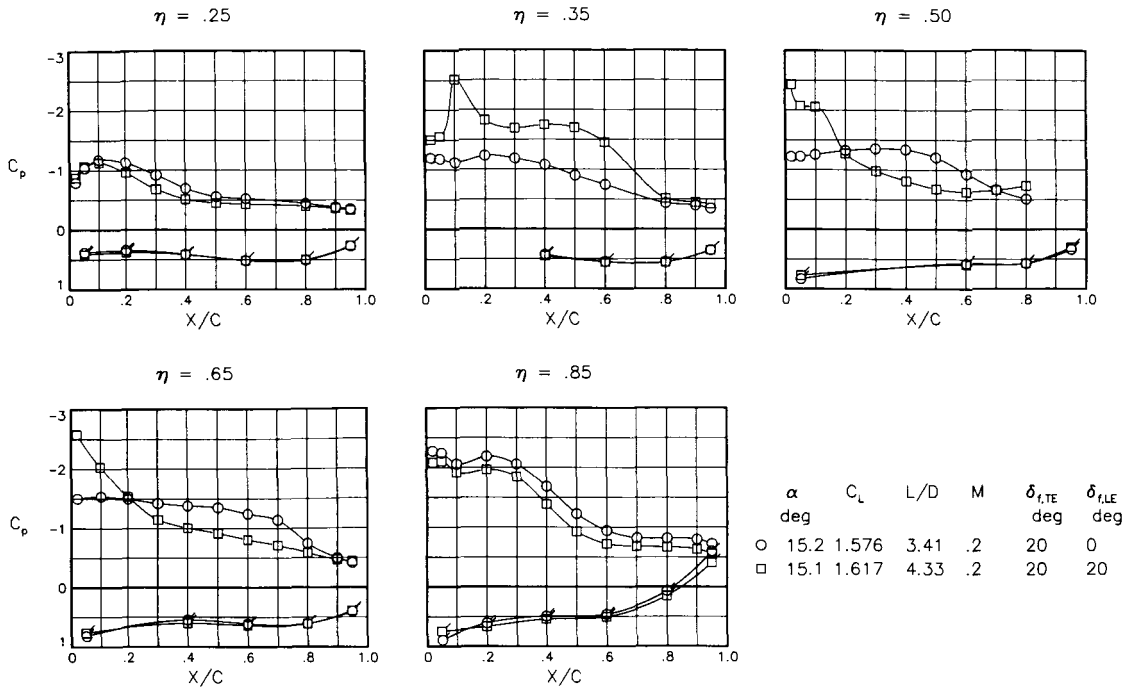


(d) Wing pressure distributions. $\alpha \approx 15°$; $\beta = 0°$.

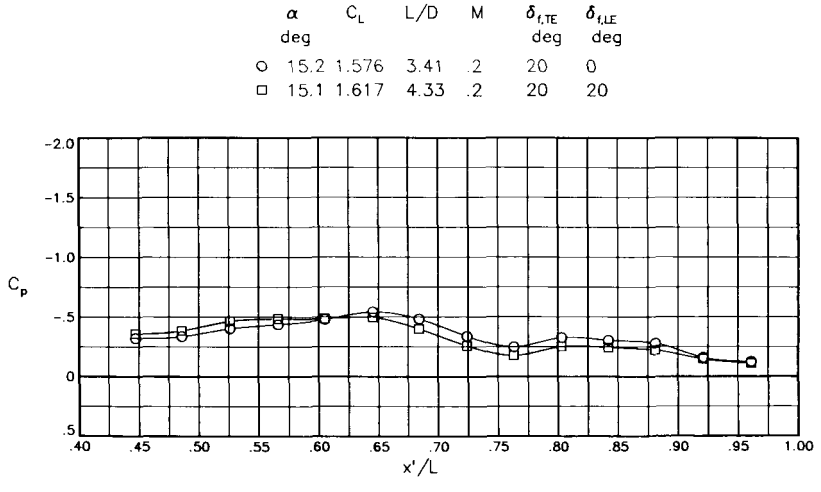


(e) Fuselage pressure distributions. $\alpha \approx 15°$; $\beta = 0°$.

Figure 13. Concluded.

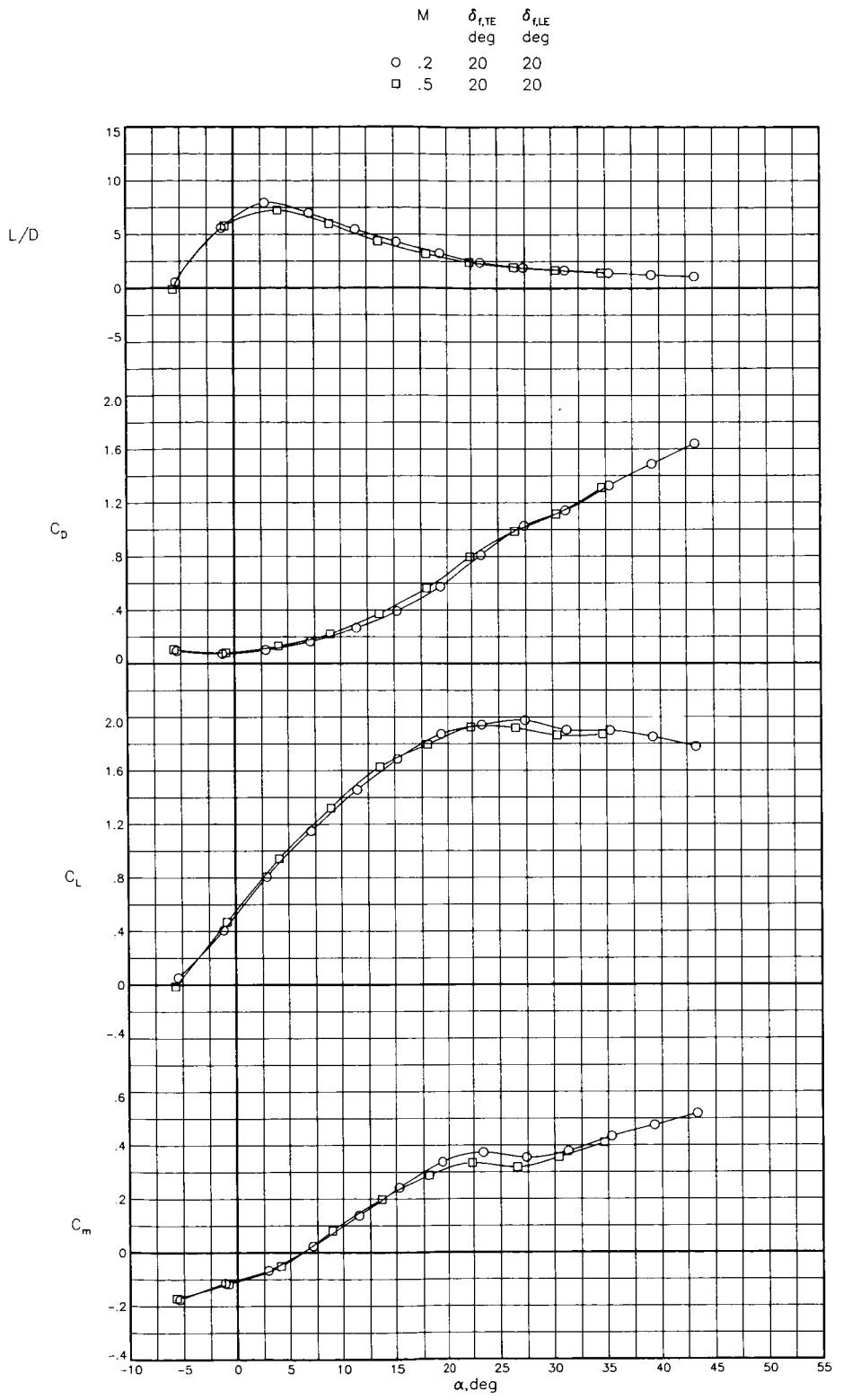


(a) Effect of Mach number on longitudinal characteristics. $\beta = 0°$.

Figure 14. Characteristics of strake-canard–wing-body configuration with canard on at zero incidence and strake on. $\delta_{f,\mathrm{LE}} = \delta_{f,\mathrm{TE}} = 20°$.

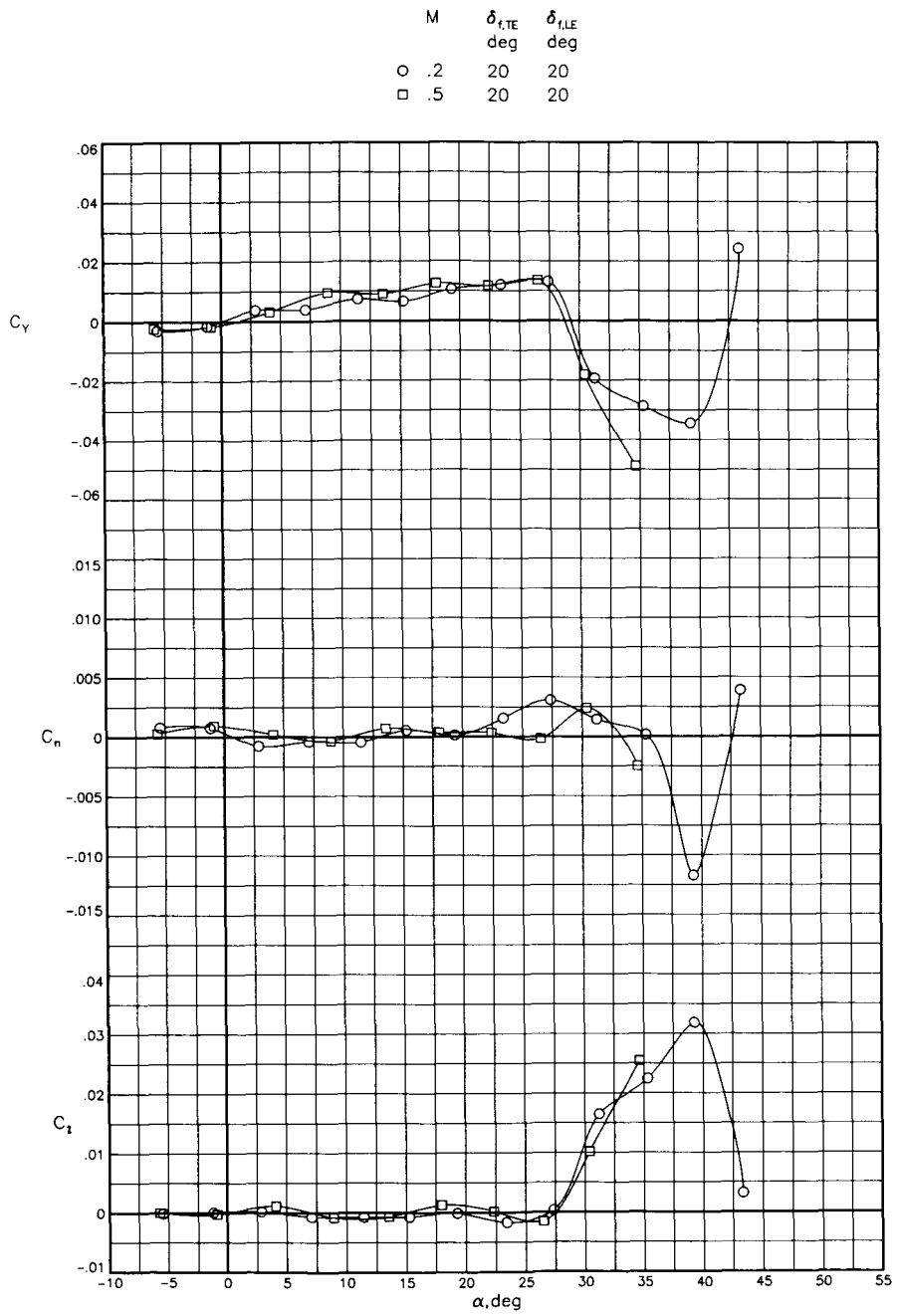


(b) Effect of Mach number on lateral-directional characteristics. $\beta = 0°$.

Figure 14. Continued.

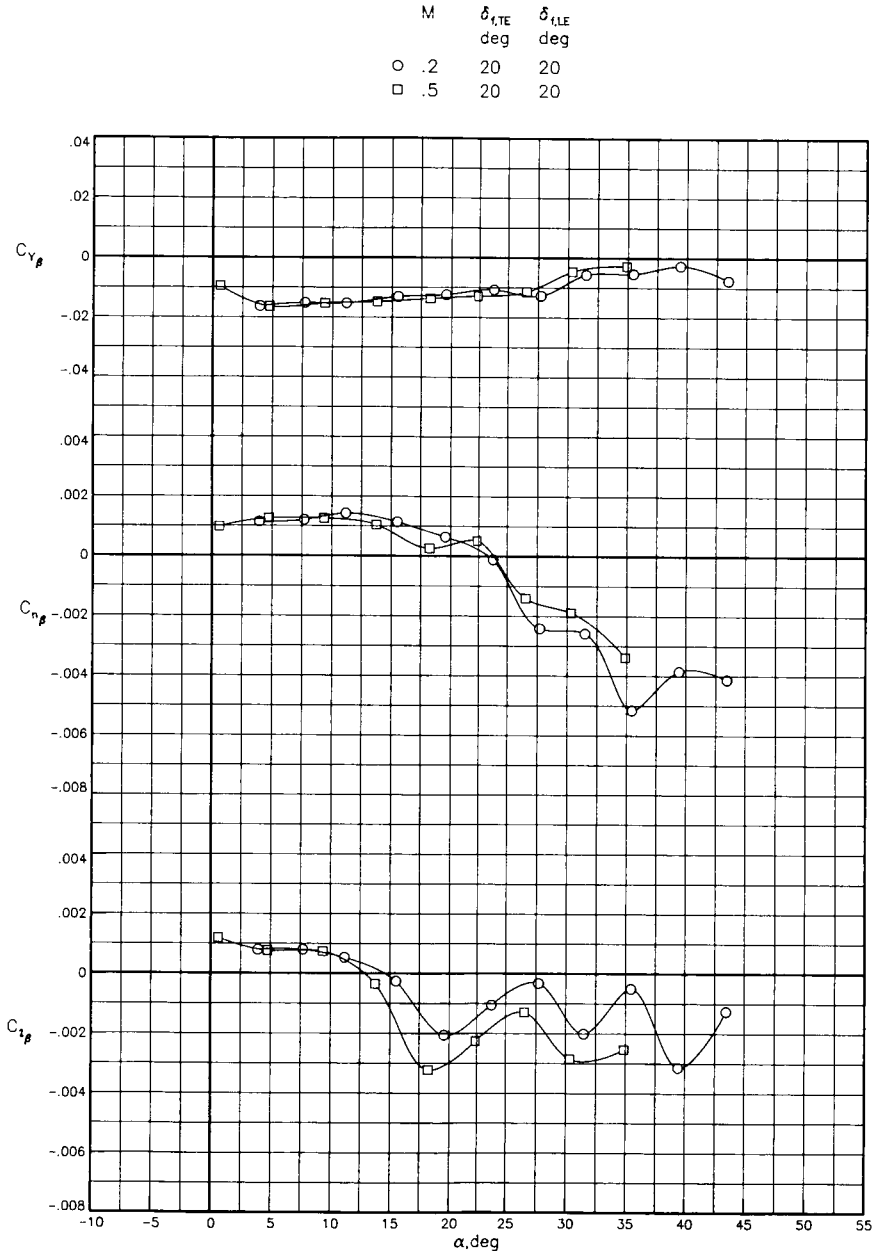


(c) Effect of Mach number on lateral-directional stability.

Figure 14. Continued.

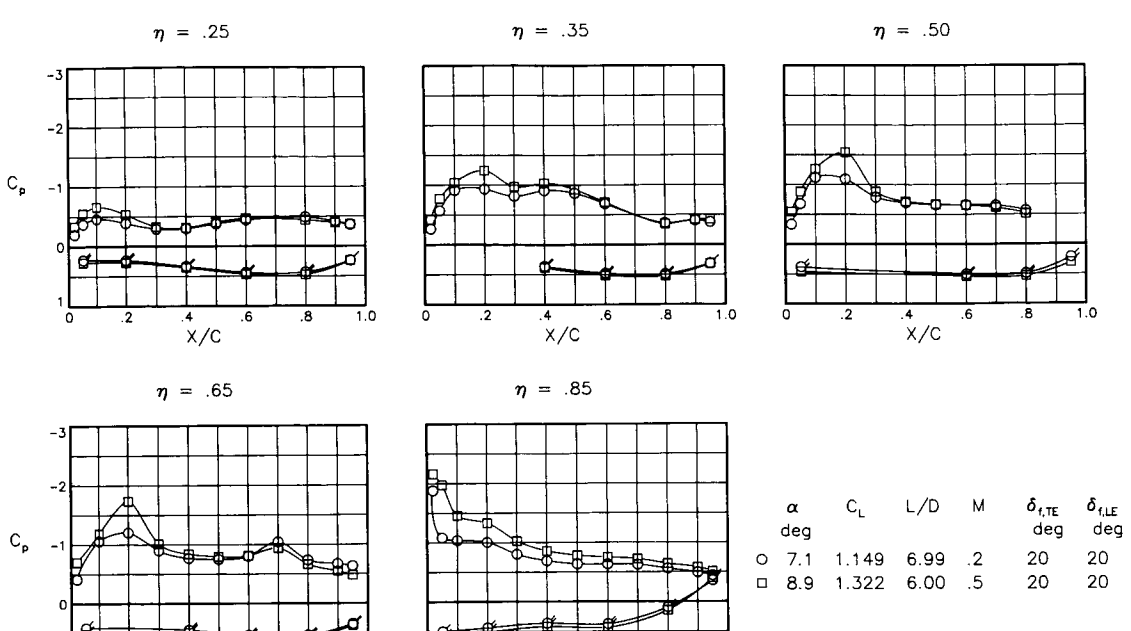


(d) Effect of Mach number on wing pressure distribution for lift coefficient near 1.0. $\beta = 0°$.

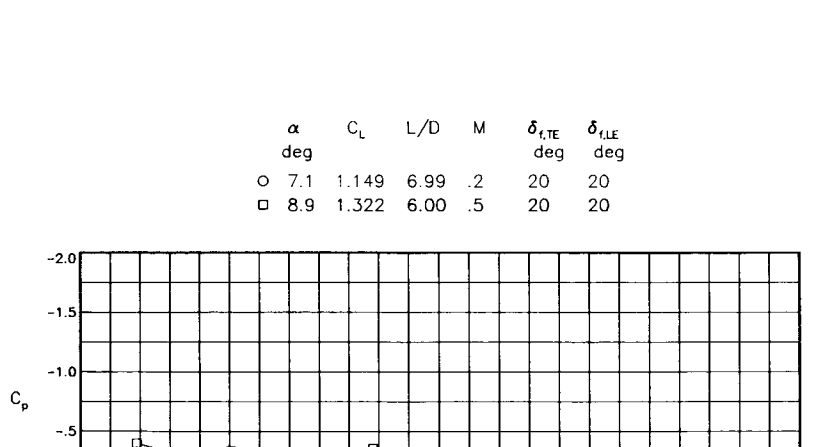


(e) Effect of Mach number on fuselage pressure distribution for lift coefficient near 1.0. $\beta = 0°$.

Figure 14. Continued.

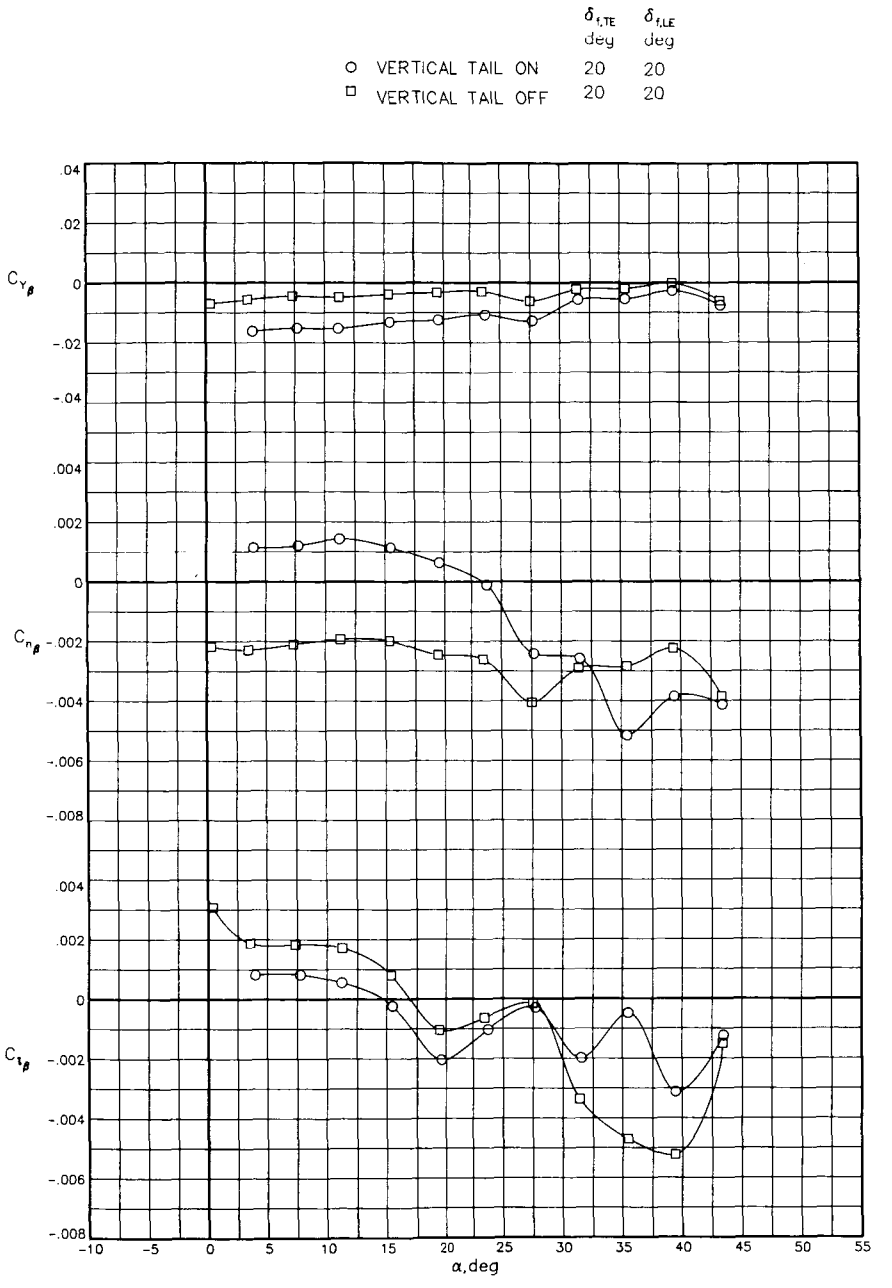


(f) Effect of vertical tail on lateral-directional stability. $M = 0.2$.

Figure 14. Continued.

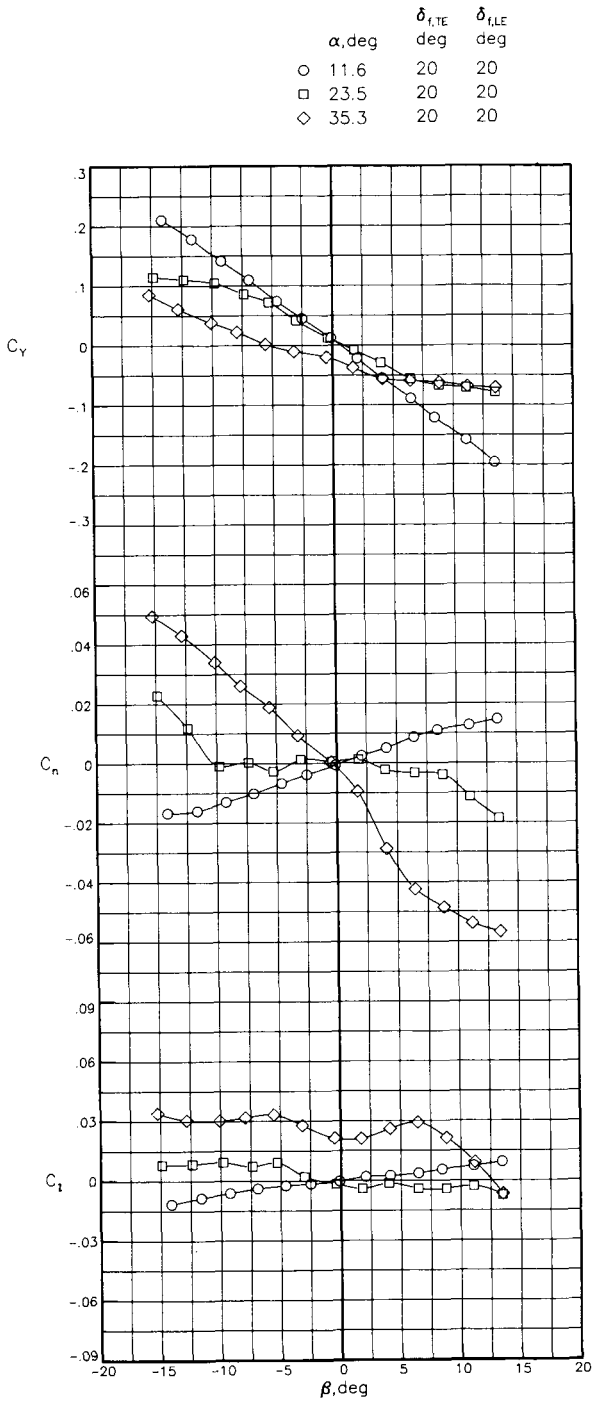


(g) Effect of angle of sideslip on lateral-directional characteristics. $M = 0.2$.

Figure 14. Concluded.

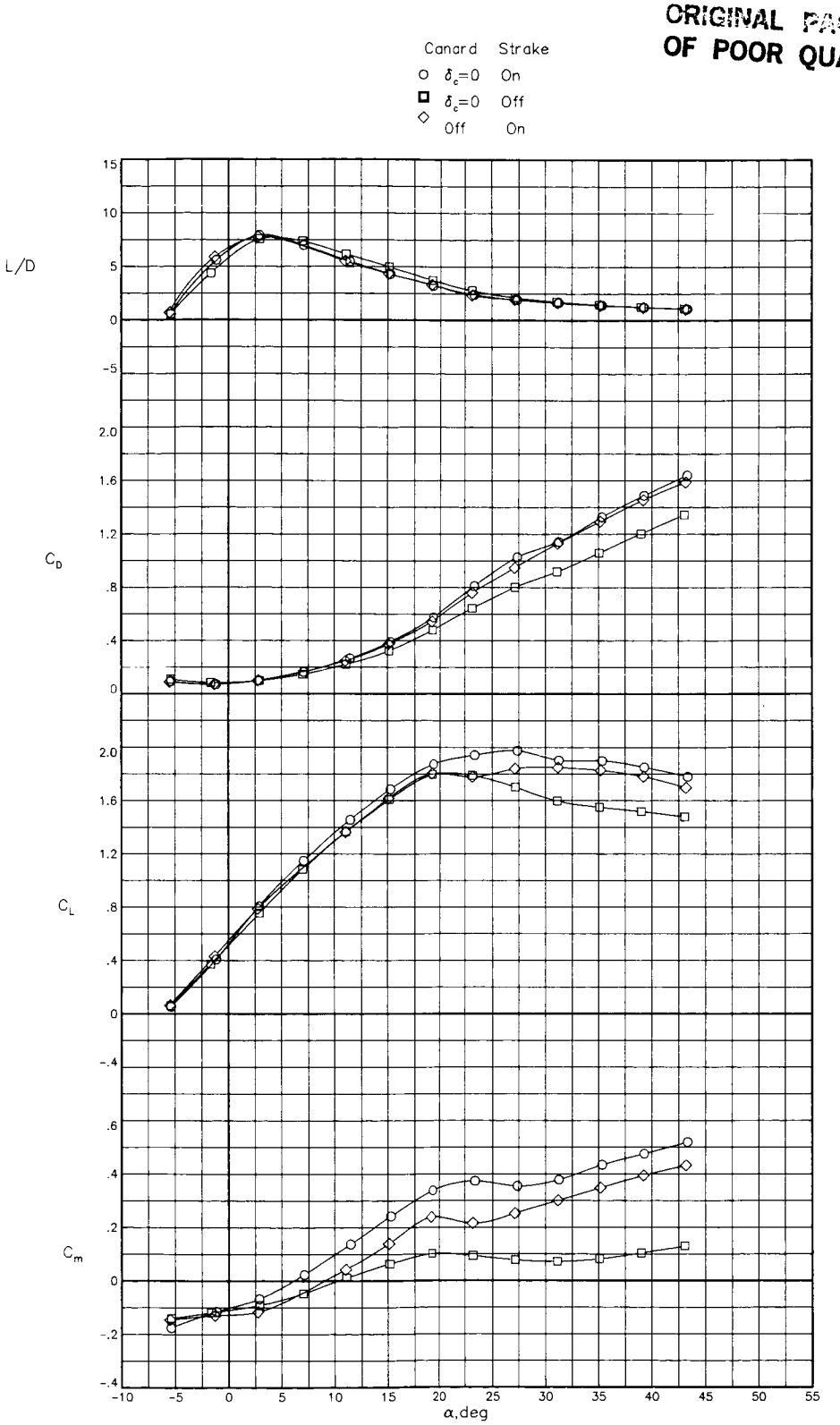


(a) Longitudinal characteristics for $M = 0.2$. $\beta = 0°$.

Figure 15. Comparison of canard, strake, and strake-canard configurations. $\delta_{f,\mathrm{LE}} = \delta_{f,\mathrm{TE}} = 20°$.

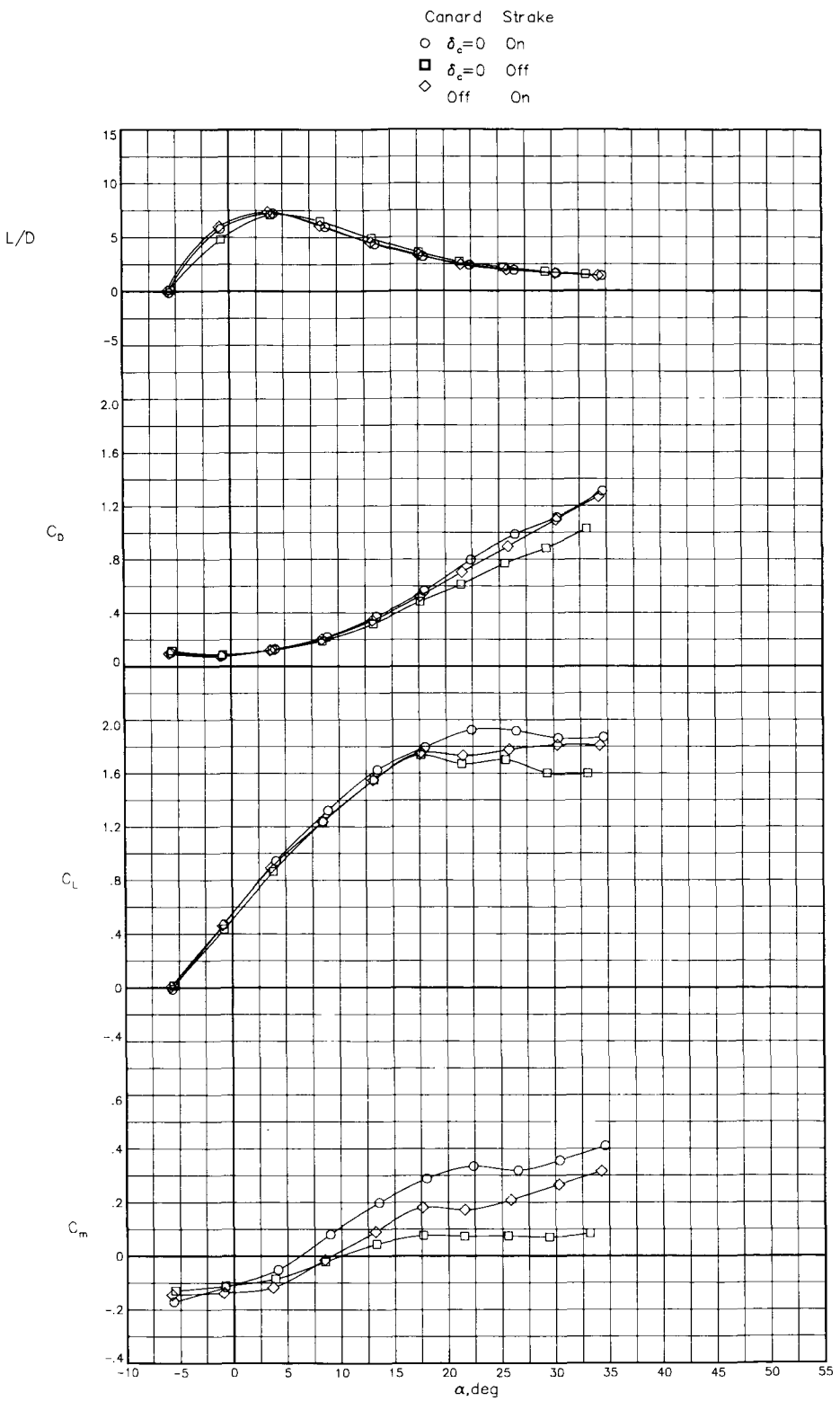


(b) Longitudinal characteristics for $M = 0.5$. $\beta = 0°$.

Figure 15. Continued.

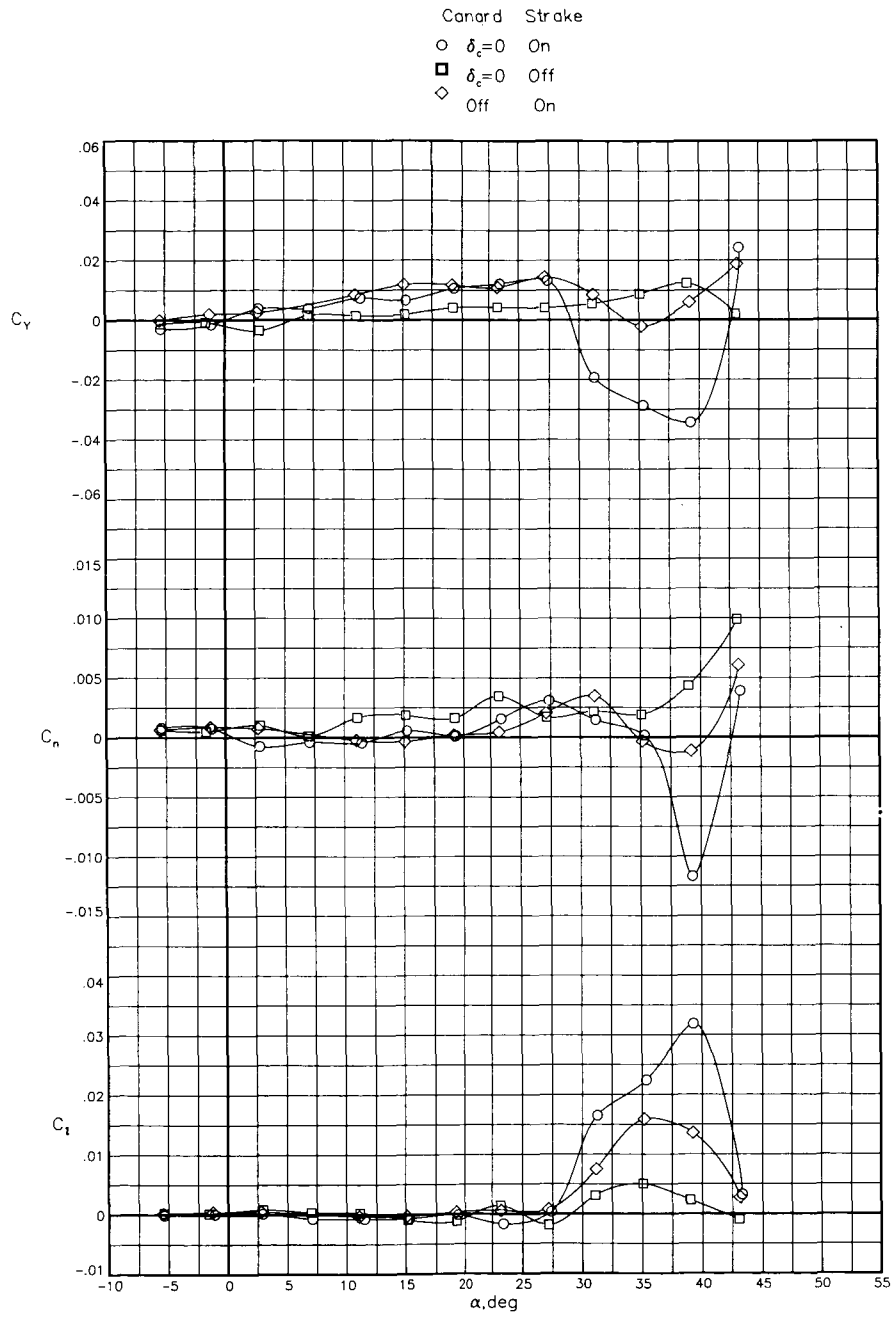


(c) Lateral-directional characteristics for $M = 0.2$. $\beta = 0°$.

Figure 15. Continued.

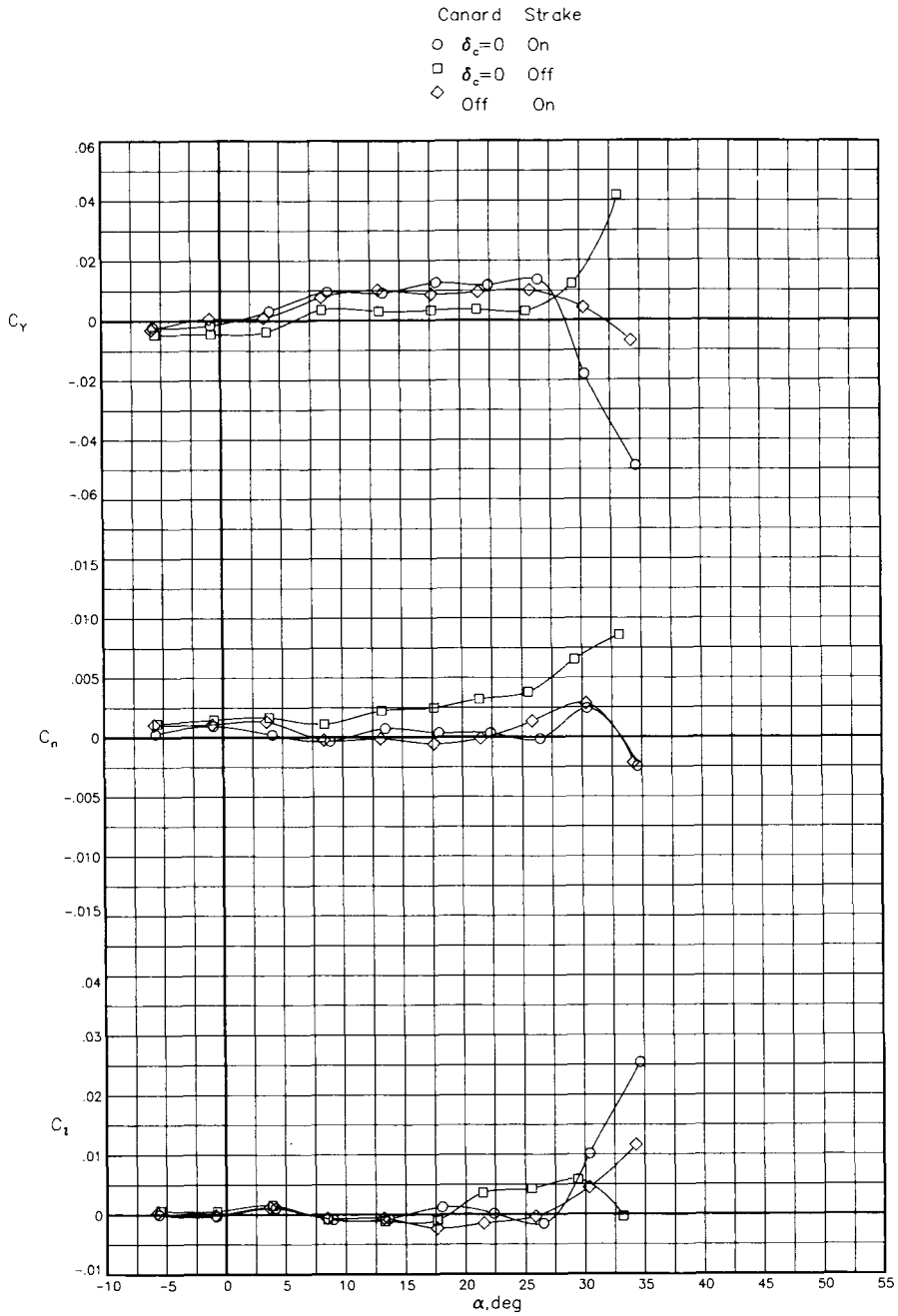


(d) Lateral-directional characteristics for $M = 0.5$. $\beta = 0°$.

Figure 15. Continued.

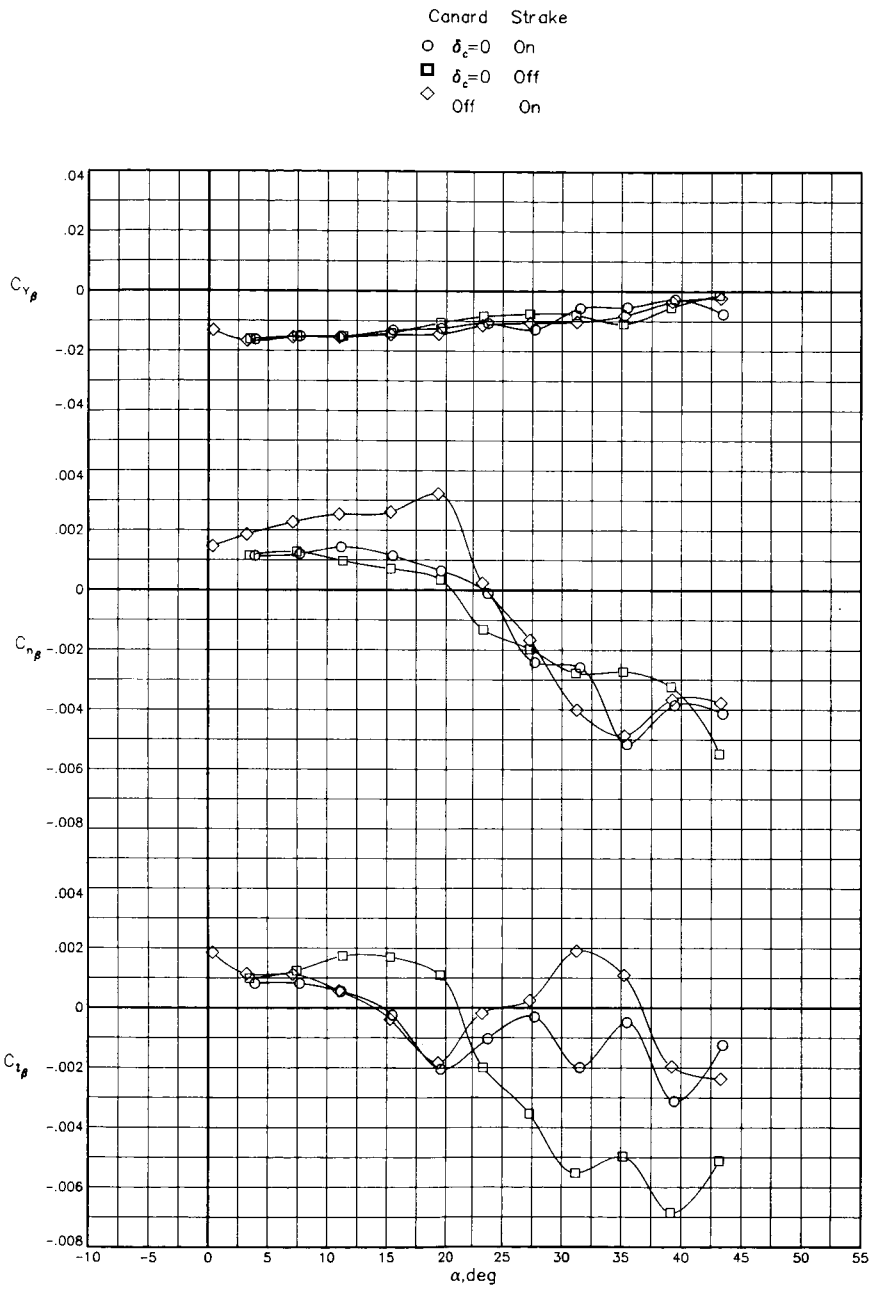


(e) Lateral-directional stability for $M = 0.2$.

Figure 15. Continued.

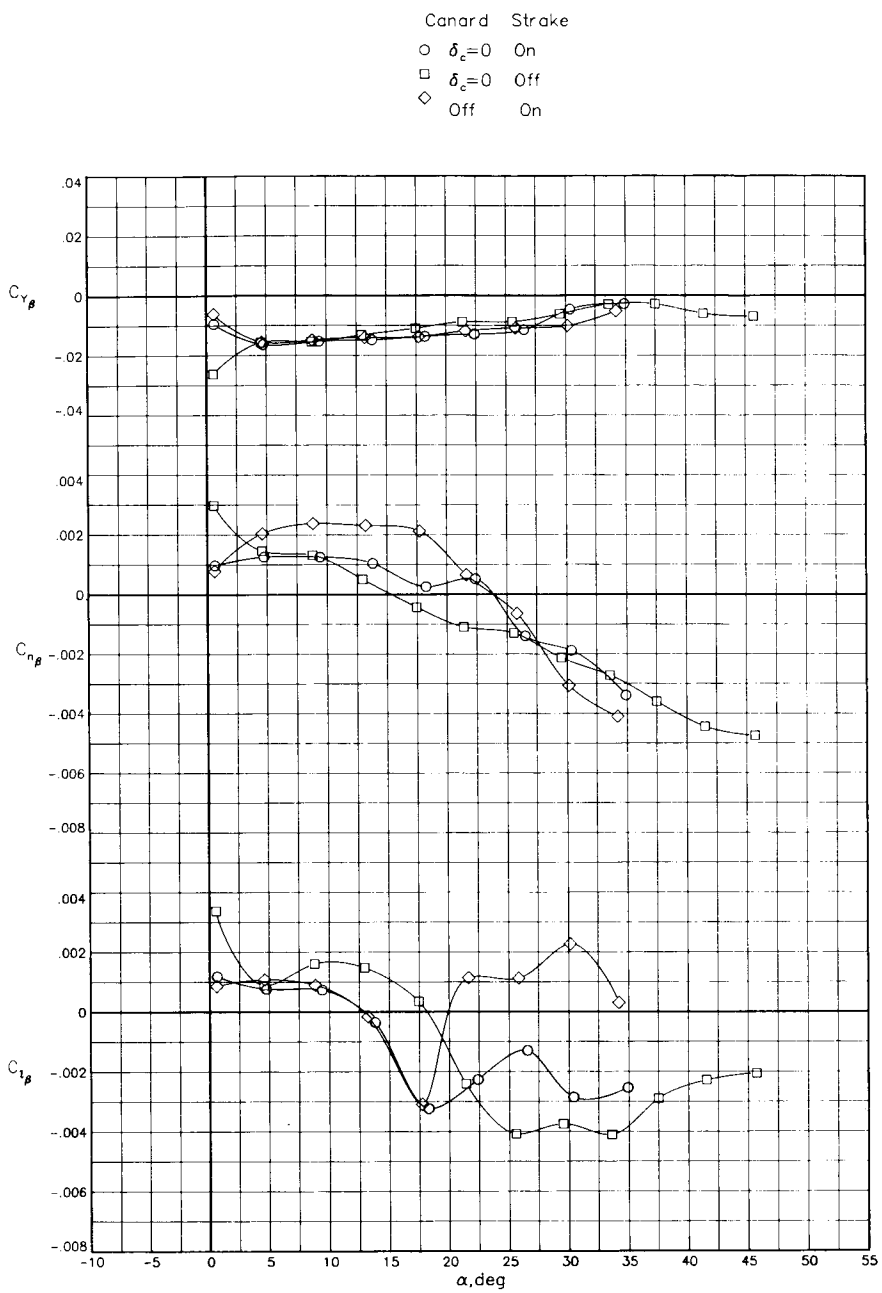


(f) Lateral-directional stability for $M = 0.5$.

Figure 15. Concluded.

C-2a

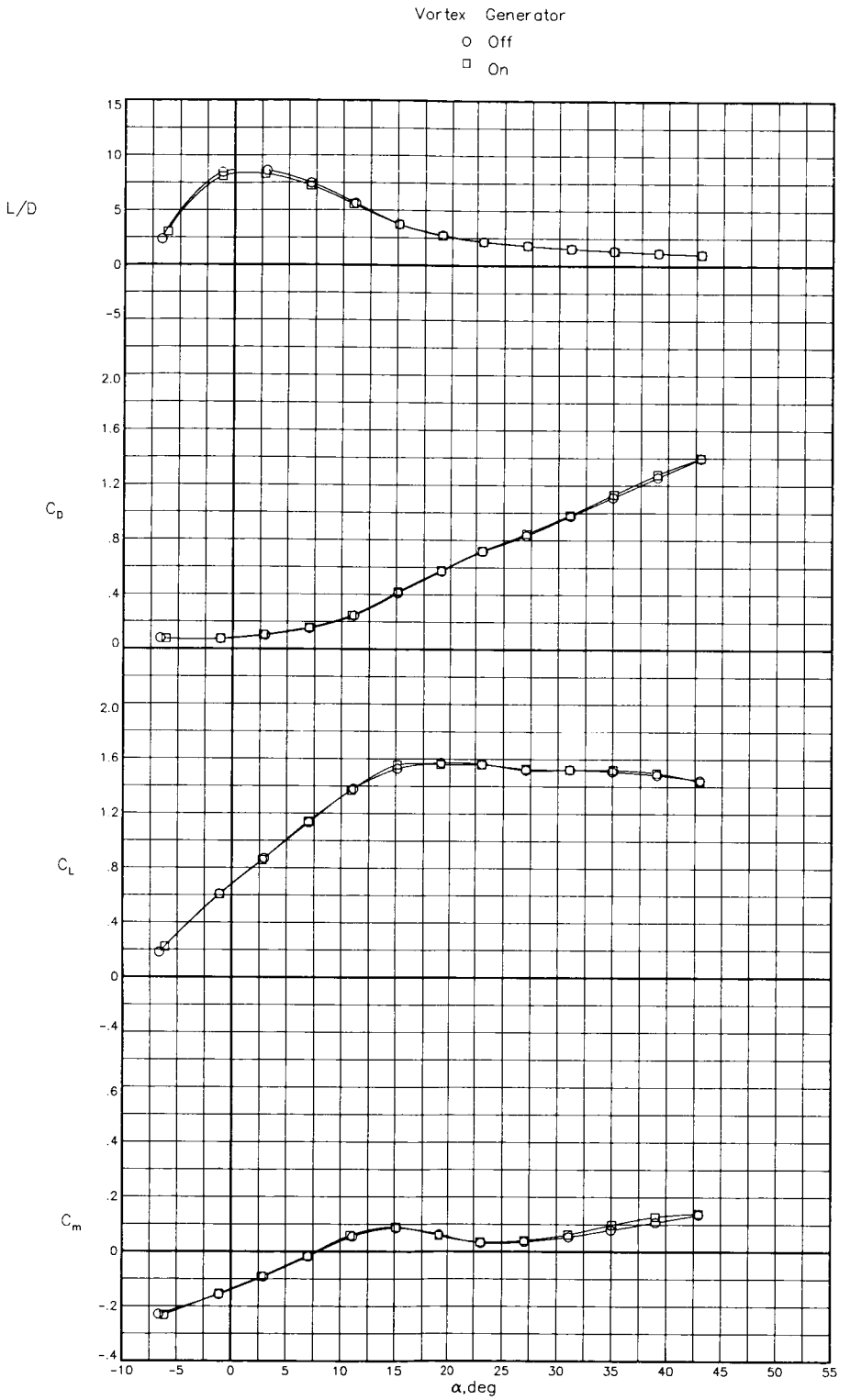


(a) Longitudinal characteristics.

Figure 16. Effects of vortex generators on canard-wing-body configuration with canard on at zero incidence and strake off. $\delta_{f,\mathrm{LE}} = 0°; \delta_{f,\mathrm{TE}} = 20°; \beta = 0°; M = 0.2$.

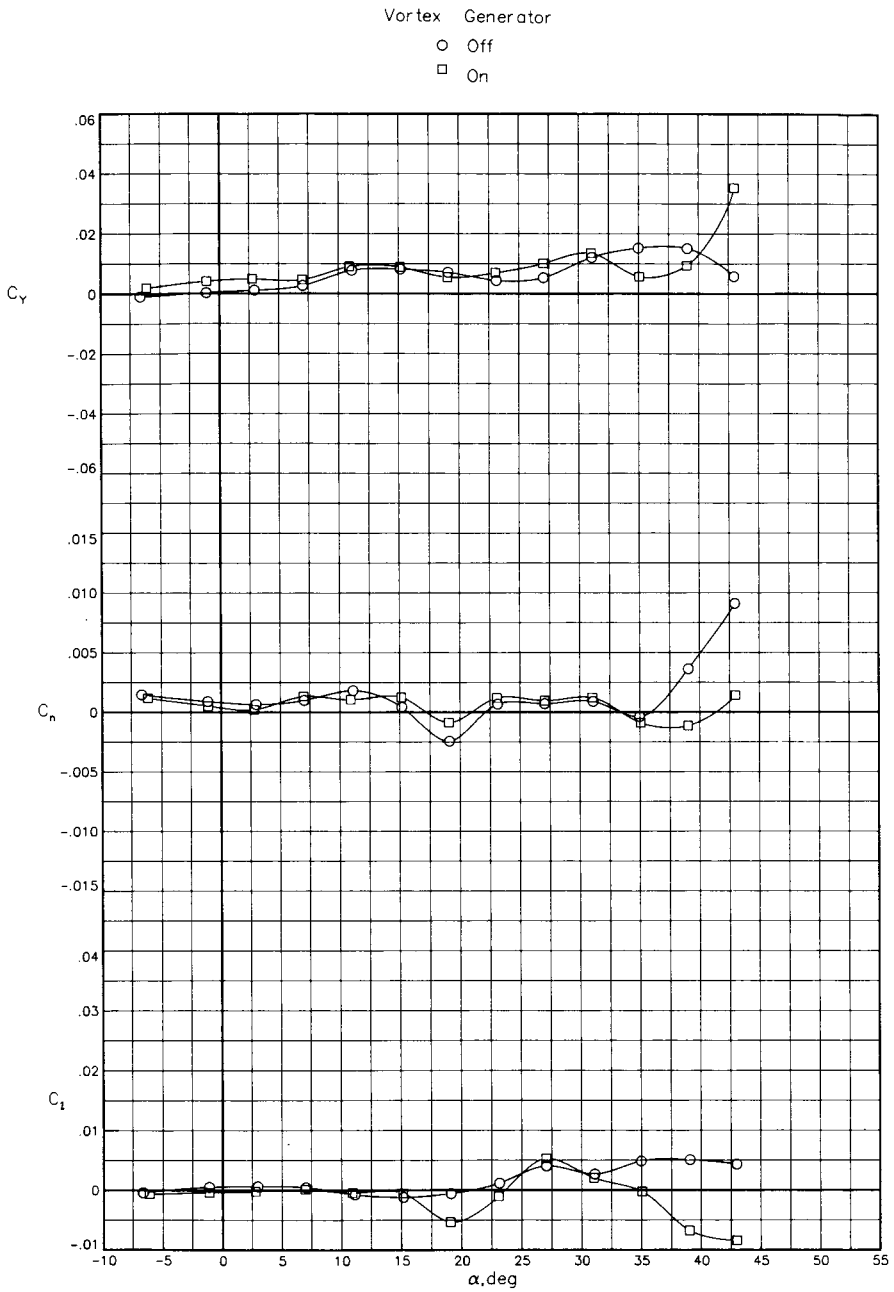


(b) Lateral-directional characteristics.

Figure 16. Concluded.

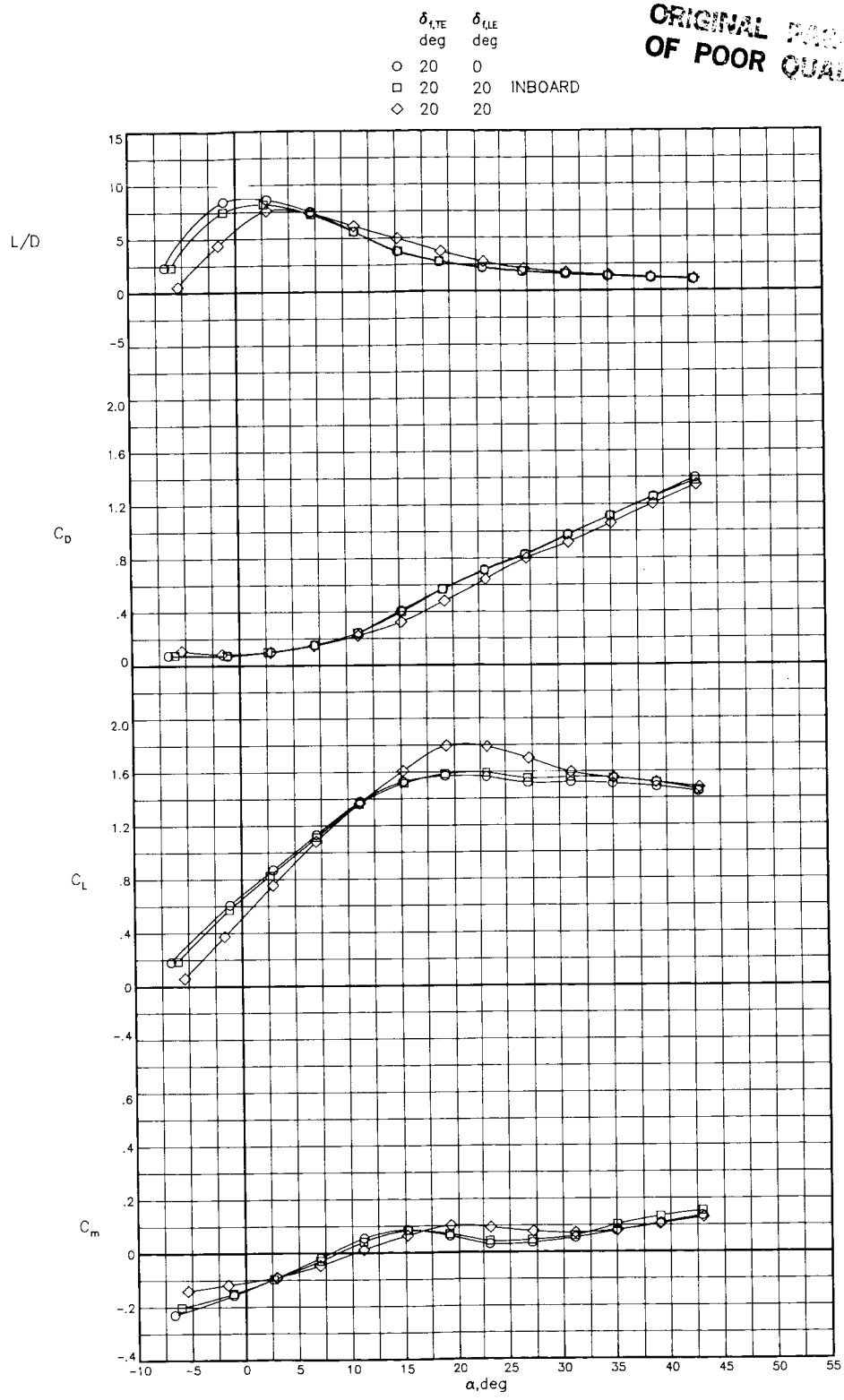


(a) Longitudinal characteristics.

Figure 17. Effects of segmented leading-edge flap on canard-wing-body configuration with canard on at zero incidence and strake off. $\delta_{f,\mathrm{TE}} = 20°$; $\beta = 0°$; $M = 0.2$.

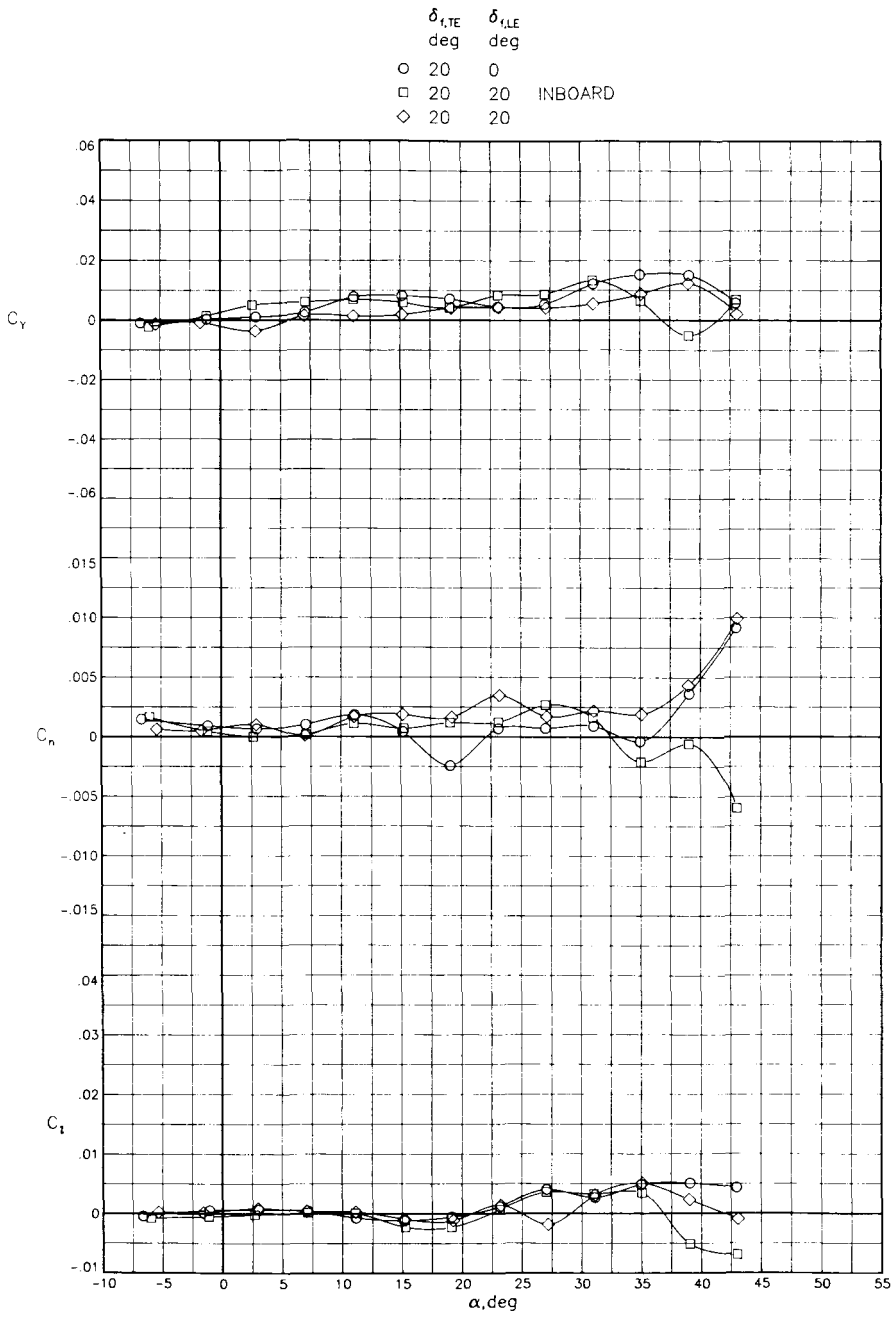


(b) Lateral-directional characteristics.

Figure 17. Concluded.

NASA
National Aeronautics and Space Administration

# Report Documentation Page

| 1. Report No. | 2. Government Accession No. | 3. Recipient's Catalog No. |
|---|---|---|
| NASA TP-2727 | | |

**4. Title and Subtitle**
Subsonic Longitudinal and Lateral-Directional Characteristics of a Forward-Swept-Wing Fighter Configuration at Angles of Attack up to 47°

**5. Report Date**
September 1987

**6. Performing Organization Code**

**7. Author(s)**
Michael J. Mann, Jarrett K. Huffman, and Charles H. Fox, Jr.

**8. Performing Organization Report No.**
L-16206

**9. Performing Organization Name and Address**
NASA Langley Research Center
Hampton, VA 23665-5225

**10. Work Unit No.**
505-61-71-03

**11. Contract or Grant No.**

**12. Sponsoring Agency Name and Address**
National Aeronautics and Space Administration
Washington, DC 20546-0001

**13. Type of Report and Period Covered**
Technical Paper

**14. Sponsoring Agency Code**

**15. Supplementary Notes**


**16. Abstract**

Subsonic lateral-directional and longitudinal characteristics of a forward-swept-wing fighter configuration were examined in wind-tunnel tests at Mach numbers of 0.2 and 0.5 for angles of attack from $-7°$ to $47°$ and over a sideslip range of $\pm 15°$. The effects of a canard, strakes, vertical tail, and leading- and trailing-edge flaps are examined. The canard and strakes both reduce asymmetric moments and side forces at zero sideslip for angles of attack up to about $30°$. The canard has a small influence on lateral-directional stability; however, strakes produce a substantial reduction in lateral stability for angles of attack greater than about $20°$. The vertical tail improves directional stability for angles of attack up to $30°$. Deflection of the leading-edge flap to $20°$ at high angles of attack on the strake and canard configurations degrades lateral and directional stability. Deflection of the trailing-edge flap to $20°$ on the canard configuration generally increases lateral and directional stability at high angles of attack. Leading- and trailing-edge flaps on the wing-body and canard configurations are effective for increased lift only for angles of attack up to about $40°$. The leading-edge flap remains effective on the strake configuration over the entire angle-of-attack range tested.



**17. Key Words (Suggested by Authors(s))**
Forward-swept wing
High angle of attack
Lateral-directional aerodynamics
Canards
Strakes

**18. Distribution Statement**
Unclassified—Unlimited

Subject Category 02


| 19. Security Classif.(of this report) | 20. Security Classif.(of this page) | 21. No. of Pages | 22. Price |
|---|---|---|---|
| Unclassified | Unclassified | 101 | A06 |